MATHEMATICAL MODELS FOR THE EVOLUTION AND DEVELOPMENT OF THE CEREBRAL CORTEX IN MAMMALS

A Thesis

Presented to the Faculty of the Graduate School

of Cornell University

In Partial Fulfillment of the Requirements for the Degree of

Doctor of Philosophy

by

Diarmuid John Cahalane

August 2013

© 2013 Diarmuid John Cahalane

MATHEMATICAL MODELS FOR THE EVOLUTION AND DEVELOPMENT OF THE CEREBRAL CORTEX IN MAMMALS

Diarmuid John Cahalane, Ph.D.

Cornell University 2013

This is a pivotal time in neuroscience as modern imaging techniques and methods in network reconstruction are elucidating the structure of the brain as never before. Ultimately, our insights into these networks of connections will be the foundation for a better understanding of cognitive function and dysfunction in humans and other species. Comprehending why these structures are as we find them can be helped by knowing their developmental programs. Mathematical models will play a key role in understanding how developmental programs are orchestrated by the genome and refined by evolution to construct the brain.

In this thesis I present mathematical models for two early stages of the development of the cerebral cortex in mammals: neurogenesis and the emergence of early network structure. Both models are informed by empirical developmental and anatomical data. The first, an ordinary differential equation model for the kinetics of cortical neurogenesis, shows how those kinetics shape the basic architecture of the cortex. A massive increase in the number of cortical neurons, driving the size of the cortex to increase by 5 orders of magnitude, is a key feature of mammalian evolution. Not only are there systematic variations in the cortical architecture across species, but also within a given cortex (affecting the type of information processing which happens in each part of the cortex). The mathematical model presented here accounts for both the cross-species and within-cortex variation as arising from the same developmental mechanism.

For the second model, data from an axon-tracing study in rodents informs a network model of early connectivity between neurons in the cerebral cortex. Analysis of the model shows that early axon out-growth has an anisotropic spatial distribution which reduces the volume occupied by the axons without causing a significant decrease in the efficiency of the resulting network. Moreover, the preferential connectivity observed along the medial-lateral axis of the cortex my seed the emerging layout of the cortical areas which are specialized for various types of information processing.

BIOGRAPHICAL SKETCH

Diarmuid Cahalane was born in Cork, Ireland in 1982 and grew up in the small, rural town of Dunmanway in West Cork. He attended local schools and worked in the family construction business during summers and on weekends. As an undergraduate at University College Cork (UCC) he studied physics and applied mathematics. He spent one year as a visiting student at the Physics Department at Boston College in Massachusetts. Diarmuid was a member of the UCC's Mountaineering Club and "Philosophical" (debating) Society, receiving an honorary life membership of that society. Having received his bachelor's degree, he pursued a master's degree by research in applied mathematics, also at UCC.

In 2007, Diarmuid enrolled in the applied mathematics PhD program at the Center for Applied Mathematics (CAM) at Cornell University. He joined a small group of his fellow first-year students in a side research project with Professor Finlay of the Psychology Department. Shortly thereafter he was the only remaining student on the project and six years later the project had developed into his PhD thesis. During his time at CAM, Diarmuid was actively involved in the various student initiatives intended to help keep the CAM ship afloat.

At Cornell, Diarmuid enjoyed spending time with CAM students and others from across the campus, and tried to make the most of Ithaca's great outdoors: skiing at Greek Peak; cycling with Finger Lakes Cycling Club and CU Cycling; swimming in Cayuga Lake. Upon leaving CAM, Diarmuid will take up a position as a Scientist with the Oracle Corporation in Boston.

ACKNOWLEDGMENTS

Many people have been involved in opening the doors for me to pursue a PhD in applied mathematics, in helping me to complete it, and in ensuring that I emerged with the modicum sanity I still have. The list of people to whom I am grateful is too long to write out in its entirety, so here a few words about some of the central characters.

Firstly and foremost, Barbara Finlay has been a wonderful mentor and friend as well as providing inspired guidance for this project from its very inception. I recall that Barb once described her approach to advising students as "libertarian". Well, whatever the descriptor, it is expertly and caringly done. Working with her was always fun, edifying and never once a chore. Thank you, Barb, for so many fascinating conversations.

I would like to thank to my Special Committee members Veit Elser, Steven Strogatz and Olaf Sporns – all of whom I expected to have more sense than to be talked into this crazy endeavor in the first place. I am very grateful for their support of this work and their sage advice over the years, which has added enormously to the quality of the outcome. Thanks also go to Steve for being the Center for Applied Mathematics' leader for so many years – he's helped CAM to be a unique program in affording a diverse group of graduate students the latitude to discover how they can best contribute and be happy in the world of research.

Christine Charvet, a postdoctoral student in the Finlay laboratory, skillfully collected anatomical results which are foundational to models presented in this thesis. Her knowledge of developmental neuroanatomy is immense and she has been generous in sharing that. Thank you, Christine, for working with me this past few years.

I have been supported by both Irish and American research funding agencies, which is an indirect way of saying that the tax payers of those two countries have been good to me. I hope that my debt to both those economies will eventually be repaid.

The community at the Center for Applied Mathematics has been a joy to be a part of during my time at Cornell. To all of the senior students who provided a supportive and welcoming environment on my arrival, to the students in my own cohort, who have all come to be among my best friends, and to the students in subsequent years, whom it's great to now see keeping the CAM flag flying high, thank you. I'm also grateful to Dolores, Bridget, Selene, Michelle, Tara, Jessica and the other administrators who have deftly kept the wheels from falling off.

Beyond academics, my time in Ithaca has been made enjoyable by kind friends in numerous circles. First must be the "Irish Mafia", including its honorary non-Irish members: Inish, Deirdre, Eoin, Declan, Srikant (Indian) and Ryan (a New Zealander whose devout royalism jeopardizes his membership). When not meeting at its headquarters in the Chapter House, the Mafia was known to relax at Cayuga Lake, thanks to the fine hospitality of Cheni, Candy and Achilles Filios. To the CAM students who occasionally ventured to The Moonshadow Tavern and The Chanticleer for dancing (you know who you are but I won't name you in print): thank you. I'm also obliged to acknowledge Tim Novikoff because he acknowledged me in his thesis but, much more so, because he's been a loyal friend and confidant.

Further afield, my family and friends back home have been enormously supportive. In particular, I'd like to thank my parents, Teresa and Conor, for their love and encouragement, and for affording Donal, Cian, Colm and I wonderful opportunities.

TABLE OF CONTENTS

INTRODUCTION

Among complex systems the brain stands distinguished by several features but one is often overlooked: it is self-assembling. No planners, engineers or technicians are at hand, just a developmental program which has been honed by evolution. This thesis presents two mathematical models, each built on a foundation of anatomical data, which elucidate how aspects of that developmental program evolved in mammals. The models illustrate how changes to the developmental program, whether in healthy or disrupted development, impact the emergence of the brain's network structure from the growth of billions of individual neurons.

This is a pivotal time in neuroscience as sophisticated imaging techniques are making the field rich with data. The remarkable conjunction of modern axon tract-tracing techniques and methods from complex networks are elucidating the structure of the brain as never before. Bewildering volumes of data on the complex topology of connections formed by axons running between brain regions are being tamed in light of network concepts like hubs, centrality, motifs and small-world connectivity. Even greater volumes of connectional data will soon flow from the Human Connectome Project and possibly from the proposed Brain Activity Map (a.k.a. the BRAIN initiative). Ultimately, our insights into these patterns of connections will be the foundation for a better understanding of cognitive function in humans and other animals.

However, quite apart from the functions these anatomical networks support, their structure is determined in large part by their early development. Comprehending why brain networks are as we find them will require understanding what is possible within their developmental program. Equally, understanding how misalignments in development lead to

malformed brain networks may illuminate the origin of pathologies such as autism and ADHD which implicate brain connectivity. That understanding is currently lacking. Efforts to catalog developmental and adult patterns of gene expression across the brain in multiple species are yielding a burgeoning volume of data. Some of those data buttress existing theories but many demand to be included in more comprehensive quantitative developmental models.

The models presented in this thesis are focused on the cerebral cortex (more specifically, the isocortex), the thin sheet which forms the outer surface of the mammalian forebrain. In larger brains, such as those of primates, the cortex takes on the familiar folded appearance as its area is massively expanded while it maintains a sheet-like form. The expansion of the cortex is the defining feature of mammalian brain evolution; as brains got bigger, the cortex gained neurons at a greater rate than any other brain structure. It is widely held that the expanded cortex underlies the superior cognitive capabilities of primates. The mathematical models presented here explicate aspects of the formation of the cortical network. Specifically, they address two subsequent stages in cortical development: (i) the process of neurogenesis which populates the cortex with neurons and (ii) the formation of the early cortical network as neurons first begin to connect. The work is differentiated by its evolutionary developmental perspective: the models are not only built on a developmental time axis but also on an evolutionary axis, speaking to how developmental programs differ across species.

An evolutionary-developmental perspective guided the choices made in constructing the models. Evidently, the brain architecture of our shrew-like mammalian ancestors had not only evolved to be functional – the developmental programs generating it had also been filtered to be "evolvable", capable of producing an architecture with enough adaptability to meet the demands

of many different body types living in disparate niches. The necessary design principles were in place to successfully scale up the number of constituent neurons by more than five orders of magnitude. That massive expansion notwithstanding, developmental programs exhibit a large degree of conservation across taxa. The basic components of the network are also largely unchanged: neurons make comparable numbers of connections via axonal and dendritic arbors of similar size; also conserved is the structure of cortical columns, the basic functional units within cortical areas. Thus, the models presented here reflect the fact that similar developmental rules and components can achieve practicable network structure in cortices with vastly different sizes. In this sense we can view the neural architecture as an adaptive system, not only in the usual sense of learning, development and environmental response, but also as adaptive with respect to the demands of growing and wiring very differently sized brains.

Features of the mature brain network, such as its hubs and small-world, modular architecture, facilitate the processing and integration of information in an efficient manner. How such felicitous global features emerge from the rules guiding the growth and development of individual neurons is not understood. Considering the sheer number of connections, it becomes plain that at most a tiny fraction of them could be explicitly programmed in the genome. Thus the mature cortical network is largely the result of adaptive self-assembly, re-wiring itself in response to endogenous activity and sensory input. We know that neurons are electrically active and begin to form provisional connections soon after they are born, creating a preliminary network structure. That structure will adapt under the influence of its nodes' spontaneous activity and newly arriving sensory input. This adaptive self-assembly surely sets this network apart. It

suggests that a deep understanding of the resulting structure will require us to pay attention to the details of its growth.

Evolution cannot act directly on network properties, unilaterally adjusting, for example, the efficiency or clustering of the resulting network. Just as a baker can only affect the quality of his product by adjusting the ingredients and cooking time and temperature, evolution must work by adjusting developmental parameters. To help understand how features of the mature cortical network emerge and are affected by developmental parameters, models for the two stages of cortical development outlined above were developed. Some of those features of cortical anatomy, such as the trend of neuronal packing density increasing along the anterior to posterior axis of the cortex, are characterized in Chapter 1, along with a discussion of the developmental origins and computational consequences of that anatomical gradient.

A neuron's location and role within the layers of the cortex is determined by the developmental time at which it is born. Neurons within different cortical layers have distinct connection profiles, some layers being mostly input or output layers, others routing signals locally. Thus we see that the time course of neuron production molds the future structure of the cortical network. Chapter 2 introduces a model for neurogenesis which accounts for how changes in parameters such as the size of the neural stem-cell pool, the cell-cycle duration and cell death rate determine features of the adult cortex, including the gradient in neuronal density discussed in Chapter 1.

Chapter 3 describes a model addressing how the neurons newly produced in neurogenesis establish an early cortical network. Using anatomical data from an axon tracing study in the Finlay laboratory, a spatially embedded network growth model for early connectivity was

developed. The anatomical data revealed an unexpected tendency for axons to grow predominantly along one axis of the cortical sheet in preference to the perpendicular axis. Analyzing the resulting network structure offered the following explanation: the degree of directional preference in the axons' growth lies precisely at a level which reduces the volume required to pack the axons in space while not adversely affecting the efficiency of the resulting network. The spatial model also establishes a framework for future investigations of how the growth of the cortical sheet during development and its expansion across species affect the resulting network structure. Asking how cell-based rules have evolved to connect progressively larger cortices will inform our understanding of the connectome.

As alluded to above, neuroscience now has a plethora of available data. In short supply, however, are interpretive and predictive quantitative models. Not only does modeling add value to projects focused on gathering empirical data (structural and functional imaging studies, gene expression and gene manipulation studies, etc.) but provides testable predictions about the highly complex process of brain development which can guide future empirical work. Apart from illuminating the evolutionary origins of healthy cognitive function, well informed models of brain development hold another promise: that complex pathologies in brain networks which underlie cognitive dysfunctions might be simply explained by changes to parameters in the embryonic brain. The heretofore elusive origins of debilitating conditions such as autistic spectrum disorders could thus become clear.

CHAPTER 1

SYSTEMATIC, BALANCING GRADIENTS IN NEURON DENSITY AND NUMBER ACROSS THE PRIMATE ISOCORTEX[1]

Abstract

The cellular and areal organization of the cerebral cortex impacts how it processes and integrates information. How that organization emerges and how best to characterize it has been debated for over a century. Here we demonstrate and describe in the isocortices of seven primate species a pronounced, anterior-to-posterior gradient in the density of neurons and in the number of neurons under a unit area of the cortical surface. Our findings assert that the cellular architecture of the primate isocortex is neither arranged uniformly nor into discrete patches with an arbitrary spatial arrangement. Rather, it exhibits striking systematic variation. We conjecture that these gradients, which establish the basic landscape that richer areal and cellular structure is built upon, result from developmental patterns of cortical neurogenesis which are conserved across species. Moreover, we propose a functional consequence: that the gradient in neurons per unit of cortical area fosters the integration and dimensional reduction of information along its ascent through sensory areas and towards frontal cortex.

[1] This text was first published in Frontiers in Neuroanatomy under the same title with authors Diarmuid J. Cahalane, Christine J. Charvet and Barbara L. Finlay.

1.1 Introduction

Two hypotheses about the fundamental organization of the cerebral cortex (or, isocortex or neocortex) define the poles of a debate which has endured for close to a century. Crisp borders drawn on the cortical surface to delimit areas with distinct cellular architecture, as first penned by Brodmann and von Economo, seeded the "modularist" paradigm (Brodmann, 1913; Economo and Koskinas, 2008). In this view, each cortical region is described by its unique input and output connectivity, along with intrinsic circuitry corresponding to a particular type of data integration and transformation, the output of which is recombined in subsequent areas (Kaas et al., 2002). Even if sharply defined borders are no longer expected between most areas (Rosa et al., 2005), current functional imaging studies suggest that specific cortical regions can be associated with distinct cognitive tasks, isolating areas for identifying faces (Kanwisher et al., 1997), for judging others' actions (Saxe and Kanwisher, 2003), for linguistic functions (Fedorenko et al., 2011) and so on. Gene expression studies have sought to discover molecular mechanisms which imprint these areas on the developing cortex (Fukuchi-Shimogori and Grove, 2001; Sansom and Livesey, 2009; Yamamori, 2011) in the spirit of the "protomap" hypothesis (Rakic, 1988).

An alternative paradigm, initially "connectionist" (Elman et al., 1998) but which has extended to various second-generation architectures and network analyses, has roots in the mass action hypothesis of Lashley (1931) and echoes the "protocortex" model (O'Leary, 1989). It discounts the role of genetically determined regions and it highlights the uniform nature of the transformation and recombination performed by the cortex on any input. Neuroimaging studies

in support of this view note the distributed and often redundant nature of cortical activation during most operations (O'Toole et al., 2005; Smith et al., 2009; Anderson, 2010). The connectionist paradigm envisions the embryonic cortex as largely undifferentiated; as synaptic connections form and refine under the influence of sensory input and endogenous cortical activity, areal specializations emerge (Johnson and Vecera, 1996).

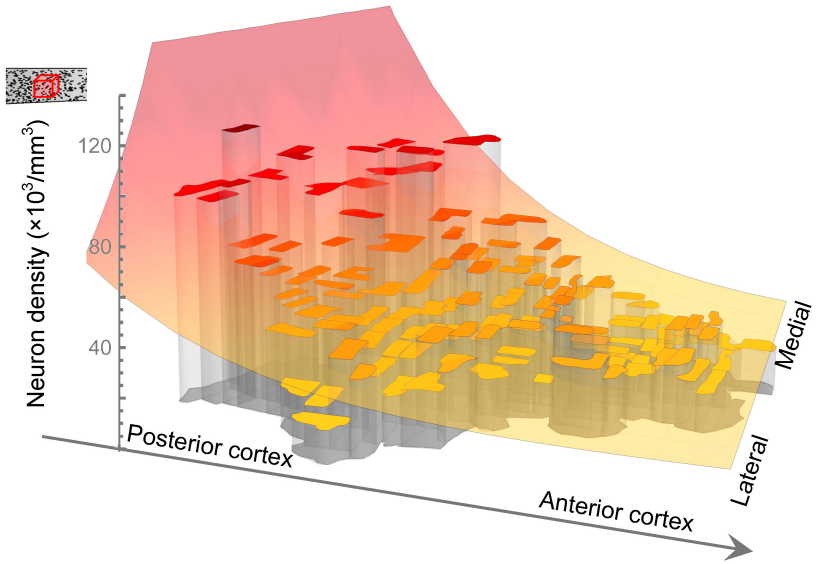

Figure 1.1. Fitting a model to neuron density recorded in each sample in baboon. Collins et al. removed and flattened the entire cortical sheet, cut it into samples and measured the density of neurons and number of neurons in each. The outlines of the samples of Collins et al. are as represented here and the height of each surface indicates the density of neurons measured in the corresponding sample. Also illustrated is the model function, increasing along an axis from anterior-lateral to posterior-medial cortex, which we have fitted to describe the global trend in neuron density.

A third paradigm is now emerging in which systematic variation across the cortical sheet may force the roughly hierarchical integration of information as is seen to occur both within and

across sensory and motor systems (Felleman and Van Essen, 1991; Barone et al., 2000). We will argue that such variation derives from a conserved pattern of neurogenesis. The protomap and protocortex are increasingly recognized as not mutually exclusive and as both being important concepts for understanding the emergence of order in the cortex (Dehay and Kennedy, 2007). The paradigm we present here promises to contribute another key concept to our understanding of cortical development and organization.

The density and number of both neurons and glial cells across the isocortical expanse were analyzed with respect to known cortical areas in a recent study using the isotropic fractionator method (Herculano-Houzel and Lent, 2005) in four primate species (the galago, *Otolemur garnetti*; the owl monkey, *Aotus nancymae;* the macaque, *Macaca mulatta*; and the baboon, *Papio cynocephalus anubis*) (Collins et al., 2010a; Collins, 2011). The authors noted that primary sensory areas in the isocortex had higher neuron numbers than other regions and noted other inter-areal variability along with potential phylogenetic and niche-related variability. However, they did not comment on what appeared to be pronounced anterior-to-posterior (or, more precisely, anterior-lateral to posterior-medial) gradients both in neuron density and in the number of neurons under a unit area of cortical surface (see Figure 1.1). For brevity, we will refer to the latter quantity as "neurons per unit column", but we wish to be clear that our definition is independent of anatomical or functional definitions of a "cortical column". In this report we analyze the data published by Collins et al. to demonstrate and describe those gradients in neuron number and density. Furthermore, we add data collected by microscopy in sectioned material from four additional New World monkey species. Not only do we find analogous

gradients in those species, but the morphological detail and precise location of neurons that we describe in sectioned material also complements the data obtained using the isotropic fractionator method.

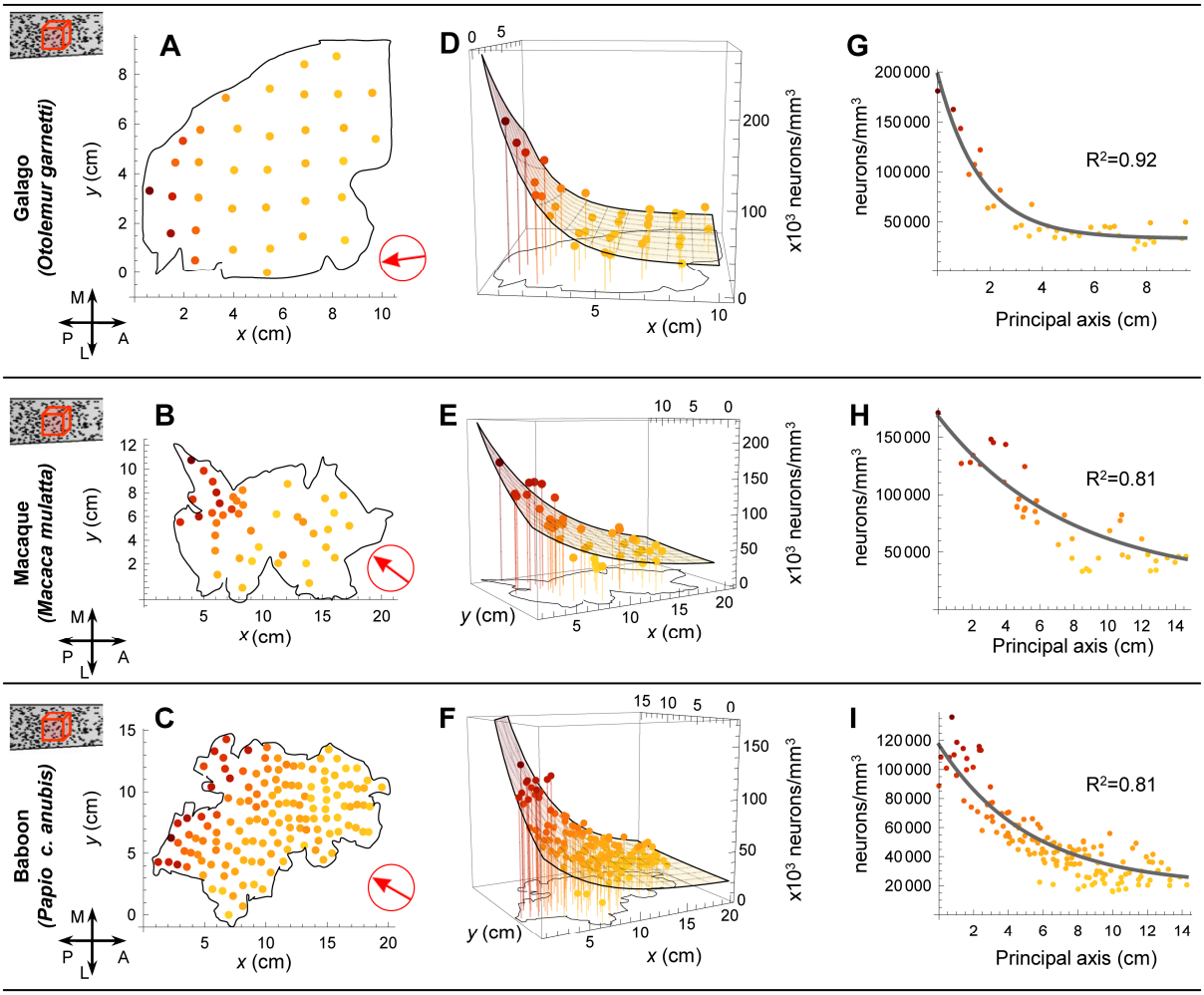

Figure 1.2. Modeling neuron density. In three primate species Collins et al. dissected the cortex into multiple samples and recorded the density of neurons in each dissected piece. In A, B and C we denote the locations of the samples on the flattened cortical sheet. We fitted model surfaces (D, E, F) which allowed us to project the data onto a principal axis of variation (G, H, I). In A, B

and C the red arrow indicates the alignment of the principal axis. A: anterior; P: posterior; M: medial; L: lateral.

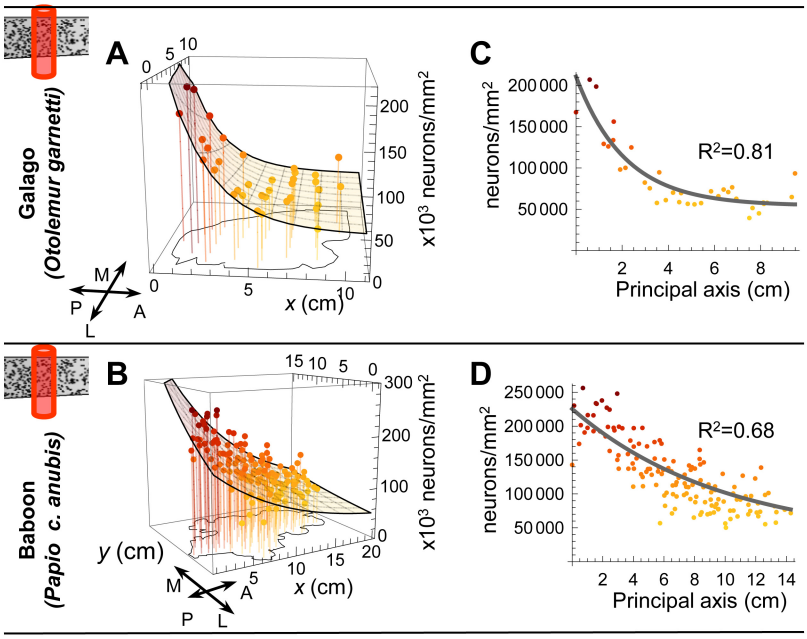

Figure 1.3. Neurons per unit column. (A and B) Model surfaces fitted to the to the number of neurons under a square millimeter of cortical surface in each of the samples tested by Collins et al. (C and D) As for the neuron density measurements (see text), we found that the data were well represented by projecting onto a single "principal axis". A: anterior; P: posterior; M: medial; L: lateral.

1.2 Results

The data collected by Collins et al. (Collins et al., 2010a) are plotted in Figure 1.2 (neuron density in galago, macaque and baboon) and Figure 1.3 (number of neurons per unit column in

galago and baboon). To collect these data for the galago and baboon the isocortical sheet was removed, flattened and cut orthogonal to the cortical surface into multiple samples having an approximately equal (top) surface area. The macaque cortex was processed similarly, but in this case the samples were cut along the borders of cortical areas, identified by reference to a map of known areas, before the cortex was flattened. Samples were processed using the isotropic fractionator to determine the number of neurons in each. The method is discussed in detail elsewhere (Collins et al., 2010b) but, briefly, entails homogenizing the samples, creating an isotropic suspension of dissociated nuclei, staining the dissociated nuclei and then counting them either under a microscope or with a flow cytometer. The samples' locations, weights, and (top) surface areas, as well as the number of neurons in each (for the galago and baboon only) were reported.

To characterize the reported variation in the density of neurons and in the number of neurons per unit column across the cortical sheet, we fitted model surfaces (see Methods). Much of the variation in each dataset occurs as a super-linear trend along a single direction, which we will term the "principal axis" (see Figure 1.2 and Figure 1.3). To model that variation, we chose functions from a family whose members' level sets are straight lines orthogonal to that principal axis – loosely speaking, the resulting surfaces are ramps, rising along the direction of the principal axis with increasing slope (see Figure 1.1). We used the same functional form to model neuron density in the galago, macaque and baboon (Figure 1.2D, E and F) and the number of neurons per unit column in the galago and baboon (Figure 1.3C and D). Typically, the principal axis was found to point in an anterior-lateral to posterior-medial direction on the cortical sheet.

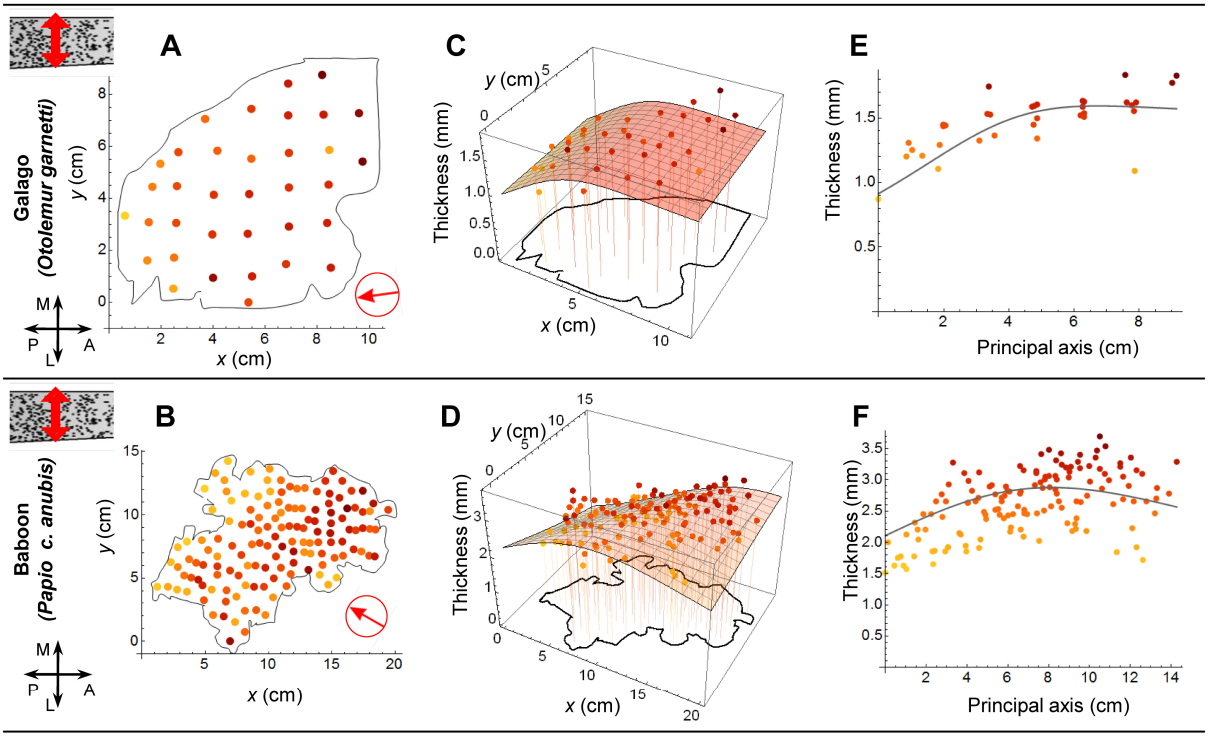

Figure 1.4. Cortical Thickness. Sample average thickness of cortex as calculated by dividing the number of neurons per column by the density of neurons for each sample in the study by Collins et al. Cortical thickness is seen to, on average, be reduced in posterior regions. The surfaces (in C and D) and the curves (in E and F) were calculated by dividing our respective model functions for neurons per column by those for neuron density. The arrows in A and B indicate the orientation of the principal axes.

For the galago and baboon, where both neuron density and number of neurons per unit column were available, the axes of variation of both those quantities were found to align to within a fraction of a degree (see Methods). Assuming a constant specific gravity of cortical tissue (Stephan et al., 1981), the collinear trends in the density and number of neurons in a unit column have consequences for cortical thickness along that same axis (Figure 1.4). Posterior cortex, despite having more neurons per unit column, is nevertheless thinner, on average, as a

result of increased neuron density (see Figure 1.5 for a schematic summary). Thus our analysis of the isotropic fractionator data reveals unambiguous trends capturing a large fraction of the variance in the neuron density and number of neurons per unit column in the isocortex. Consistent with MRI (Fischl, 2000) and stereological (Pakkenberg and Gundersen, 1997) studies of human cortical thickness, we find that average cortical thickness varies over a much lesser range (by approximately two-fold) than do the underlying density and number of neurons (approximately five-fold) – a fact which may explain why such striking gradients spanning the cortex have gone unnoted.

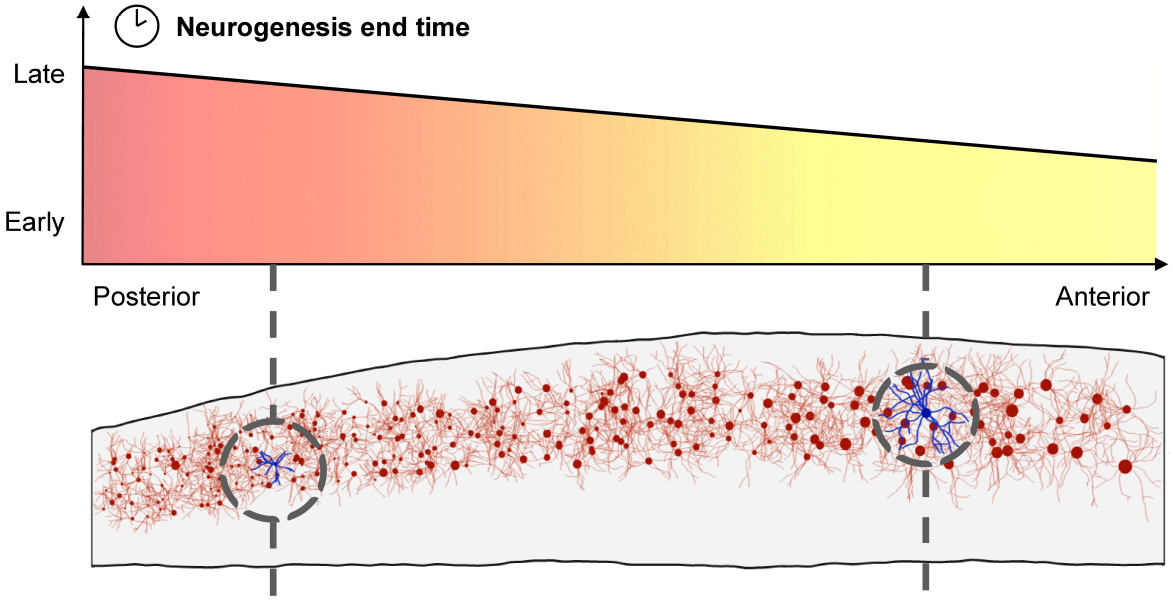

Posterior Cortex (Layer II/III)		Anterior Cortex (Layer II/III)
• neurogenesis ends later		• neurogenesis ends earlier
• more neurons per unit column		• fewer neurons per unit column
• higher neuron density		• lower neuron density
• smaller soma ⇒ shorter processes		• larger soma ⇒ longer processes

Figure 1.5. Schematic depiction of the neurogenesis timing gradient and balanced gradients in neuron density and number per unit column. In posterior regions neurogenesis continues for longer, resulting in a higher total number of neurons in each unit column. Higher neuronal density in those regions means that the increased number of neurons does not result in greater cortical thickness. We also found that the average size of a neuron's cell body in cortical layers II and III increases towards anterior regions. Larger neuron cell bodies are associated with longer axonal and/or dendritic processes.

Are such gradients in neuron density and neurons per unit column common to the cortices of all primates or perhaps to a still larger phylogenetic group? To assess the generality of these features, we estimated neuron density in the isocortices of four New World monkeys (a golden-handed tamarin, *Saguinus midas*; a northern owl monkey, *Aotus azarae*; a black howler monkey, *Alouatta caraya*; and a tufted capuchin, *Cebus apella)*. Using light microscopy we examined serial sections along the anterior-posterior axis (see Methods). In all four species, neuron density increased in progressively more caudal regions (Figure 1.6A-D). Taken together, the results from seven primate species suggest that these systematic cortical variations in neuron density are general to the primate order.

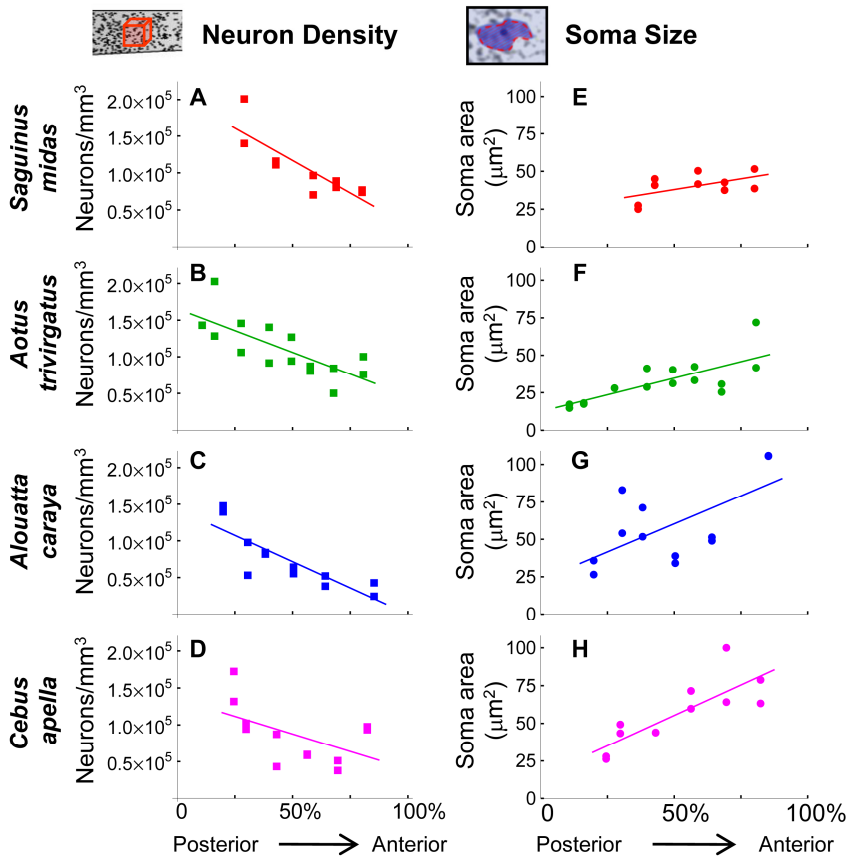

Figure 1.6. (A-D) Stereological measurements of neuron density in four species of New World monkeys. Neuron density decreases toward the anterior. Linear regression confirms the high significance ($p<0.002$, one-tailed t-test) of the trend in A, B and C. For D, *Cebus apella,* ($p=0.08$). (E-F) Neuron soma size in cortical layers II and III. Soma size increases toward the anterior isocortex (in E, $p=0.09$; F, $p=0.0008$; G, $p=0.03$, H, $p=0.001$ using a one-tailed t-test).

We sought to better understand what variations in neural architecture underlie the observed differences in neuron density. The differences in density across cortical locations could be due to one or both of two factors. Firstly, the dosage of densely packed granule cells, particularly in isocortical layer IV, is known to vary across the cortex. Secondly, a varying amount of connectivity of pyramidal neurons, with their axonal and dendritic processes

occupying relatively more space as connectivity increases, could contribute to reduced neuron density. Here we present evidence of such increased connectivity. Since isocortical layers II and III together are both an important source and target of intracortical axonal projections, and because the volume and extent of a neuron's processes can be a factor in determining the volume of its soma (e.g. Elston et al. (2009)), we measured the soma sizes of neurons found in layers II and III. In the four New World monkeys we examined sites distributed along the posterior-to-anterior axis selected in the same manner as those for the stereological measurements of neuron density reported above (see Methods). Figure 1.6 (E to H) shows that neuronal soma size in isocortical layers II and III increases as neuron density decreases from the posterior to anterior in these cortices. In three of the four species examined, the global trend in soma size reaches significance ($p<0.05$, one sided t-test), but outliers are present in all cases. The noisy nature of the trend hints that local effects are also influencing soma size, e.g. axon length, cortical area and the effects experience (pruning or enlarging arbors) are all known to affect soma size. However, the global trends are consistent with the hypothesis that decreased neuron density in anterior regions is due, at least in part, to the greater amount of neuropil produced by increased intracortical connectivity.

To characterize the cortical architecture as varying systematically seems at odds with the notion that areas assume their properties idiosyncratically, prompted by genetic markers, projections from subcortical structures (Finlay and Pallas, 1989) or other locally present cues. For example, Collins et al. noted that areas involved in sensory processing had higher neuron densities than some adjacent areas (Collins et al., 2010a). Identifying the data points which related to primary sensory areas in the baboon, we noted that neuron densities at such sites

typically lay above the model surface we had fitted (Figure 1.7). We used a two-factor model, incorporating each sample's location and whether or not it was from a primary sensory area, to show that primary areas have a density of neurons which is 1.26 times higher than that predicted for a non-primary area in the same cortical location (an F-test confirms that the two-factor model is the better descriptor of the data; F=28.3, $p<10^{-6}$, $d.f.$=(1,135), see Methods). Lower levels of neuron death during early development have been reported in putative sensory areas (Finlay and Slattery, 1983) relative to other areas and we suggest that this may contribute to the greater number of neurons per unit column in these regions. We offer this as an example of how local deviations are overlaid on the basic landscape set up by the global gradient in neuron number. We posit that the gradient itself is established by an isocortex-wide developmental pattern and acts in combination with more local mechanisms to develop the cortex's richer structure.

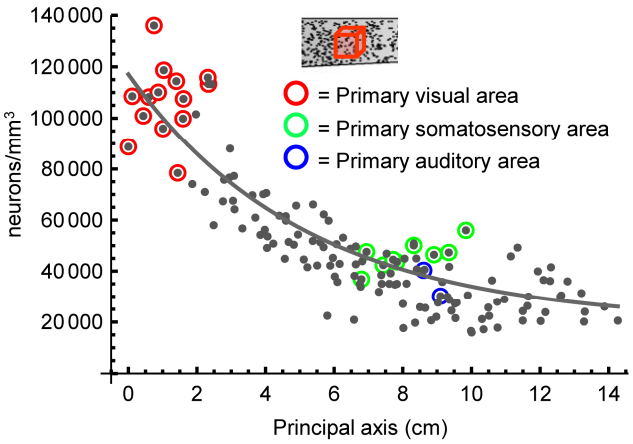

Figure 1.7. Highlighting primary sensory areas in baboon. Fitting all data points with a one-factor model (as described in the text) yielded the black curve. A two-factor model (not illustrated, see text) suggests primary sensory areas (those highlighted here) have an expected density 1.26 times greater than would a non-primary area in the same location.

1.3 Discussion

The global gradients in neuron density and number per unit column that we have described are matched with a prominent gradient of cortical neurogenesis that is conserved across species (see Figure 1.5 for a schematic summary). In every mammalian isocortex that has been studied, the non-cingulate isocortex is populated with neurons in an anterior-to-posterior progression, the progression being more pronounced in larger brains (Bayer and Altman, 1991; Kornack and Rakic, 1998; Miyama et al., 1997; Smart et al., 2002; Jackson et al., 1989; Luskin and Shatz, 1985; Rakic, 2002). For primates particularly, despite beginning at approximately the same time in all regions, neurogenesis generally ends earlier in frontal cortical regions than in posterior cortex (by as much as 3 weeks for some frontal regions in macaque, but with exceptions such as area 46) (Rakic, 1974, 2002). A neurogenetic interval of progressively longer duration in progressively more posterior regions, allowing a greater number of cell division cycles, would account for the greater number of neurons per unit column in those regions (Kornack and Rakic, 1998). Previously, it was suggested that in primates elevated levels of neurogenesis were specific to primary visual areas (Dehay and Kennedy, 2007). However, the location of the visual cortex, typically at the highest point on the density gradient, and the known reduction of cell death in primary sensory regions (Finlay and Slattery, 1983) may be sufficient to explain its high density of neurons. As to the lower density of neurons in anterior cortex, we offer the related developmental possibility that the earlier completion of neurogenesis in these regions may afford its neurons a head start and a lengthier interval to elaborate neuronal processes – it is known that isocortical neurons begin to establish their arbors from the earliest stages of cortical development

(Goldman-Rakic, 1987). That hypothesis is compatible with our finding of increased neuron soma size in cortical layers II and III, with studies showing enlarged pyramidal dendritic arbors in pre-frontal cortex (Elston et al., 2009), and with the approximately constant number of synapses per unit volume across adult visual, auditory and pre-frontal cortex (Huttenlocher and Dabholkar, 1997). Process development should be distinguished from synaptogenesis however, as synapse formation appears to occur approximately simultaneously across the primate cortical sheet (Rakic et al., 1986).

Apart from aligning with a developmental axis, we point out that the cortical variations we have highlighted are also aligned with important functional and processing axes. The gradients have consequences for the makeup neural circuitry, implying a rostral-to-caudal shift in the ratio of space apportioned to neurons' cell bodies versus their connective processes. So, it is of interest that higher stages of information processing and integration in the cortex occur at progressively more anterior locations. Higher visual areas and association areas integrating visual information are located anterior to the primary visual areas (Van Essen et al., 1992). The motor areas, which integrate somatosensory information in motor control, are located anterior to the primary areas receiving somatosensory input. However, such an alignment in the auditory processing areas is not so clearly evident (Kaas and Hackett, 2004). We note that the auditory areas differ from the other sensory areas in lacking a spatial topography and in occupying a much smaller proportion of the primate cortical surface. That small spatial extent means the global gradient in neuron number would imply little change in cellular architecture across these areas in any case. Network analysis of structural connectivity in the cortex also suggests an anterior-to-posterior gradient whereby frontal regions have more integrative roles, evidenced by the

preponderance of network hubs being located in those regions (Modha and Singh, 2010). We conclude that the architectural gradients we have identified foster successively higher and more integrative stages of neural processing: as information is represented in successively higher (i.e. progressively anterior) areas, their reduced areal extents and lower numbers of neurons per unit column imply the dimensional reduction or other compression of that information. Considering the opposing direction, the gradients discussed here also align with established and hypothesized contra-flows of neural information issuing from frontal regions. It has been shown that progressively anterior regions of prefrontal cortex execute "progressively abstract, higher control" of behavior (Badre, 2008). The control of attention has been shown to propagate backward through visual areas (Buffalo et al., 2010). Merker has hypothesized that a "countercurrent" from frontal regions provides more caudal regions a context to associate with sensory information (Merker, 2004). The so-called Bayesian brain hypothesis also posits an anterior to posterior flow of context-relevant predictions about future input, priming relevant representations and ultimately acting on lower sensory areas to guide perception (Bar, 2007).

We wish to be clear that the cortex-wide gradient in cellular architecture we describe here does not preclude the presence of abrupt anatomical borders between cortical areas. Neither the data of Collins et al. nor the histology we report has a sampled the cortical surface at sufficient density to resolve, for example, the border between visual areas 17 and 18, which is readily visible in stained sectioned material from primates even at low magnification. Our hypothesis is that cellular architecture changes in an ordered progression at the isocortex-wide scale. Examining the cortex with suitable methods at a higher resolution would refine local features such as areal borders. Perhaps a useful analogy is that of a staircase: to discuss to the overall

slope or pitch of the staircase, a global measure, is not to deny the presence of discrete steps. Evidence for the modular, hierarchical genetic organization of the cortex at the intermediate scale of lobes and regions has been found by analysis of the cortical surface in twins (Chen et al., 2012).

The isotropic fractionator, being a high throughput method, is ideal for comparative studies examining large numbers of cortical loci. For example, the large number of samples examined by Collins et al. (N=141 in baboon) and the uniformity of their distribution in the cortical sheet stand in contrast to the sampling of just six sites (V1, S1, M1 and Brodmann areas 7, 9, and 22) in an oft-cited report of the "basic uniformity" of cortical structure by Rockel et al. (1980). That report concluded the number of neurons per unit column is the same in all of non-visual cortex and constant across five species (mouse, rat, cat, macaque and human). Rockel did find that the number of neurons in primary visual cortex in primates was elevated by a factor of 2.5 over that in other cortical areas, and the data of Collins et al. support a comparable contrast between primary visual areas and some neighboring areas, but there the similarities end. Under-sampling of the cortex by Rockel et al. may have contributed to their finding of constant neuron number, with just one of the six sites examined being in frontal cortex. Numerous previous studies have contradicted the conclusions of Rockel et al. regarding both within cortex variation and cross-species variation, e.g. Pakkenberg and Gundersen (1997), Beaulieu and Colonnier (1989), Cheung et al. (2007), Cheung et al. (2010) and several others discussed in Collins et al. (2010a), but the definitive contribution of Collins et al. surely provides closure on this matter.

Despite the value of the isotropic fractionator as a comparative tool, it does have limitations. Firstly, it is unclear whether every neuronal nucleus present in the tissue samples

survives the dissociation step, is successfully stained and then detected at the counting step. However, any under-counting of nuclei would result in the same fractional error in the estimated neuronal density of each sample. Thus, while the absolute number of neurons might be under-estimated, comparing estimates across samples is still useful. Secondly, the isotropic fractionator cannot tell apart different neuronal cell types, examine their morphology, nor identify the layers those neurons had occupied in the intact cortex. For that reason, traditional histology in sectioned material can usefully compliment results from fractionator studies by providing additional information at a subset of the cortical sites examined. For example, in sectioned material in the present study we identified those neurons in cortical layers II and III and estimated their soma size by tracing cell body outlines at high (60×) magnification. In future work, such methods will allow us to investigate in detail how each layer contributes to the gradient in neuron number and how neuron density varies within layers.

In summary, we emphasize the empirical finding that two gradients - an increase in the density of neurons and an increase in the number of neurons per unit column - align on an axis from the frontal to occipital poles of the mature primate cortex. The gradients are balanced in the sense that their net effect is to produce a cortex whose thickness changes, by comparison, to a much lesser extent. Variation in the cellular architecture across cortical regions surely also implies a corresponding variation in the types of neural processing tasks that regions are most apt to support. Understanding the interaction of the global variations we have described with local features, such as the presence of genetic markers or subcortical sensory projections, will be central to understanding how cortical areas assume and execute their respective roles in neural processing. To conclude, we propose that the modularist's vision of the embryonic isocortex as a

patchwork and the connectionist's view of it as a blank computational canvas would be better replaced by the metaphor of a staircase, with position along the staircase having significance for the nature of the computation carried out there. The connectionist must acknowledge that not all steps are equal and the modularist must acknowledge their global trend. The entwined challenges of understanding the evolution, development, anatomy, function and pathologies of the isocortex will surely demand such integrative perspectives.

1.4 Materials and Methods

1.4.1 Species. This report includes analysis of previously published data (Collins et al., 2010a; Collins, 2011) relating to a baboon (*Papio cynocephalus anubis*), a rhesus macaque (*Macaca mulatta*) and a prosimian galago (*Otolemur garnetti*) collected using the isotropic fractionator method. We collected original data in sectioned tissue from four species of New World monkeys: one golden-handed tamarin (*Saguinus midas*), one northern owl monkey (*Aotus trivirgatus*), one black howler monkey (*Alouatta caraya*), and one tufted capuchin (*Cebus apella*). These samples came from previous studies conducted in this laboratory (Kaskan et al., 2005; Chalfin et al., 2007). The animals had been bred or housed in the Centro Nacional de Primatas in Pará, Brazil. The sex, brain weight and specimen ID of these animals are listed Table 1.

1.4.2. Ethics Statement. The original data in this report was collected from animals housed and treated in compliance with the principles defined in the National Institutes of Health Guide for the Care and Use of Laboratory Animals, as certified by Cornell University's Institutional Animal Care and Use Committee as part of a larger study.

1.4.3. Sample Preparation. For *Saguinus midas*, *Aotus trivirgatus, Alouatta caraya* and *Cebus Apella*, the animals were adapted to dark conditions for 30 minutes while a light anesthetic was administered by intramuscular injection (a 1:4 mixture of 2% xylazine hydrochloride and 5% ketamine hydrochloride). The same preparation was then used to deeply anesthetize the animals. They were perfused with a phosphate-buffered saline solution (PBS) with a pH of 7.2 prior to perfusion with 4% paraformaldehyde. The brains were removed and weighed. One to two weeks later, the brains were stored in a 2% paraformaldehyde solution. Prior to sectioning, the brains were placed in a 30% sucrose/PBS 0.1M preparation having a pH of 7.2. Coronal sections were made at 60μm using a freezing microtome. Every fifth or seventh section was kept, mounted on a gelatinized slide and stained with cresyl violet.

1.4.4. Estimating neuron density and neuron soma size. Sections were examined using a Leitz Diaplan micropscope and a Neurolucida imaging system with a mechanical stage (Mircrobrightfield Inc., Colchester, VT). Coronal sections were selected, approximately equally spaced along the rostral-caudal axis, excluding the most caudal and rostral sections (Figure 1.6). The number of sections chosen for each species is given in Table 1. We did not correct for shrinkage of the sectioned material – the within-cortex comparisons we present are unaffected by

this. Cells with small and condensed somas were not included so as to exclude glial cells from the analysis.

1.4.4a Site selection. In each section, we randomly selected two regions in the right or left (see Table 1) isocortical hemisphere within which to estimate neuron size and density. Within the randomly selected regions, we overlaid a grid on the magnified image to randomly select a column of cortex. At the selected location, the axes of a grid were aligned to be (respectively) tangential and normal to the cortical surface at that location. For the purpose of this description, we refer to the axis normal to the surface at each sampling site as a "sampling axis".

1.4.4b Neuron density estimates. We placed counting boxes measuring 41 μm × 41 μm at 50-200 μm intervals along each selected sampling axis, beginning at layer I and until the boundary between layer VI and the white matter was reached (see Figure 1.8). We used the optical disector method (Williams et al., 2003) to estimate the number of neurons contained in each box's volume. The 60 μm sections were thick enough to employ a three-dimensional, 5 μm thick, guard zone, whereby neurons that lay on the three exclusion planes (*x*, *y* and *z* planes) were not counted. Details of how many counting boxes were used to calculate density along each sampling axis are given in Table 2.

1.4.4c Neuron soma size estimates. We estimated neuron size in isocortical layers II/III. Beginning at the layer I/layer II interface and ending at the layer III/layer IV interface, we placed counting boxes measuring 41 μm × 41 μm at intervals of 100 μm along the sampling axis.

Within each box, once the focal plane was fixed we identified those neurons whose nuclei were clearly visible. This ensured only neurons were counted. Moreover, it ensured that our estimates of soma area were consistently made, using a cross-section of the neuron that contained the nucleus rather than an arbitrary cross-section. For the range and mean of the number of neurons selected per sampling axis see Table 3.

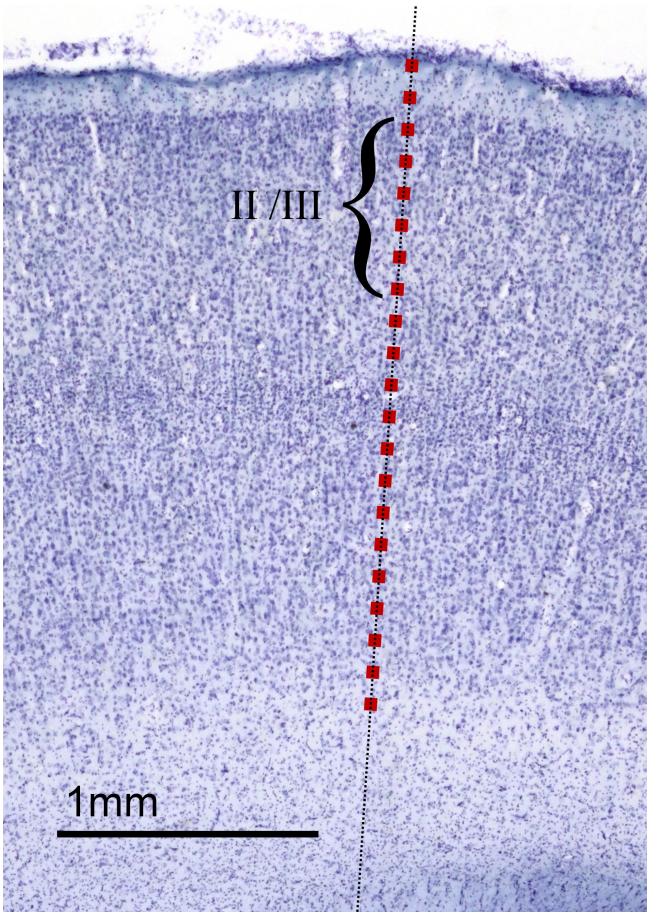

Figure 1.8. Counting boxes for neuron density and neuron soma size estimates. As outlined in the Methods section, and as illustrated here in a section from *Aotus trivirgatus* temporal isocortex, sampling axes (dashed line) were placed normal to the cortex's outer surface at chosen sites in cortical sections. Along each sampling axis, counting boxes measuring 41 µm × 41 µm (red squares, drawn to scale) were placed, typically at 100 µm intervals, from the surface to the

white matter. Neuron density estimates were made within each counting box. In those counting boxes that lay in cortical layers II and III (indicated by the bracket), estimates of neuron soma size were also made.

1.4.5. Mathematical and statistical methods.

1.4.5a. Modeling neuron density and number per unit column. In samples cut from the flattened cortical sheet, Collins et al. recorded neuron density and the total number of neurons along with the top surface area and a tracing of each sample's outline on the cortex prior to sectioning. We assigned Cartesian coordinates *(x, y)* to denote, in the two-dimensional plane of the flattened cortical sheet, approximately the centroid of each sample. For both the neuron density and neurons per unit column measurements, we noted in species that (a) there was a super-linear trend in the data and (b) most of the variation in the data was in a roughly anterior-lateral to posterior-medial direction. For these reasons, we chose to fit the following surface (with fitting parameters *a, b, c,* and *d*) to quantify the trend and to identify the principal axis of variation: $f(x,y) = a + \exp[b + c(dx + (\sqrt{1-d^2})y)]$. This function grows as an exponential along one direction and is level along all lines parallel to the orthogonal direction. The direction of the principal axis of variation is given by the fitted parameter *d* via $\theta = \arccos(d)$. In each case, we fitted the surface to the data by minimizing the sum of the squared errors using the "FindFit" function in Mathematica (Version 7, Wolfram Research, Champaign, IL.). The fitted values of the parameters, as well as the coefficient of determination R^2 for each case, are as in Table 4. The results of projecting the data on to the principal axes are shown in Figure 1.2, parts g, h and i, for neuron density and in Figure 1.3, parts c and d, for neurons per unit column. This provides visual

confirmation that one axis captures much of the variance. To validate that observation, in each case we projected the model's residuals onto the orthogonal axis and carried out a linear regression to test for trends in the data. In no case was there a significant trend along the orthogonal axis (p>0.15 and R^2<0.07 in all cases).

1.4.5b Two-factor model for neuron density. In the baboon neuron density dataset, we tagged each data point with a binary descriptor of whether or not it belongs to a primary sensory area (V1, S1 or A1). Collins et al. had identified the samples from such areas by viewing the flattened cortex on a light box, whereby myelin-dense sensory areas are opaque relative to the surrounding areas. Samples for which more than half of their surface area lay within a primary sensory area were tagged as belonging to that primary sensory area. We let q_i denote the density of neurons as measured in the i^{th} sample and let (x_i,y_i) be the sample's location. We let s_i equal 1 if the i^{th} sample belongs to a primary sensory area and let it equal 0 otherwise. We obtained our fit by adjusting the parameters *a, b, c, d* and *e,* to minimize the quantity $\sum_i \left[(1-e\times s_i)q_i - f(x_i,y_i)\right]^2$ with $f(x,y) = a + \exp[b + c(dx + (\sqrt{1-d^2})y)]$, as in the location-only model described above. This minimization amounts to carrying out a least squares fit of the location-only model with the added parameter *e* now discounting the densities of primary sensory areas. Loosely speaking, the discount term *e* quantifies by what fraction the density of primary sensory areas would need to be reduced to fall "in line" with their non-primary sensory neighbors. The result of fitting the two-factor model (using the "NMinimize" function in Mathematica) is shown in Table 5. The coefficient of determination, R^2=0.84, is seen to be higher than in the location-only model

(R^2=0.81). We note that the location-only model is nested within the extended model (to see this, take $e = 0$), and so an F-test can be used to confirm the high significance of the improvement in the value of R^2 (F=28.3, p<10^{-6}, $d.f.$=(1,135)). The value of e=0.206 yielded by the fitting procedure can be interpreted as primary sensory area having a density which is 1/(1-e)≈1.26 times greater than would be predicted in this model for a non-primary sensory area at the same location.

Acknowledgements

This work was supported by National Science Foundation/Conselho Nacional de Desenvolvimento Cientifico e Tecnologico grant 910149/96-99 to Luiz Carlos de Lima Silveira and B.L.F., NSF grant number IBN-0138113 to B.L.F., an Eunice Kennedy Shriver National Institute of Child Health and Human Development fellowship No. F32HD067011 to C.J.C., and support from the G. Harold and Leila Y. Mathers Foundation to C.E.C. and Jon H. Kaas. D.J.C. was supported by a National University of Ireland Traveling Studentship and NSF grant CCF-0835706 to Steven Strogatz. The content is solely the responsibility of the authors and does not necessarily represent the official views of any supporting agency.

We thank Christine Collins for helpful discussions and for comments on this manuscript, Nicole Young for collecting quantitative data for the baboon cortex, Richard Darlington for statistical consultation, Luiz Carlos de Lima Silveira for sponsorship of the New World Monkey study in which the sectioned material was collected, Peter Kaskan for brain histology, Veit Elser for helpful discussions. We thank three anonymous reviewers for their comments and helpful suggestions.

Appendix 1A

SUPPLEMENTARY INFORMATION FOR

CHAPTER 1: SYSTEMATIC, BALANCING GRADIENTS IN NEURON DENSITY AND NUMBER ACROSS THE PRIMATE ISOCORTEX

Species	*Saguinus midas*	*Aotus trivirgatus*	*Alouatta caraya*	*Cebus apella*
Specimen ID	SM 970108B	AT 980115A	AC 970111A	CA 970913
Sex	F	F	M	M
Brain weight (g)	9.09	14	54.3	62
Hemisphere examined	Right	Left	Left	Right
Magnification	60×	60×/40×	40×	60×
Section thickness (µm)	60	60	60	60
Section thickness, shrunken (µm)	28	25	28	28.1
Number of sections examined	5	8	7	6
Guard zone (µm)	5	5	5	5

Table 1A.1. Species data for New World monkeys specimens used in stereological measurement of neuron density and layer II and III soma size.

Species	*Saguinus midas*	*Aotus trivirgatus*	*Alouatta caraya*	*Cebus apella*
Mean number of locations sampled per column	17.4	16.1	18.8	20.1
Min. number of locations sampled per column	6	8	10	8
Max. number of locations sampled per column	27	27	32	45

Table 1A.2. Numbers of sites along a sampling axis at which counts were made to determine neuron density.

Species	*Saguinus midas*	*Aotus trivirgatus*	*Alouatta caraya*	*Cebus apella*
Mean number of neurons selected per column	13.8	15.1	9.8	14.6
Min. number of neurons selected per column	6	9	6	8
Max. number of neurons selected per column	19	25	13	26

Table 1A.3. Numbers of layer II and III neurons measured along a sampling axis to estimate soma size.

Species	Measurement	N	a	b	c	d	θ	R^2
Otolemur g.	Neurons per column	35	5.41×10^4	12.5	-0.476	0.989	8.6˚	0.81
	Neuron density	35	3.33×10^4	12.7	-0.613	0.989	8.4˚	0.92
Papio c. a.	Neurons per column	141	3.16×10^4	12.0	0.118	-0.858	-30.9˚	0.68
	Neuron density	141	1.98×10^4	11.1	0.225	-0.854	-31.3˚	0.81
Macaca m.	Neuron density	41	2.21×10^4	11.6	0.155	-0.839	-32.9˚	0.81

Table 1A.4. Parameters for curve-fitting of neuron density and neurons per unit column. N is the number of points in each data set. R^2 is the coefficient of determination for each fit.

Species	Measurement	N_p	N_{np}	a	b	c	d	e	θ	R^2
Papio c. a.	Neuron density	25	116	1.19×10^4	11.0	0.158	-0.846	0.206	-32.2˚	0.84

Table 1A.5. Parameters for fitting our two-factor model for baboon neuron density. In this model we discount the recorded density at primary sensory areas by a factor of (1-e). N_p is the number of data points from primary sensory areas and N_{np} is the number of data points from non-primary areas. R^2 is the coefficient of determination.

CHAPTER 2

A COMPUTATIONAL, EVOLUTIONARY-DEVELOPMENTAL MODEL LINKING CROSS-SPECIES AND INTRA-CORTEX VARIATION IN ISOCORTICAL NEURON NUMBER IN MAMMALS

Abstract

A massive increase in the number of isocortical neurons, driving the size of the isocortex to increase by 5 orders of magnitude, is a key feature of mammalian evolution. Not only are there systematic variations in the isocortical architecture across species, but also across spatial axes within a given isocortex. In this report we present a computational model that accounts for both types of variation as arising from the same developmental mechanism. The Ordinary Differential Equation model presented demonstrates that changes to the kinetics of neurogenesis (specifically to the cell cycle rate, the cell death rate and the "quit rate", i.e. the fraction of cell divisions which are terminal) are sufficient to explain the great diversity in the number of cortical neurons across mammals. Moreover, spatio-temporal gradients in those same parameters in the embryonic cortex, such as have been recorded in several species, can account for cortex-wide, graded variations in the mature neural architecture. Consistent with emerging anatomical data in several species, the model predicts (i) a greater complement of neurons per cortical column in the later-developing, posterior regions of intermediate and large cortices, (ii) that the extent of variation across a cortex increases with cortex size, reaching five-fold or greater in primates, and (iii) that when the number of neurons per cortical column increases, whether across species or

within a given cortex, it is the later-developing superficial layers of the cortex which accommodate those additional neurons. We posit that these graded features of the cortex have a functional (computational) significance and so must be subject to evolutionary selection.

2.1 Introduction

By considering the patterns of brain variation from present day sharks and rays to today's mammals including primates, we can infer the trajectory of brain evolution over a period of approximately 450 million years in the vertebrate lineage. Changes in brain structure follow a remarkably stable pattern: it is always the same brain parts that have become enlarged when overall brain size increases (Yopak et al., 2010). In particular, the cortex (or its forebrain homologue) is preferentially enlarged whenever brains become large. Moreover, in studies of individual variation in humans, minks, pigs, and mice, when overall brain size is larger, those same divisions as would be predicted by looking at brain enlargement across taxa are found to be preferentially enlarged (Finlay et al., 2011; Charvet et al., 2013). That is despite the range of variation between individuals being orders of magnitude less than that across taxa. Such regularities in brain scaling suggest that the developmental mechanisms which generate central nervous systems are strongly conserved across species (Finlay and Darlington, 1995).

To tease apart the features of the isocortex contributed by the scaling of conserved developmental mechanisms from those features which might be specially selected for in a given niche or species, we have created a formal, quantitative model of cortical neurogenesis. The

model elucidates how the dials and levers made available by conserved developmental mechanisms allow selection to shape the basic landscape of the embryonic cortex. The extent to which any particular cortical area (e.g. a visual or language area) has been a special subject of selection can then be better evaluated given the baselines provided by this evolutionary developmental or "evo-devo" model.

For decades, the developmental mechanisms which generate the mammalian cerebral cortex have been the subject of extensive investigations and competing theories, e.g. "protomap" (Rakic, 1988) versus "protocortex" (O'Leary, 1989). More recently, investigators have cataloged developmental and adult gene expression across the cortex in multiple species. Some of that data sits well with existing theories but more comprehensive mechanistic models are needed to interpret much of it (Kang et al., 2011; Hawrylycz et al., 2012). What has become clear is that rather than there being a singular, definitive mechanism to coordinate the structure and layout of the cortex, many mechanisms and sources contribute order throughout development (Dehay and Kennedy, 2007; Sansom and Livesey, 2009; Yamamori, 2011). Early polarization and regionalization of the cortex is directed by morphogens issuing from signaling centers in the cortical primordium (Fukuchi-Shimogori and Grove, 2001a). Spatial gradients in the kinetics of neurogenesis change the extent and timing of neuronal production from location to location (Rakic, 1974b, 2002a; Bayer and Altman, 1991). Molecular signals guide axons of the various sensory modalities to enter the growing cortex at particular locations (Finlay and Pallas, 1989). The axons of those projections are kept in topological register and that orders the various topographic maps in the cortex. The structure of correlations in sensory information flowing through those same projections further refines the adult cortical architecture (Johnson and

Vecera, 1996). As we unravel how this complex ontogeny is orchestrated by the genome, formal models for developmental mechanisms will be pivotal in synthesizing data on developmental gene expression patterns (Lewis, 2008).

The mechanics of mammalian cortical neurogenesis are patently adaptable: changes in duration and kinetics result in the production of five orders of magnitude more neurons in the largest cortices compared to the smallest. What developmental parameters must change to accommodate the much greater number of neurons required to populate larger cortices? Several computational models have been proposed which reconcile the limited empirical data available on the kinetics of the cortical neurogenesis with aspects of the mature distribution of cortical neurons (Kornack and Rakic, 1998; Caviness et al., 2003; Gohlke et al., 2007). Most published models focus on a single species but some comparative studies address a few species. We have developed a model to investigate the key parameters contributing to the variations in neural architecture observed not only across the mammalian order but also across the cortical surface of a given species. The model is purposefully simplistic, so as to make it's mechanics transparent: it tracks two populations, namely the precursor pool and the neuronal progeny of those precursors, as the size of each changes during neurogenesis. Studies have suggested that separate compartments within the embryonic ventricular region are respectively responsible for producing the deep and superficial layer neurons of the cortex (for a review, see Dehay and Kennedy (2007)). For simplicity, we model the ventricular region as a homogeneous source of neurons, their layer assignment being dependent on their time of production. Also not included in our model are the inhibitory neurons which migrate (tangentially) into the embryonic cortex from the ganglionic eminence and contribute a small part of the total population of cortical neurons.

Given a unit founder population of precursors, the model predicts the time course of neuronal output at a ventricular zone location in terms of amplification of the unit founder population. Parameters in the model which change over the time course of neurogenesis include the quit fraction (the instantaneous probability that the product of a cell divisions is a neuron and will not undergo further rounds of cell division), the cell-cycle duration and the probability that either of the two cells resulting from a division die.

Empirical data to inform the model's inputs and to test its predictions against measured numbers of neurons, postnatally or in adulthood, are in short supply. Estimates of the number of precursor cells, of the adult distribution of cortical neurons and for the kinetic parameters (cell cycle rates, death rates and the quit fraction) have been published for only a handful of mammalian species. We collate what information is to hand in order to estimate targets for precursor amplification and adult layer distribution of neurons across the range of mammalian brain sizes from small rodents to primates. For the kinetic parameters, we use what published data is available to inform initial guesses of these parameters. Then, for each cortex size, we search over many candidate sets of the parameters to find those producing the best match to the targets for amplification and layer assignment of neurons.

Our model explains recently demonstrated global gradients (reaching up to 5-fold variation, but also subject to local, areal deviations) in the number of neurons per column across the anterior to posterior axis of primate cortices (Cahalane et al., 2012; Collins et al., 2010a) as arising from intra-cortical gradients in the kinetics of neurogenesis which are known to exist in rodents, carnivores and primates (Luskin and Shatz, 1985; Jackson et al., 1989; Bayer and Altman, 1991; Miyama et al., 1997; Kornack and Rakic, 1998; Rakic, 2002a; Smart et al., 2002).

The model produces the empirically testable hypotheses that (i) rodent brains exhibit a much lesser gradient in neuron number per column and (ii) mammalian cortices of intermediate size (e.g. in cat or ferret) exhibit an intermediate gradient of approximately 2-fold variation. Accompanying the spatial gradient in neuron number, the proportion of neurons populating the upper versus lower layers of the cortex is predicted to shift, preferentially swelling upper layers as neuron number per column increases.

2.1.1 Overview of Cortical Neurogenesis The following is an abridged overview of the basic processes by which cortical neurons are produced and assigned to a particular layer of the cortex. A founding population of precursor cells in ventricular zones near the wall of the cerebral vesicles initially undergoes rounds of symmetric division, whereby both daughter cells are precursors, thus swelling the precursor pool. Neurogenesis begins when some divisions in the precursor pool become asymmetric: with some probability a daughter cell is now a differentiated neuron which will not undergo further rounds of cell division and will migrate out of the ventricular zone towards the developing layers of the cortex. We refer to the probability of a daughter cell being a neuron as the "quit fraction". As long as the quit fraction remains close to zero, the precursor population increases approximately exponentially. As neurogenesis proceeds, the quit fraction becomes larger. The precursor population peaks exactly when the quit fraction is one half: now, in expectation, every precursor that undergoes cell division produces one precursor and one neuron, thus the growth phase of the precursor pool has ended. Eventually the majority of the cells produced are neurons and the precursor pool becomes further depleted with each round of divisions. Young neurons migrate out of the ventricular zone to populate the

developing layers of the cortex in an "inside-out" manner (Rakic, 2002a). It has been established that the neurons of the deep cortical layers (VI and V) are produced first. Neurons destined for the progressively more superficial layers (VI through II) subsequently migrate through the already-present layers. These events take place over approximately 8 days in rat and 60 days in the rhesus macaque (Kornack and Rakic, 1995).

2.2 Methods

2.2.1 Modeling the Neuronal Output of the Ventricular Zone. A system of two ordinary differential equations (ODEs) models the dynamics of precursor cell replication and neuron production in the ventricular zone. Denoting the number of precursor cells present at time t by $P(t)$ and the number of differentiated neurons present by $N(t)$, the following differential equations prescribe how those populations change in time during neurogenesis:

$$\frac{dP(t)}{dt} = P(t)\frac{\ln(2)}{c(t)}\left[1 - 2d(t) - 2q(t)(1 - d(t))\right]$$

$$\frac{dN(t)}{dt} = P(t)\frac{\ln(2)}{c(t)}[2q(t)(1 - d(t))],$$

where $c(t)$ is the cell-cycle duration, $d(t)$ is the independent probability that each daughter cell dies after a cell division, and $q(t)$ is the probability that a daughter cell is a differentiated neuron which quits the precursor pool and does not undergo further rounds of cell division. To interpret the equations, note that if d and q were equal to zero, the precursor pool would undergo

exponential growth, doubling in number at a rate inversely proportional to the cell cycle duration $c(t)$. Allowing $d(t)$ to be non-zero accounts for the probability of cells dying after a division, thus reducing the overall growth rate. As the quit fraction becomes non-zero, this accounts for that fraction of daughter cells which does not die but leaves the precursor pool. It is precisely those quitting cells which swell the neuronal population and so that same "non-dead, quitting" quantity subtracted from the equation for precursors also appears as the positive contribution in the equation for the neuronal population. As no neurons are present at the start of neurogenesis, the initial number of neurons, $N(0)$, is equal to zero. So that the final output can be interpreted as the "amplification factor" of the initial precursor population, the initial precursor population is written as $P(0)=1$. This description of a "unit" precursor population is made possible by the fact that the output of the model is linear with respect to the initial precursor population. Hence, the amplification factor is determined in the model by the time course of the kinetic parameters, $c(t)$, $d(t)$, and $q(t)$.

2.2.2 A Universal Time Axis for Neurogenesis. Researchers have shown not only that the order of neurodevelopmental events is strictly conserved across mammals, but also that the timing of events can be predicted with high precision across species (Clancy et al., 2001; Finlay and Darlington, 1995). The mathematical form of the "translating time" model allows the scaling of early developmental intervals across mammals in a linear fashion. The developmental interval of interest in the present study is that between the onset and the completion of isocortical neurogenesis. The neurogenetic interval of any mammal can be stretched to lie between zero and one on a universal time axis (see Supplementary Figure 2A.1). In terms of our model, this

corresponds to the time in development between the moment when the quit fraction $q(t)$ first becomes non-zero (which we call t=0 on the universal time axis) and when $q(t)$=1, signaling that all divisions will be terminal and thus ending neurogenesis (at what we will call t=1). Differences in the length of neurodevelopmental schedules across species are reflected in the translating time formalism in the "species scores". For the purposes of this study, those scores provide a convenient axis on which to line up brains, the larger brains generally having higher species scores due to their longer developmental interval.

As the present study focuses on the cortex, a slight modification of the species score is used, which we will term the "cortex score" and denote s_c. Neurodevelopmental events relating to the generation of the cortex in the primate order occur later in the developmental interval than might be predicted by looking at timing in other mammalian orders. Within the translating time model, a primate-cortex factor is included to model such events. The cortex score used here is simply the species score in the case of non-primates and for primates a primate-cortex correction is added (a difference of 0.21722, (Clancy et al., 2001)). For those species where a species score was not available in the literature, adult brain weight is used as an *ad hoc* proxy to estimate the species score and the primate-cortex correction is added as appropriate (see Supplementary Information in Appendix 2A).

2.2.3 Modeling the Layer Assignment of Cortical Neurons. It is well established that the time of a neuron's production during neurogenesis predicts in which of the cortex's layers it will assume its adult location. Developmental cell-labeling studies in rat (Bayer and Altman, 1991) and monkey (Rakic, 1982) have illustrated on which days the neurons destined for each layer of

the cortex are produced. Data from the cell-labeling studies is employed to parameterize a function which assigns the neuronal output of the ODE model either to lowers (layers V and VI) or upper (layers II-IV) according to the time of production. Although the model could accommodate further separating the output into any number of layers, sufficient empirical data to test such model predictions are not currently available. At a given time t in the neurogenetic interval for a cortex score of s_c, the fraction $u(t; s_c)$ of total neuronal output is routed to the upper layers, and 1-$u(t; s_c)$ to the lower layers, where $u(t; s_c)$ is a sigmoid-shaped function given by

$$u(t; s_c) = \frac{1}{2}\left(1 + \mathrm{erf}\left(\frac{t - t_{switch}(s_c)}{w}\right)\right).$$

The parameter t_{switch} determines the time at which $u(t; s_c) = 0.5$ and w determines the width of the sigmoid's cross-over (see Supplementary Figures 2A.3 and 2A.4). For a given cortex score, empirical data from rat and monkey are used to estimate the parameter t_{switch}, while the parameter w is fixed at 10.3% of length of the neurogenetic interval as that is the mean value measured in both rat and in monkey (see Supplementary Information §2A.3). Based on the rat and monkey empirical data and assuming a linear relationship between cortex score s_c and t_{switch}, it is estimated that $t_{switch}(s_c) = 0.675 - 0.114 s_c$.

2.2.4 Estimating the amount of Neuronal Amplifications and the Adult Layer Distributions of Neurons.

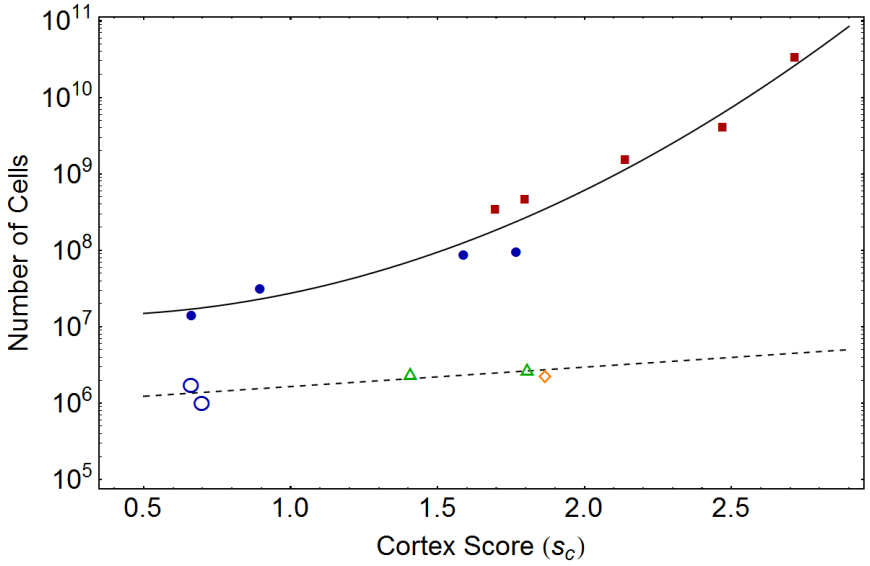

Figure 2.1. Estimates for the founder population (dashed line) and total neuronal output of the ventricular zone (solid line) as a function of cortex score s_c. The solid symbols represent adult cortical neuron counts in rodents (blue disks) and primates (red squares), each multiplied by a factor of 1.5 to allow for the large fraction of neurons that dies after reaching the cortex. The open symbols represent empirical counts of cells in the precursor pools of rodents (blue circles), carnivores (green triangles) and a sheep (orange diamond). The ratio of the two fitted functions gives an estimate for the amplification factor for a given cortex score. See Supplementary Tables 2A.1 and 2A.2 for data and sources.

To establish by what factor the precursor pool ought to be amplified for a given cortex score, and in what proportion neurons produced should be allotted to the upper and lower layers, data from the literature were collated and stereological measurements were carried out in this laboratory to asses adult neuron numbers, neuron layer distribution, and precursor population sizes (see Supplementary Tables 2A.1, 2A.2 and 2A.3). To allow for the substantive fraction neurons that dies after reaching the cortex, the adult neuron population numbers are multiplied by a factor of 1.5 to estimate the total output of cortical neurogenesis (Burek and Oppenheim, 1996; Underwood, 2013). Functions relating both total output and precursor pool populations to cortex

score s_c (see Figure 2.1) were fitted to data and their ratio used to estimate the amplification factor a as a function of cortex score, obtaining $a(s_c)=\exp(2.81-1.254s_c+1.256s_c^2)$.

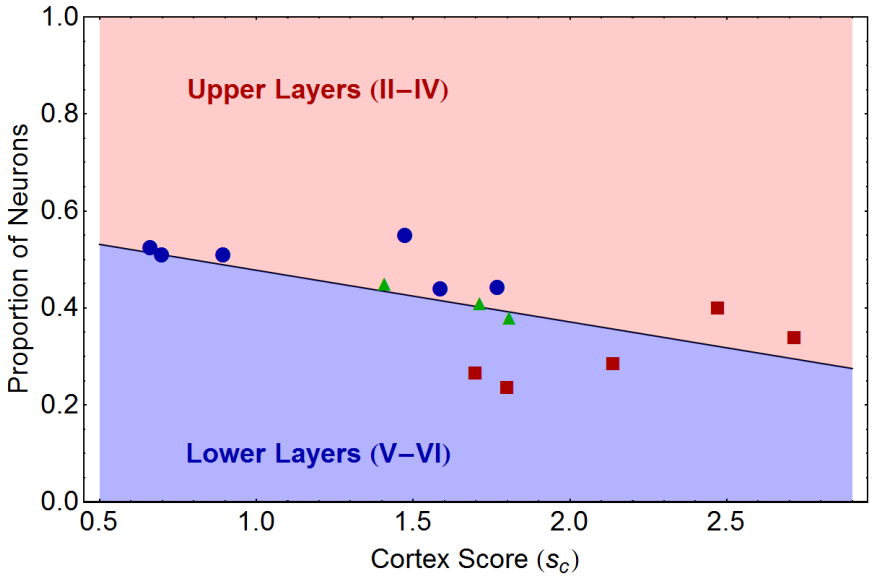

Figure 2.2.To estimate the proportion of neurons whose adult location is in the upper layers (II-IV) versus lower layers (V and VI) of the cortex, a linear regression of the proportion as assessed in six rodents (blue disks), three carnivores (green triangles) and five primates (red squares) against cortex score s_c is carried out. For species and sources, see Supplementary Table 2A.3.

Figure 2.2 displays a fit of the adult layer distribution of neurons versus cortex score. Although there is a significant trend of increased proportions of neurons in upper layers with increasing cortex score ($p<0.02$), this accounts for only a modest fraction of the variance in the data ($R^2=0.41$). On inspection, the data suggest the relationship of layer proportion to cortex score might be also be a function of the species' order, with rodents, carnivores, primates *et cetera* adopting different patterns of layer scaling – a possible extension of the model would distinguish

between taxa and not make the approximation that cortical architecture is a function of cortex score, or cortex size, alone.

2.2.5 Assimilating Empirical Data for Kinetic Parameters

Despite there being many qualitative accounts of the mechanics cortical neurogenesis in the literature, there have been few quantitative studies of the parameters governing the kinetics of the process. In that context, it not possible to supply the mathematical model, whose behavior is designed to mimic empirical qualitative observations, with the necessary kinetic parameters across the range of species based on what data are available in the literature alone. To address this shortfall, what data are available are used to generate initial estimates of the parameters determining the shape of functions modeling the quit fraction $q(t)$, the cell cycle duration $c(t)$ and the cell death rate $d(t)$ for each value of the cortex score (i.e. across the range of cortex sizes). Given the initial estimate for each parameter, a range of neighboring values is considered. The final choice of the parameter set for a given species contains those parameters for which the model produces the best results in terms of matching the target population of neurons in the upper and lower layers, and having a precursor pool which is depleted at the end of neurogenesis.

The progression of the quit fraction is modeled as a modified sigmoid $q(t;\alpha,\beta)$, constrained to have $q(0)=0$ and $q(1)=1$. The width of the sigmoid's crossover is controlled by the parameter α and the midpoint of the crossover is reached at time $t=\beta$ (see Supplementary Information §2A.6 for details). Initial estimates for α and β are established for all cortex scores based on empirical data on the progression of the quit fraction in mouse as no data are available for other species (Takahashi et al., 1996) (see Supplementary Figure 2A.5).

The cell cycle duration, expressed as a fraction of the duration of neurogenesis, is modeled as changing linearly in time over the developmental interval as $c(t) = c(t;\gamma,\delta) = \gamma + (\delta - \gamma)t$. Fitting a line to the initial cell cycle durations (i.e. those at the beginning of neurogenesis) for mouse, rat and macaque provides an estimate for γ as a function of cortex score, and similarly δ is estimated using data on the cell cycle duration at the end of neurogenesis for mouse, rat, ferret and macaque (Takahashi et al., 1995; Miller and Kuhn, 1995; Reillo and Borrell, 2012; Kornack and Rakic, 1998; Lukaszewicz et al., 2005) (see Supplementary Information §2A.6).

The progression of the cell death rate is modelled as linearly increasing over the time interval as $d(t) = d(t;\varepsilon,\phi) = \varepsilon + \phi t$. To our knowledge, measurements of the cell death rate are available only in rat (Thomaidou et al., 1997). Those data inform the estimates ε=0.1 (the value at t=0) and ϕ=0.15 (resulting in $d(1)$=0.35), and it is assumed, in the absence of other data, that these values apply across the range of cortex scores.

The final parameter introduced relates to the layer assignment function, $u(t;\ s_c)$. The parameter fitting algorithm is allowed to move the layer assignment function back or forward slightly on the time axis via the parameter τ. In this manner, any misalignment between the empirically informed $u(t;\ s_c)$ and the end-points of the model's time axis can be amended.

2.2.6 Finding the Best Fit for Kinetic Parameters. For a given candidate set of parameter values $m_i = \{\alpha_i, \beta_i, \gamma_i, \delta_i, \varepsilon_i, \phi_i, \tau_i\}$, the ODE's for the corresponding $P_i(t)$ and $N_i(t)$ are solved numerically using an implementation of the Runge-Kutta 4th order method in the c++ computer language. The parameter values which investigated for each species score are given in

Supplementary Table 2A.4. The resultant upper and lower layer components of the neuronal output, labeled U_i and L_i, respectively, are calculated from $N_i(t)$ as follow

$$U_i = \int_0^1 N_i(t)(u(t+\tau_i))dt; \quad L_i = \int_0^1 N_i(t)(1-u(t+\tau_i))dt\,.$$

To evaluate how well U_i, L_i and $P_i(1)$, as arising from the choice of parameters m_i, match the target values for the given cortex score, the "error"

$$E_i = |P_i(1)| + |U_i - U_T| + |L_i - L_T|$$

is calculated. Here U_T and L_T are the upper and lower layer neuronal output targets for the given species (as in Figure 2.1) and $P_i(1)$ ought to be zero if the precursor pool has been successfully depleted at the end of neurogenesis. The particular set of parameters m_i which minimizes E_i for a given cortex score is denoted $m_* = \{\alpha_*, \beta_*, \gamma_*, \delta_*, \varepsilon_*, \phi_*, \tau_*\}$. We label the corresponding upper and lower layer neuronal output as U_* and L_*, respectively. Checking 5×10^5 parameter sets takes approximately one minute on a desktop computer.

2.2.7 Modeling the Effects of Spatial Gradients in Neurogenesis. Neurogenesis is known to end earlier in the anterior cortex and relatively later in the posterior cortex of several species including mouse (Smart, 1983; Miyama et al., 1997), rat (Bayer and Altman, 1991), ferret (Jackson et al., 1989), cat (Luskin and Shatz, 1985) and monkey (Smart et al., 2002). We extended the model outlined above to examine the effects on neuronal output of those known spatial gradients in the progress of neurogenesis across the surface of the embryonic cortex. Viewing the parameters m_* identified above as applying to the "average" location in cortex, the effects of progressing the corresponding parameter functions, from their starting values through

to their end values, more quickly in anterior cortex and more slowly in posterior cortex may be examined. The mathematical formulation for how time in the parameter functions is scaled according spatial position x in the model cortex is given in the Supplementary Information (§2A.8). At position x=0.5 the functions are unaffected by the scaling (this is the "average cortical location"), while at x=0 the scaled time variable $\hat{t}$ is given by $\hat{t} = t/(1+\Delta)$ and at x=1 by $\hat{t} = t/(1-\Delta)$. To reflect the extent of empirical anterior-posterior time differences, the value of Δ=10% is chosen. Solving a separate pair of differential equations for each spatially indexed $P_x(t)$ and $N_x(t)$ produces outputs U_x and L_x.

2.3 Results

The model presented in this report can account for the massive increase over mammalian evolution in the number of cortical neurons as arising from biologically plausible, continuous changes to the kinetic parameters of a developmental mechanism which is conserved across species. Moreover, the initial cortical precursor population is not required to change significantly across species to support the change of approximately five orders of magnitude in the size of the adult cortical neuronal population. The increase in total adult number of cortical neurons is predicted to have a concomitant increase in the proportion of those neurons which occupy the upper layers (II-IV) of the cerebral cortex.

Intra-cortical variations in neural architecture are predicted by modeling the spatial differences in the kinetics of neurogenesis which are known to be present across the embryonic cortex. Across the range of brain sizes, the model predicts that cortices of larger sizes will have a gradient of increasing slope in the number of neurons per cortical column (Figure 2.4). In all cases, the gradient rises from the less neuron-dense anterior cortex along an axis towards the denser posterior cortex.

2.3.1 Cross-species Increases in Neuron Number and Upper Layer Proportion. We have identified coordinate changes to the progression of the quit fraction $q(t)$, the cell cycle duration $c(t)$ and the cell death rate $d(t)$ which can account, to high accuracy, for the changes seen in upper and lower cortical neuron numbers across the range of mammalian cortex sizes. The accuracy with which the empirical targets for those neuron numbers are reproduced is within 4% of the target values in all cases and within less than 1% for intermediate and larger cortices, as shown in Figure 2.3. Our search scheme does not exhaust the space of biologically plausible parameters, so it may be assumed that higher accuracy is possible. However, the current absence of empirical data with which to compare such predictions, along with the approximate nature of the targets, means the pursuit of higher accuracy predictions is of uncertain value at this time. For example, future anatomical data may support the suggestion that the layer proportion of neurons varies by taxonomic group and not only by cortex size. In that eventuality, the model's targets ought to also reflect group differences in upper and lower neuron number, and this would necessarily change the best fit parameters for the species in question.

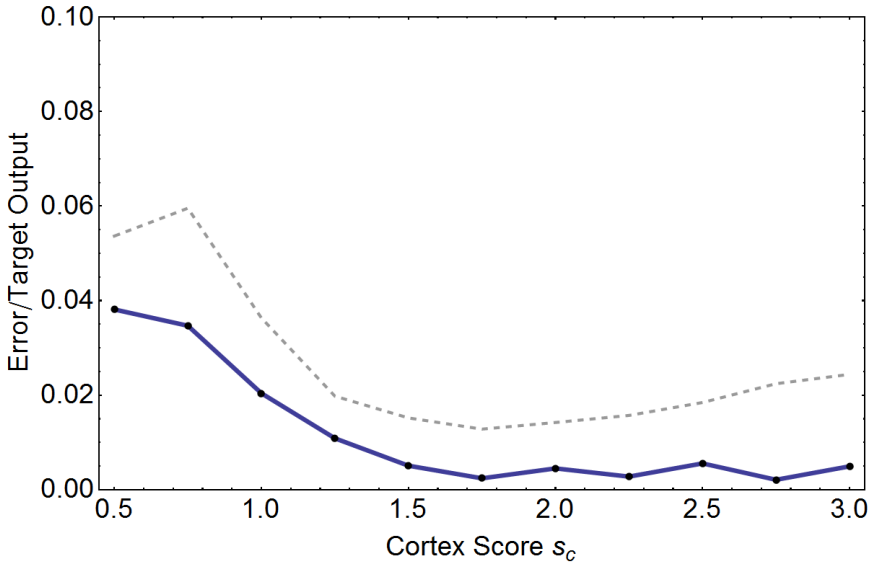

Figure 2.3. Accuracy of model output for a range of cortex scores. The solid line joins points indicating the error E_* of the best fitting parameter set m_* found for each cortex score examined. In each case, the best 50 parameter sets m_i had an error less than that indicated by the dashed line.

The parameter sets which can reproduce target neuron numbers for a given cortex score to high accuracy are not unique (see Supplementary Figure 2A.7). For each cortex score, circa 5×10^5 parameter sets were examined and in each case 50 parameter sets had an accuracy better than that depicted by the dashed line in Figure 2.3. Evidently, compensating changes to the various parameters can result in similar neuronal output. Future empirical observations will help to constrain the search space, revealing some parameter sets as implausible and thus refining the model's predictions concerning those parameters which remain unobserved.

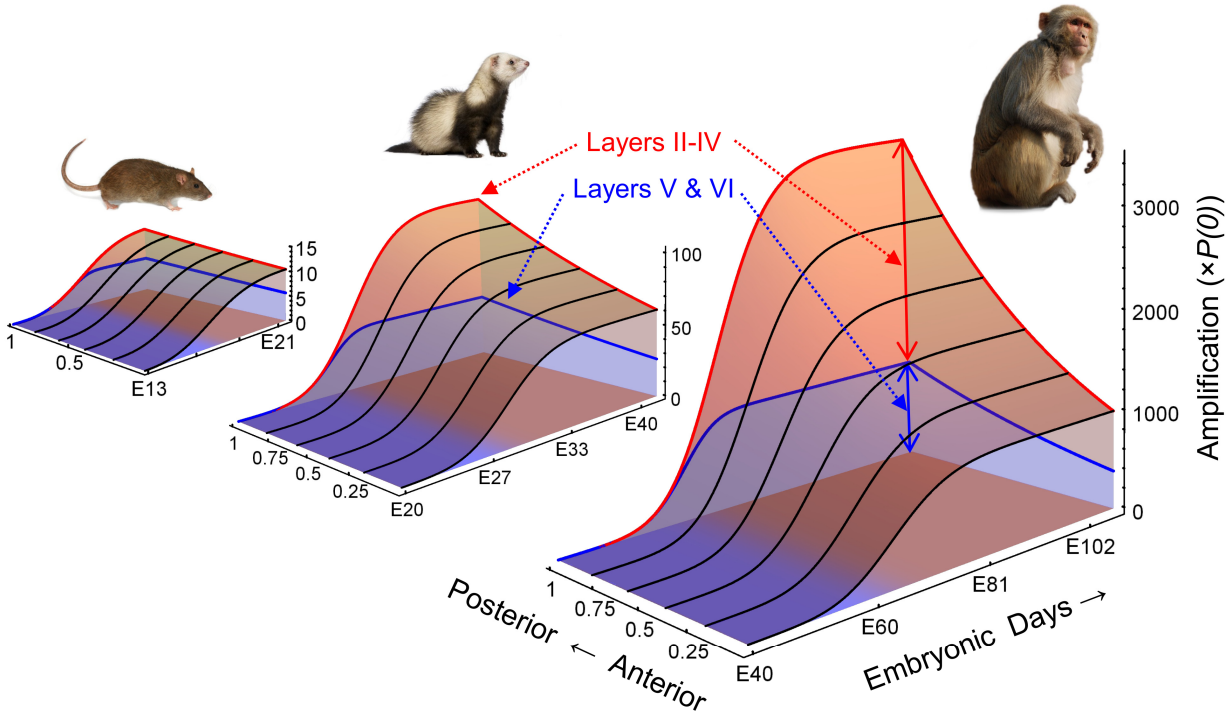

Figure 2.4. Model-predicted inter-species and intra-cortex differences in the timing, extent and layer assignment of cortical neuron output. Shown here are the predicted amounts of neuronal output (in terms of amplification of a unit precursor pool) across the anterior-posterior (spatial) axis of the cortex over the course of embryonic neurogenesis (time axis) for three different cortex scores (1.0, similar to a rat; 1.75, similar to a ferret; 2.5 similar to a macaque monkey). The larger cortices have a longer developmental interval, produce orders of magnitude more neurons in total and, in particular, have a greater complement of upper layer neurons. The anterior-posterior gradient in neuron number becomes more pronounced in larger cortices and it is the upper layers which accommodate the greater proportion of the increasing quantities of neurons. Species photo credit: Wikimedia Commons.

2.3.2 Intra-cortex Increases in Neuron Number and Upper Layer Proportion. Neurogenesis is known to progress at location-dependent rates, varying across the embryonic cortices of rodents, carnivores and primates (Luskin and Shatz, 1985; Jackson et al., 1989; Bayer and

Altman, 1991; Miyama et al., 1997; Kornack and Rakic, 1998; Rakic, 2002a; Smart et al., 2002), whereby the non-cingulate isocortex is populated with neurons in an anterior to posterior progression. Modeling the effect of such spatial gradients in developmental timing (by adjusting the progression of the parameters in neurogenesis, as described in the Methods section), the predicted outcome is an anterior to posterior gradient in the number of neurons per column. The extent of the gradient in neuron numbers, reaching up to five-fold in large primate cortices, is consistent with known anatomical gradients in primate neuron number (Cahalane et al., 2012; Collins et al., 2010a). The model predicts an accompanying shift in the layer proportion of neurons, favoring upper layers in the later-developing posterior cortex. Stereological measurements of upper and lower neuron numbers carried out in the Finlay laboratory confirm that the increased complement of neurons per column in the posterior of primate cortices is largely contained in the upper layers; the absolute numbers of neurons per column in layers V and VI vary relatively little across the cortex.

To understand the mechanics of how changes to the timing of neurogenesis across an embryonic cortex can affect neuronal output, we modeled the effect of delaying the rise of the quit fraction by 30% in a cortex of intermediate size (cortex score of 2.25) (see Figure 2.5). The moderate adjustment to $q(t)$ results in a disproportionate, 4-fold boost in the neuronal output. Moreover, the shift in the average time at which those are produced is also relevant, later born neurons having a greater chance of adopting an upper layer fate.

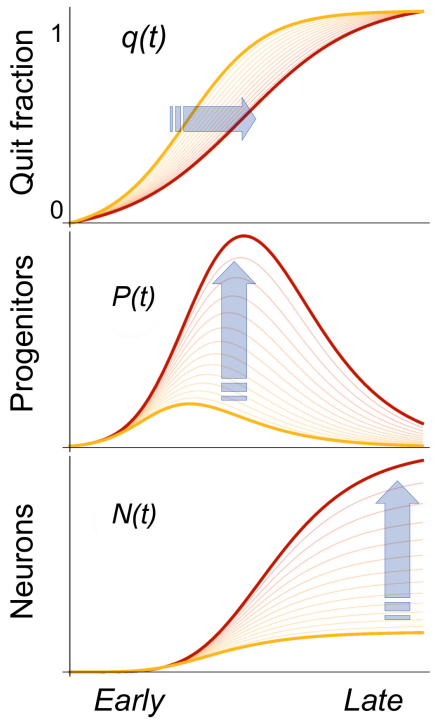

Figure 2.5. Modeling the effect on neuronal output of delaying the progression of the quit fraction $q(t)$ (top panel) by approximately 30% (the red curves are delayed relative to yellow curves) in a cortex of intermediate size. The precursor pool (middle panel) stays in a state of near-exponential growth for longer, peaking later and larger, resulting in the production of approximately 4-fold more neurons (bottom panel), the bulk of which are born relatively late.

2.3.3 Cross-species Differences in the Extent of Intra-cortical Variation. Across species, the model predicts that larger cortices will have a far more pronounced anterior-posterior gradient in neuron number and layer proportion: varying by five-fold in large primates and by just a few percent in small rodents. The longer period of gestation in primates makes the difference in neurogenesis end-dates more notable in those species than in rodents. In the macaque monkey, despite beginning at approximately the same developmental time in all regions, neurogenesis ends as many as three weeks later in posterior cortex – an intra-cortex difference of more than

30% in the length of the interval (Rakic, 2002a). By comparison, the anterior-posterior timing difference in rat may be as long as 2 days, amounting to perhaps a 25% percent intra-cortex difference in the duration of neurogenesis (Bayer and Altman, 1991). Hence the fractional differences in neurogenesis duration across species are not dissimilar. The impact of lengthening the period of neurogenesis by a given percentage depends, however, on how many additional rounds of cell-division that extension will allow. Hence, larger brains, where many more of rounds of cell-division take place during neurogenesis, will realize a disproportionate boost in neuronal output in those regions with extended neurogenesis. This leaves open the possibility that the intermediate-sized brains (of, e.g. some carnivores) exhibit a gradient of intermediate slope.

2.4 Discussion

Considering the plethora of developmental mechanisms which co-operate in directing the ontogeny of the cortex, it is perhaps not surprising that selection may not be able to address particular circuits or cortical areas without also affecting others. That is to say, rather than being mosaic as implied in the "proper mass" hypothesis (Jerison, 1973), adaptations might necessarily be coordinate in nature. For example, it could be that the only way to provide an increased number of neurons per cortical column in visual area 1 would be to boost neurogenesis output according to position along the anterior-posterior axis. Such an adaptation would have an impact

beyond the borders of that cortical area under direct selection pressure. A reasonable first reaction to the hypothesis that developmental mechanisms admit only such coordinated change is that it sounds highly restrictive, forbidding the selection of a myriad of potentially expedient mosaic adaptations. However, appropriate, "evolvable" developmental mechanisms might provide useful structure. They might leave available to selection the most useful reduced set of parameters from a search space far too large for the genotype to sample extensively.

2.4.1 Interaction with Other Mechanisms. We have outlined a model for how the kinetics of neurogenesis could give rise to an embryonic cortex whose architecture varies smoothly and systematically from the anterior to posterior poles. We conjecture that these gradients establish the basic landscape that richer areal and cellular structure is built upon, as prompted by genetic markers, projections from subcortical structures or other locally present cues (Kingsbury and Finlay, 2001). We offer the following as an example of how local deviations can be overlaid on the basic landscape set up by the global gradient in neuron number. In their investigation of neuronal densities across the cortex, Collins et al. noted that areas involved in sensory processing had higher neuron densities than some adjacent areas (Collins et al., 2010a). Identifying the data points of Collins et which related to primary sensory areas in baboon, we used a two-factor model, incorporating each sample's location and whether or not it was from a primary sensory area, to look for significant differences in neuronal density from what a "location-only" model predicted (Cahalane et al., 2012). We found that primary areas have a density of neurons which is 26% higher than that predicted for a non-primary area in the same cortical location (Figure 4). So, clearly, a mechanism other than smooth, location dependent changes in neurogenesis is

required to fully explain the variations in neuron density. Lower levels of neuron death during early development have been reported in developing sensory areas relative to other areas (Finlay and Slattery, 1983). We suggest that mechanism, in combination with the smooth gradients in neurogenesis output described above, and possibly in concert with further local mechanisms, may explain the greater number of neurons per unit column in primary sensory regions.

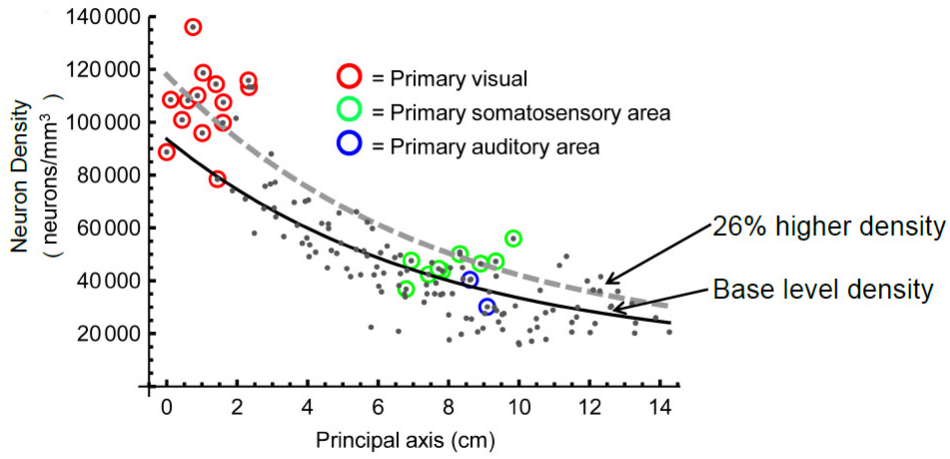

Figure 2.6. Using a two factor model (location and an indicator for primary or non-primary area) of neuronal density is better than a location-only model. In the two factor model, primary sensory areas have a neuronal density 26% higher than would a non-primary sensory area at the same location. The origin of the spatial "principal" axis is at the posterior medial pole of the flattened cortex and it extends towards the anterior lateral pole.

2.4.2 Structural & Functional Implications. The anterior-to posterior changes in cortical neuron number imply a corresponding variation in the types of neural processing that the respective regions of the cortex are most apt to support. Indeed, the cortical variations we have

highlighted are aligned with important functional and processing axes: higher stages of information processing and integration occur at progressively more anterior locations in the cortex. For example, higher visual areas and association areas integrating visual information are in regions anterior to the primary visual areas (Van Essen et al., 1992). From somatosensory areas, information flows in the anterior direction to the motor areas where it informs motor control. The notion that frontal regions have more integrative roles in neural processing is also indicated by their structural network connectivity, with most of the cortex's hubs being located in frontal regions (Modha and Singh, 2010). We surmise that successively higher and more integrative stages of neural processing might be best supported by the less neuron-dense architecture bestowed on frontal cortex by developmental gradients. Thus, the developmental mechanisms which lead to within-cortex variations in neural architecture impact cortical function and so are presumably a target of selection.

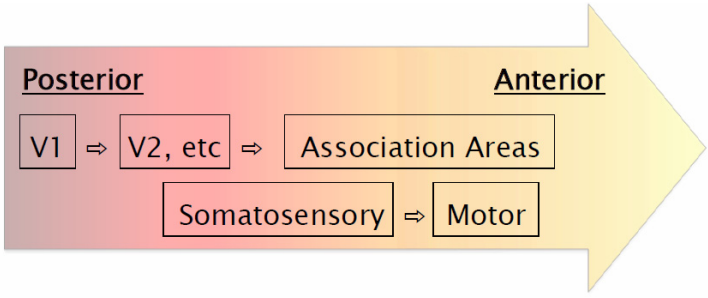

Figure 2.7 Considering the layout of cortical areas, we see that regions with more integrative roles in information processing are typically located anterior to those cortical areas receiving primary sensory input.

2.4.3 Questions Arising. The strikingly regular scaling of brain component sizes across species is a key feature of vertebrate brain evolution. As we have argued, those regularities hint at the strong conservation across taxa of the developmental mechanisms which produce the central nervous system. We have given a model of cortical neurogenesis which demonstrates how a conserved mechanism can explain both cross-species scaling and within-cortex variations. We conclude by addressing the following two questions raised by such an argument. Firstly, what further empirical data may soon be available to support or challenge the degree to which coordinate changes, arising from conserved mechanisms, account for the structure of the cortex? Secondly, in the midst of so much conservation, what remains variable and available to selection?

Regarding empirical data, it was cross-cortex isotropic fractionator studies in primates which revealed the pronounced gradients in neuron number along the anterior-posterior axis discussed above (Collins et al., 2010a). In contrast to the primate cortices, preliminary stereological measurements of neuron number carried out in this laboratory suggest a much more uniform distribution of neurons across the rodent cortex. Would a cortex whose size is intermediate to that of the rodent and primate would exhibit an intermediate level of gradation in neuron number as is predicted by the model presented here? Are there large or intermediate brains in which neurogenesis happens in lock-step across the cortex and so no gradient in neuron number is produced? Studies systematically sampling multiple sites in the cortices of non-primates would help answer the question of whether gradients in neuron number and neuron layer assignment are an obligatory feature of an enlarged cortex or whether they are unique to primates. Apart from data on the mature anatomy of the cortex, estimates of kinetic parameters

in a greater range of species than are currently reported may support or challenge the assumptions we have made here concerning how those parameters change across species.

As to what parameters might be made accessible to selection by conserved developmental mechanisms, by means of which the brains of different groups or species become differentiated from those of common ancestors, we offer the following as a possible example. Even if neuron number were constrained to vary smoothly, in a graded manner, across the cortex, then the slope of that gradient might be a subject of selection. It seems apparent that those smaller cortices produced by relatively few rounds of cell division have a limited scope to develop gradients in neuron number by way of spatial variation of neurogenesis. It is less clear, however, if or why large cortices could not be more or less varied across their spatial extent. Can the slope of the gradient be set independent of cortex size? Answering questions such as these will further the understanding of the cellular and molecular mechanisms at work in constructing the brain and of how those mechanisms are encoded in the genome.

Acknowledgements

Thanks to Christine Charvet for stereological assessments of adult neuron number and laminar distribution in hamster, agouti, paca, owl monkey, tamarin and capuchin, and also of the precursor population in hamster, dog, cat and sheep.

APPENDIX 2A

SUPPLEMENTARY INFORMATION FOR

CHAPTER 2: A COMPUTATIONAL, EVOLUTIONARY-DEVELOPMENTAL MODEL LINKING INTER-SPECIES AND INTRA-CORTEX VARIATION IN ISOCORTICAL NEURON NUMBER IN MAMMALS

2A.1 A Universal Time Axis for Neurogenesis (SI for §2.2.2)

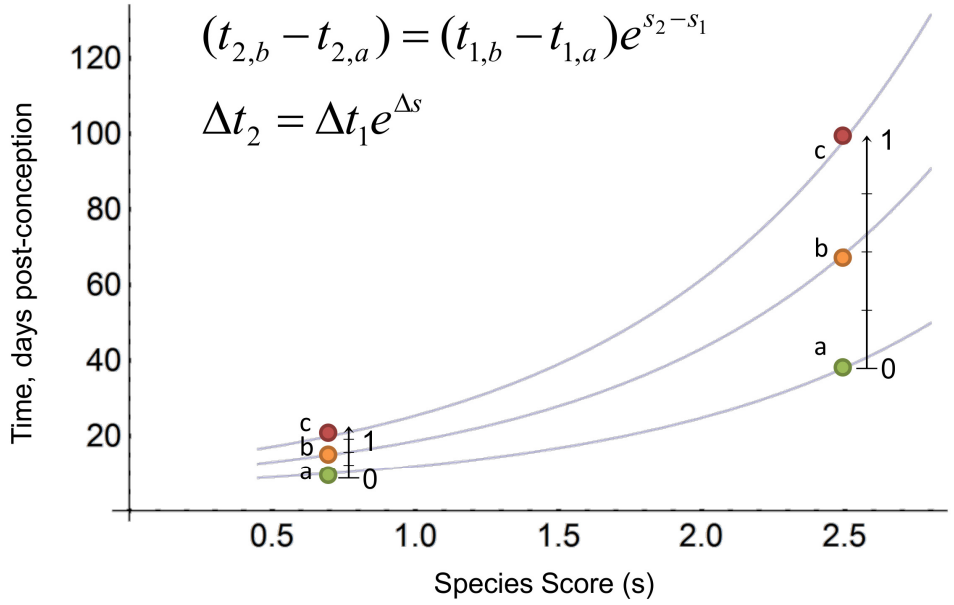

Figure 2A.1. If the date $t_{1,a}$ of a developmental event a is recorded in species 1, then the translating time model of Clancy et al. (2001) allows one to predict the date $t_{2,a}$ of that event in a species 2. The gray curves in the figure illustrate how the dates of three illustrative events a, b, and c would translate in gestational time across species with different species scores, using mouse (species score 0.701) and the macaque monkey (species score 2.255) as examples. The formulae in the inset illustrate that the interval of time between any two events in one species is

simply stretched linearly when translated to a different species. A more recent study including postnatal developmental events has shown that a non-linear model gives a better description of how developmental time translates across species (Workman et al., 2013). However, the translation in that newer model remains very nearly linear for events in early development, the epoch of relevance in the present study.

2A.2 Assigning Estimated Species Scores According to Adult Brain Weight (SI for §2.2.2)

To estimate species scores not available in the literature, we fitted a line to N=10 published species scores plotted against the natural logarithm of the corresponding adult brain weight. The approximate relationship between weight and species score s given by the regression line, $s = 0.971 + .02296 * \ln(weight)$, is used to estimate species scores from brain weight in other animals.

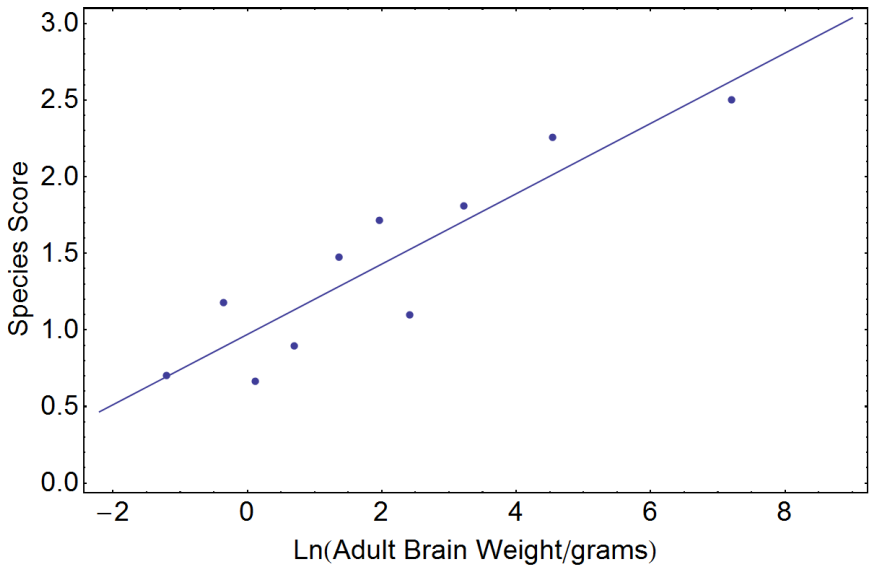

Figure 2A.2. Linear regression of species scores against log of adult brain weight. N=10, R^2=0.82, F=37, p<0.0003.

2A.3 Modeling the Layer Assignment of Cortical Neurons (SI for §2.2.3)

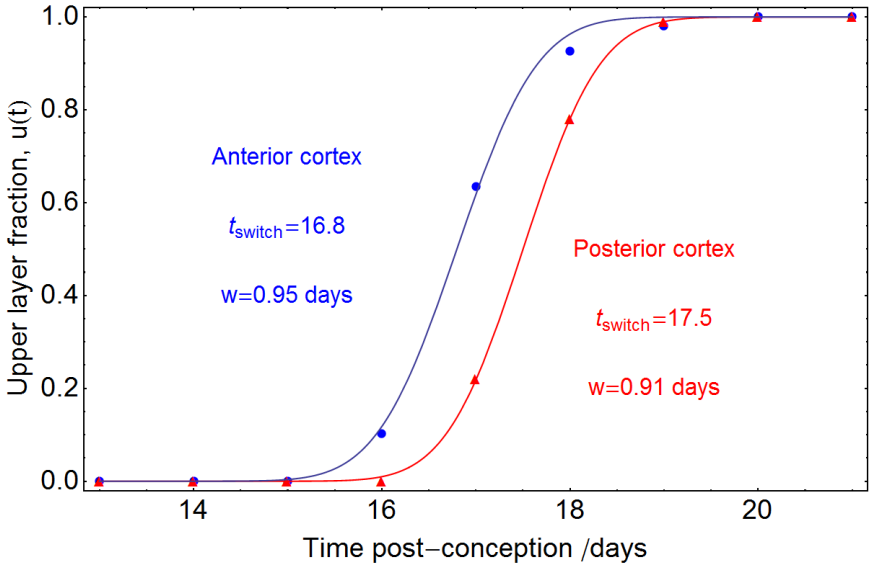

Figure 2A.3. The fraction of neurons produced on post-conception (PC) days in rat which have an upper-layer fate. The data of Bayer and Altman (1991) are used under the approximation that the number of upper (II-IV) and lower (V and VI) layer neurons is equal at each site (an approximation which is commensurate with stereological data collected in rodents in this laboratory, data not shown). The blue disks are based on measurements in anterior cortex and the red triangles show data from posterior cortex. The corresponding curves represent the best fit of the function $u(t) = 0.5\left(1 + \mathrm{erf}\left(t - t_{switch}\right)/w\right)$ achieved by adjusting the parameters t_{switch} and w using the NonlinearModelFit function in Mathematica (Version 9, Wolfram Research, Champaign IL). R^2>0.99 for both fitted curves.

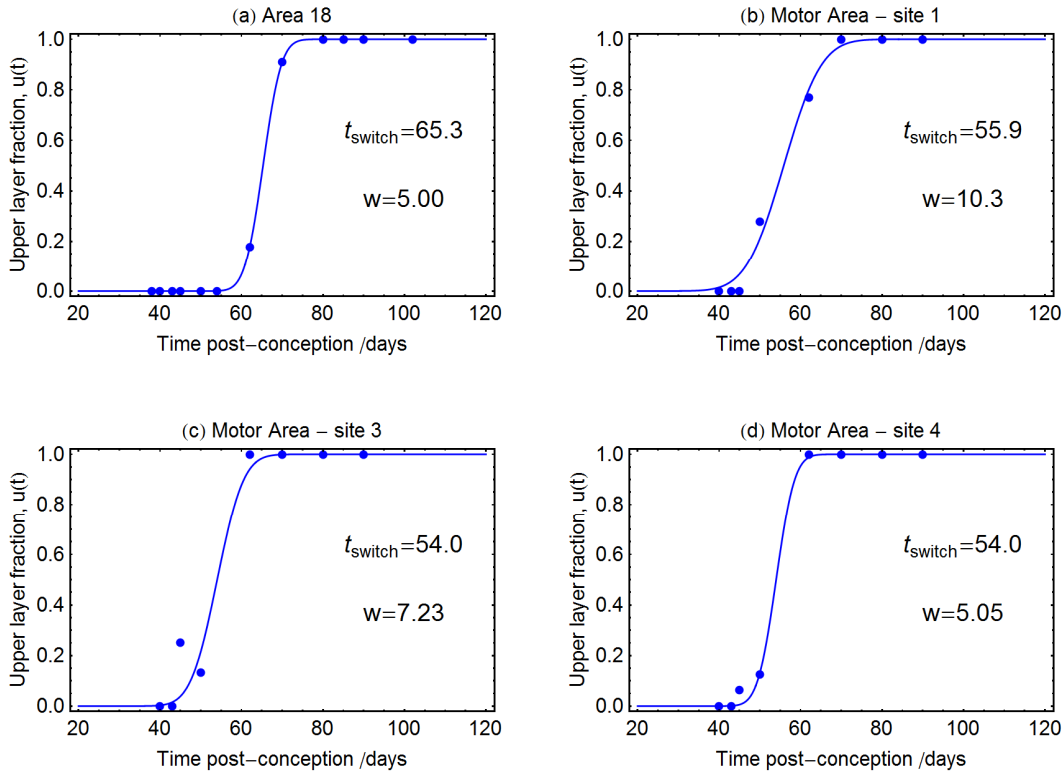

Figure 2A.4. The fraction of neurons produced on post-conception (PC) days in the macaque monkey which have an upper-layer fate; data from Rakic (1982). The blue disks are based on measurements in one posterior area (Area 18) shown in panel (a), and three distinct sites in central, motor cortex, shown in panels (b), (c) and (d). Data in the same study describe additional areas but lacked the temporal resolution to discern the width of the switch-over from lower to upper layer neuron production. The corresponding curves (solid lines) represent the best fit of the function $u(t)$ and R^2>0.98 for all fitted curves.

2A.4 Estimating the Amount of Neuronal Amplification (SI for §2.2.4)

Precursor population empirical data

Species	*Cortex Score*	*Precursors*	*PC Day*
Hamster	0.663	1.7E+06	10/11
sources/notes	*2*	*F*	
Mouse	0.701	1.0E+06	10
sources/notes	*2*	*1*	
Sheep	1.870	2.3E+06	24
sources/notes	*ebw*	*F*	
Cat	1.808	2.8E+06	17
sources/notes	*2*	*F*	
Dog (Beagle)	1.410	2.6E+06	24
sources/notes	*ebw*	*F*	

Table 2A.1. Data used in a regression of founder population against cortex score s_c resulting in the relationship *founders*=exp(13.702+0.585s_c), having R^2=0.67 and p=0.09. Table legend: (1) Haydar et al., 2000; (2) Clancy et al., 2001; (F) stereological data collected in the Finlay laboratory; (ebw) cortex score estimated from adult brain weight.

Adult cortical neurons

Species	*Cortex Score*	*Adult Neurons*
Hamster	0.663	9.2E+06
sources/notes	*2*	*F*
Rat	0.897	2.1E+07
sources/notes	*2*	*7*
Macaque	2.472	2.7E+09
sources/notes	*2*	*4*
Human	2.717	2.2E+10
sources/notes	*2*	*5*
Agouti	1.590	5.8E+07
sources/notes	*ebw*	*F*
Paca	1.770	6.3E+07
sources/notes	*ebw*	*F*
Tamarin	1.697	2.3E+08
sources/notes	*ebw*	*F*
Owl Monkey	1.797	3.0E+08
sources/notes	*ebw*	*F*
Capuchin	2.135	1.0E+09
sources/notes	*ebw*	*F*

Table 2A.2. Data used in a regression of adult neuron population against cortex score s_c resulting in the relationship $neurons=\exp(16.54-0.669s_c+1.256s_c^2)$, having $R^2=0.96$ and $p<0.04$. Table legend: (2) Clancy et al., 2001; (4) Christensen et al., 2007; (5) Roth and Dicke, 2005; (7) Korbo et al., 1990; (F) stereological data collected in the Finlay laboratory; (ebw) cortex score estimated from adult brain weight.

2A.5 Estimating the Laminar Distribution of Neurons (SI for §2.2.4)

Laminar distribution of cortical neurons

Species	*Cortex Score*	*Upper Layers (II-IV) %*
Hamster	0.663	48%
sources	*2*	*F*
Mouse	0.701	49%
sources	*2*	*19*
Rat	0.897	49%
sources	*2*	*19*
Guinea Pig	1.476	45%
sources		*19*
Ferret	1.714	59%
sources	*2*	*19*
Cat	1.808	62%
sources	*2*	*19*
Macaque	2.472	60%
sources	*2*	*19*
Human	2.717	66%
sources	*2*	*19*
Agouti	1.590	56%
sources	*ebw*	*F*
Paca	1.770	56%
sources	*ebw*	*F*
Tamarin	1.697	73%
sources	*ebw*	*F*
Owl Monkey	1.797	76%
sources	*ebw*	*F*
Cappuchin	2.135	71%
sources	*ebw*	*F*
Dog (Beagle)	1.410	55%
sources	*ebw*	*19*

Table 2A.3. Data used in a regression of the fraction of neurons occupying upper layers against cortex score s_c, resulting in the relationship $f(s_c)=0.416+0.107s_c$, having $R^2=0.41$ and $p<0.02$. Table legend: (2) Clancy et al., 2001; (19) using data from Hutsler et al. (2005), under the assumptions that (i) the data are representative of the aggregate cortical location in the respective species and (ii) the volume density of neurons in the upper and lower cortical layers is approximately equal at a given cortical location (an approximation which is consistent with stereological data collected in this laboratory in three rodent and three primate species, data not

shown); (F) stereological data collected in the Finlay laboratory; (ebw) cortex score estimated from adult brain weight.

2A.6 Assimilating Empirical Data for Kinetic Parameters (SI for §2.2.5)

Modeling the progression of the quit fraction q(t)

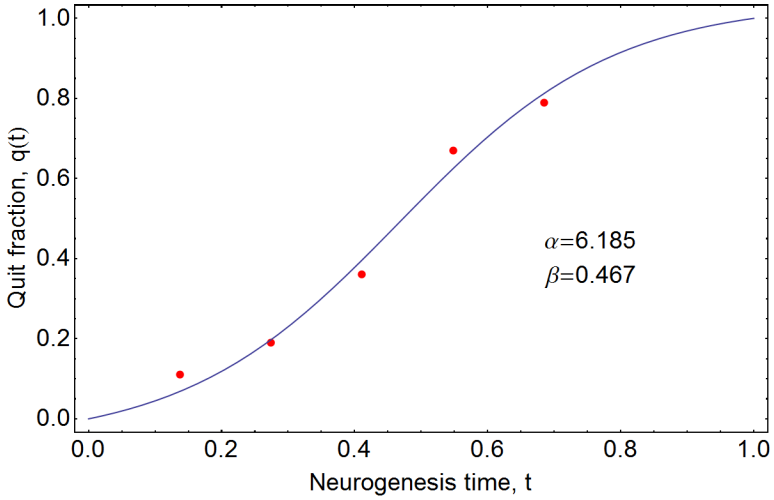

Figure 2A.5. The progression of the quit fraction $q(t)$ in mouse. The red points are empirical data (Takahashi et al., 1995) and the blue curve is the best fit of the modified sigmoid function $q(t;\alpha,\beta)$.

The function $q(t;\alpha,\beta)$ is given by

$$q(t;\alpha,\beta)=\frac{\tilde{q}(t;\alpha,\beta)-\tilde{q}(0;\alpha,\beta)}{\tilde{q}(1;\alpha,\beta)-\tilde{q}(0;\alpha,\beta)}, \text{ where } \tilde{q}(t;\alpha,\beta)=\frac{1}{1+\exp[-\alpha(t-\beta)]}.$$

Modeling the progression of the cell cycle duration d(t)

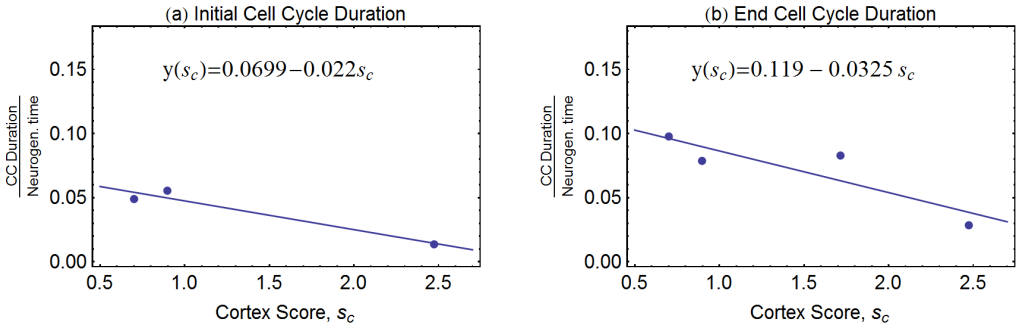

Figure 2A.6. The cell cycle duration at the beginning and end of neurogenesis in several species, expressed as a fraction of the duration of the respective neurogenetic intervals of those species. (a) Initial cell cycle duration in mouse, rat and macaque (from left to right) (Takahashi et al., 1995; Miller and Kuhn, 1995; Kornack and Rakic, 1998). (b) Cell cycle duration near the end of neurogenesis in (from left to right) mouse, rat, ferret and monkey (Takahashi et al., 1995; Miller and Kuhn, 1995; Reillo and Borrell, 2012; Lukaszewicz et al., 2005). For the end cell cycle duration in macaque, the value estimated by Lukaszewicz et al. was used rather than the estimate of Rakic et al. (1998).

2A.7 Finding the Best Fit for Kinetic Parameters (SI for §2.2.6)

Ranges of Values for Candidate Parameter Sets m_i

Function	*Parameter*	*From*	*To*	*# Steps*
$q(t)$	α	0.50	8.00	20
$q(t)$	β	0.20	0.80	20
$c(t)$	γ	$c_{start}(s_c)$-0.02	$c_{start}(s_c)$+0.02	10
$c(t)$	δ	$c_{end}(s_c)$-0.02	$c_{end}(s_c)$+0.02	10
$d(t)$	ε	0.10	n/a	0
$d(t)$	ϕ	0.15	n/a	0
$u(t)$	τ	-0.06	0.06	10

Table 2A.4. These ranges of values, resulting in 586,971 candidate parameter sets m_i for each cortex score s_c, were used in searching for the set of values m_* which minimized the prediction error E_i. The ranges for γ and δ used for a given cortex score s_c are functions of s_c: $c_{start}(s_c)=0.0699-0.022s_c$ and $c_{end}(s_c)=0.119-0.0325s_c$ as determined in §2A.6 above.

2A.8 Modeling the Effects of Spatial Gradients in Neurogenesis (SI for §2.2.7)

To model the empirical observation that the kinetic parameters for neurogenesis progress through their trajectories more quickly in anterior cortex and less quickly in posterior cortex, the following scaling of time is used in the parameter functions. The extent to which time is scaled depends on the spatial coordinate x, which ranges from x=0 at the anterior cortex to x=1 at the posterior. In the scaled functions below, the form of the layer assignment function $\hat{u}(t;x)$ is scaled to a lesser extent than the other kinetic parameters. That choice is informed by preliminary stereological data collected in the Finlay laboratory (data not shown) which indicate that the number of lower layer neurons in primates varies from anterior to posterior cortex to a much lesser extent than does the number of upper layer neurons. Scaling the layer assignment function across the anterior-posterior axis in the same manner as all other parameters would result in the model predicting a large increase in the number of lower layer neurons in intermediate and large sized cortices.

We let $\hat{t}(x) = \dfrac{t}{1+\Delta-2x\Delta}$ and the scaled parameter functions are given by

$$\begin{aligned}
\hat{q}(t;x) &= \min\left[1, q(\hat{t}(x);\alpha_*,\beta_*)\right],\\
\hat{c}(t;x) &= c(\hat{t}(x);\gamma_*,\delta_*),\\
\hat{d}(t;x) &= d(\hat{t}(x);\varepsilon_*,\phi_*),\\
\hat{u}(t;x) &= u\left(\tfrac{1}{2}\left(t+\hat{t}(x)\right)\right).
\end{aligned}$$

For each value of z, the corresponding pair of ODEs

$$\begin{aligned}
\frac{d\hat{P}_z(t)}{dt} &= \hat{P}_z(t)\frac{\ln(2)}{\hat{c}(t;z)}\left[1-2\hat{d}(t;z)-2\hat{q}(t;z)(1-\hat{d}(t;z))\right],\\
\frac{d\hat{N}_z(t)}{dt} &= \hat{P}_z(t)\frac{\ln(2)}{\hat{c}(t;z)}[2\hat{q}(t;z)(1-\hat{d}(t;z))]
\end{aligned}$$

is solved numerically for $t \in [0, \frac{1}{1+\Delta-2x\Delta}]$. The resulting, indexed values of $N_x(t)$ is used to calculate the upper and lower layer output according to

$$\hat{U}_x = \int_0^{1/(1+\Delta-2x\Delta)} \hat{N}_x(t)(\hat{u}(t+\tau_*;x))dt \text{ and } \hat{L}_x = \int_0^{1/(1+\Delta-2x\Delta)} \hat{N}_x(t)(1-\hat{u}(t+\tau_*;x))dt .$$

2A.10 Results of Parameter Search (SI for §2.3.1)

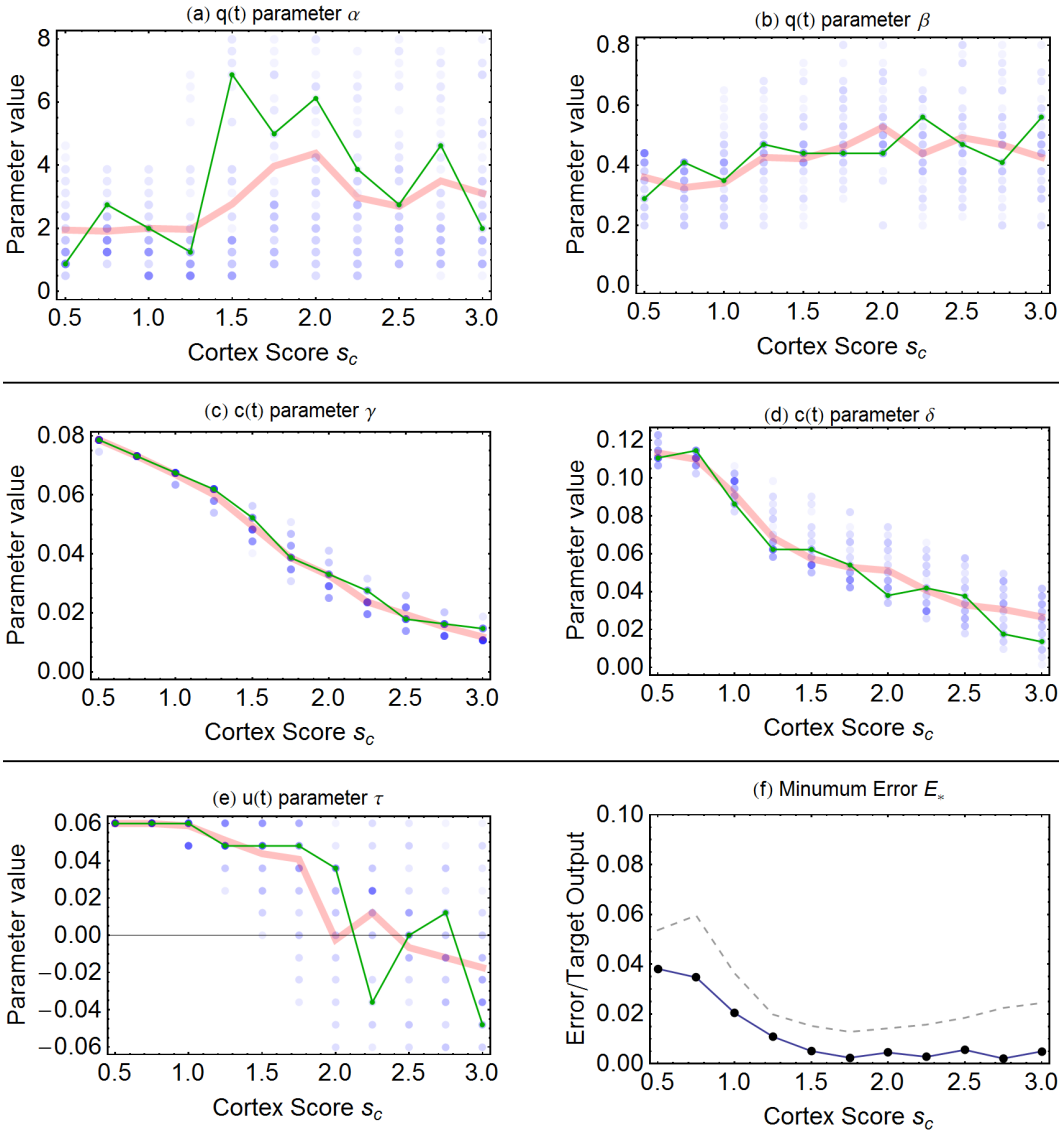

Figure 2A.7 Panels (a)-(e) show, for each cortex score, which values of the respective parameters best match the target values for neuron output with the two remaining parameters, those for $d(t)$, pinned at ε=0.1 and ϕ=0.15. The green trace shows the parameter values in the best performing parameter set m_*. The thick pink trace shows the average of the best 20 values at each cortex score. The blue dots show values which occurred in the best 50 parameter sets with opacity proportional to how frequently that particular value featured in the best 50. In panel (f) the solid line shows the minimum error E_* expressed as a fraction of the total output (upper layer plus

lower layer) for each cortex score. The value of E_i for all of the best 50 parameter sets for each value of s_c lies below the dashed line.

CHAPTER 3

NETWORK STRUCTURE IMPLIED BY INITIAL AXON OUTGROWTH IN RODENT CORTEX: EMPIRICAL MEASUREMENT AND MODELS[2]

Abstract

The developmental mechanisms by which the network organization of the adult cortex is established are incompletely understood. Here we report on empirical data on the development of connections in hamster isocortex and use these data to parameterize a network model of early cortical connectivity. Using anterograde tracers at a series of postnatal ages, we investigate the growth of connections in the early cortical sheet and systematically map initial axon extension from sites in anterior (motor), middle (somatosensory) and posterior (visual) cortex. As a general rule, developing axons extend from all sites to cover relatively large portions of the cortical field that include multiple cortical areas. From all sites, outgrowth is anisotropic, covering a greater distance along the medial/lateral axis than along the anterior/posterior axis. These observations are summarized as 2-dimensional probability distributions of axon terminal sites over the cortical sheet. Our network model consists of nodes, representing parcels of cortex, embedded in 2-dimensional space. Network nodes are connected via directed edges, representing axons, drawn according to the empirically derived anisotropic probability distribution. The networks generated are described by a number of graph theoretic measurements including graph efficiency, node

[2] This text was first published in PLoS ONE under the same title with authors Diarmuid J. Cahalane, Barbara Clancy, Marcy A. Kingsbury, Ethan Graf, Olaf Sporns and Barbara L. Finlay.

betweenness centrality and average shortest path length. To determine if connectional anisotropy helps reduce the total volume occupied by axons, we define and measure a simple metric for the extra volume required by axons crossing. We investigate the impact of different levels of anisotropy on network structure and volume. The empirically observed level of anisotropy suggests a good trade-off between volume reduction and maintenance of both network efficiency and robustness. Future work will test the model's predictions for connectivity in larger cortices to gain insight into how the regulation of axonal outgrowth may have evolved to achieve efficient and economical connectivity in larger brains.

3.1 Introduction

Understanding the nature of the network of interconnections within the cerebral cortex is of central importance to determine how information is distributed and integrated (Bullmore and Sporns, 2009). Collated neuroanatomical data sets from several species (Felleman and Van Essen, 1991; Scannell et al., 1999) on the neuroanatomical connections of multiple cortical regions have been analyzed extensively, examining hierarchical organization, clustered and modular architecture and other key network metrics such as small-world attributes (Hilgetag and Grant, 2000; Sporns et al., 2004; Modha and Singh, 2010). More recently, the functional connectivity of the human cortex has been described by analyzing time series of activations obtained in imaging studies, during resting and task-evoked activity (Fox and Raichle, 2007). Until now, only a few studies have attempted to trace the developmental origin of key features of

cortical network architecture. Understanding the early development of anatomical connectivity is important as it may help to identify the structural features that become organized prior to those which arise in the course of experience.

During the time in which anatomical information has been gathered about the connectional anatomy of the cortex, our computational understanding of it has changed continuously. The classical view of the cortex centered on operations performed by "cortical areas" with each area representing a distinct region thought to integrate specific inputs from thalamus and cortex, transform them, and pass them to "higher" areas for further integration. In accord with this theory, investigations of cortical neuroanatomy and neurophysiology catalogued in great detail patterns of input and output connections, and response properties of single neurons of specific cortical regions, to illuminate each area's essential function (e.g. (Hubel and Wiesel, 1965; Kaas, 1987), reviewed in (Olshausen and Field, 2005)). Correspondingly, early studies of the development of connectivity in the cortex focused on primary visual cortex and primary somatosensory cortex, treating each as independent entities (O'Leary et al., 1994; Fitzpatrick, 1996). Few studies were designed explicitly to compare the early establishment of cortical connectivity across areas or to link its local and global features.

Serial-processing or switchboard metaphors for the cortex have been progressively replaced, not least because of the development of functional neuroimaging techniques, by a less hierarchical and more distributed model of function (Bressler and Menon, 2010). Under this view single areas may contribute to multiple functions and vice versa (Duncan and Owen, 2000; O'Toole et al., 2005; Anderson, 2010). The assignment of "function" to single brain areas has been shown to be quite plastic, on both short and long timescales (Pallas, 2001; Burton, 2003).

Information gathered from neuroanatomical studies (Modha and Singh, 2010; Scannell et al., 1995) together with advances in graph theoretical analysis of anatomical networks (Bullmore and Sporns, 2009) suggest that patterns of cortical connectivity reflect the interplay of local and global rules of how axons become spatially distributed, rather than a fixed developmental program that assigns connections to areas according to a pre-formed list of unique inputs and outputs.

Efficiency and scaleability are key design objectives for networks specialized for information processing, and they also have implications for evolving neural systems (Bassett et al., 2010). In combination with the efficient transmission of information, neural systems must also be economical in terms of volume and energy consumption, and existing evolved brains are manifestly scalable (Murre and Sturdy, 1995; Sporns et al., 2000; Chklovskii and Koulakov, 2004). Characterization of the efficiency and scaleability of local and global connectivity patterns in the cortex has been limited by the fact that all of the information presently available for analysis falls into one of two distinct categories, differentiated by the length-scales they examine. The first category, recorded in neuroanatomical studies, by activation of functional areas in imaging studies, or by diffusion tensor and diffusion spectrum imaging, describe axonal projections at scales comparable to the size of the entire cortex but typically at the low resolution of cortical areas or "regions of interest" (Hagmann et al., 2008). The second category of studies has focused on smaller units of cortex, mapping connections within cortical columns or patterns of synaptic connectivity on individual arbors (White and Fitzpatrick, 2007).

How features at the large scale emerge from the developmental rules governing growth at the cellular level is not well understood. Anatomical studies of the establishment of connectivity

spanning those two length scales are lacking in the literature, as are any attempts to infer the global network structure arising from such wiring rules. For this reason, we undertook to examine the establishment of overall connectivity in the cortex in a small mammal, the hamster, where the cortex is recently formed and axon outgrowth is in progress at the time of birth. Furthermore, we compared the connectivity patterns of small regions across the cortex, both independently of and in relation to their cortical region of origin. Based on our empirical observations, we propose a method of generating model cortical networks. Further, we use the model to make inferences about the particular form of the axon outgrowth distribution observed, arguing that it may be favored because it reduces wiring volume while maintaining high network efficiency and robustness. The ultimate intention is to ascertain, in a small cortex, basic principles for the establishment of axon network structure at the onset of first experience, and examine how those principles scale in expanding cortical sizes.

3.2. Methods Part I: Data Acquisition and Basic Quantification

3.2.1 Ethics Statement. Throughout all experiments, animals were treated in accord with the policies and procedures set forth in The National Institutes of Health Guide for the Care and Use of Laboratory Animals and approved regulations of Cornell University's Institutional Animal Care and Use Committee (IACUC). The experiments described in this paper were conducted under IACUC protocol number 84-55-00.

3.2.2 Species. Fifty-four Syrian hamster pups (*Mesocricetus auratus*) of both sexes from timed pregnancies in the laboratory colony were used in this study. Animals were fed *ad libitum* and maintained on a 10L:14D photoperiod.

3.2.4 Tracer and Injections. According to convention, the 24-hour period following birth is designated postnatal day 0 (P0). Only hamsters born within 24 hours of the expected 15.5 day gestation period were used for this study. Biocytin was injected into pup cortex at ages P0, P2, P4, P6 and P8, with transport time optimized at 24 hours. Intracortical transport was principally anterograde with very few cortical cell bodies retrogradely labeled outside the immediate injection area. However, both anterograde and retrograde transport were observed to the thalamus, although at ages earlier than P4, transport to the thalamus was principally retrograde. This thalamic label was used to identify thalamic nuclei with connections to the cortical injection site.

3.2.5 Surgeries. Pups were anesthetized by hypothermia and maintained on an ice blanket in molded head and body restraints. The skull was exposed and a hole made overlying the cortical region of interest. A solution of 5% biocytin was injected through a backfilled micropipette (inner diameter 15-20 μm) using a Picospritzer (General Valve Co.; Fairfield, NJ), with pressure and duration adjusted to deliver >0.1 – 0.5 microliters of solution. Injections were positioned only in cortical regions that could be clearly viewed, avoiding areas of high vascularization. Because rodent intracortical connectivity originates from both infra- and supragranular layers, injections were centered at a depth adjusted for the different ages to span the full thickness of the

cortex while avoiding the underlying white matter. Following injections, the scalp was sutured; pups were rewarmed and returned to the mother. After 24 hours pups were overdosed with sodium pentobarbital and perfused transcardially with 0.9% saline followed by 4% paraformaldehyde and 0.1% gluteraldehyde in 0.1M phosphate buffer (PB, pH 7.4). Brains were cryoprotected in 30% sucrose at 4^{o} centigrade until processing.

3.2.6 Histochemistry. All brains were frozen and sectioned coronally at approximately 60 μm. Sections were treated according to a protocol adapted from Ding and Elberger (Ding and Elberger, 1995), followed by conventional diaminobenzidine (DAB) processing. Briefly, sections were rinsed in phosphate buffered saline (PBS; pH 7.2,) quenched in 1% H_2O_2, and immersed in 1% Triton-X100 (TX) in PBS. Tissue was incubated overnight in an avidin-biotin solution (1:100; Vectastain Elite Standard Kit) containing 1% TX. Sections were reacted with 0.004% tetramethylbenzidine (TMB); mounted on chromium-gelatin coated slides, dehydrated, cleared, and coverslipped with Krystalon (Fisher Scientific) with one series counterstained with cresyl violet. Dehydration of the unstained series was kept to less than one-minute immersion in each of three graded alcohols to minimize shrinkage. Following data collection, this series was also lightly stained with cresyl violet to further verify neural divisions and landmarks.

3.2.7 Reconstruction of Dorsal Cortex and Injection Sites. Reconstructions were made using a LeitzDiaplan Microscope and a Neurolucida imaging system with a mechanical stage (Microbrightfield, Inc., Colchester, VT). Measurements were obtained from each traced serial section in each of the fifty-four brains, always including sections containing landmarks

comparatively stable across development such as the furthest ventral and caudal levels of the white matter, thalamic complex, and caudate nucleus. To avoid artificially elongating in the medial to lateral plane when converting from coronal sections to dorsal views, in each traced section a midpoint contour was measured using a line drawn intermediate between the superficial white matter and the top of cortical layer I. The measurement began medially at the "point of flexure" (dorsalmedial crest separating the two cerebral hemispheres) and extended laterally to the rhinal fissure. A dorsal cortical surface view was then constructed by plotting each midline measurement to scale using Canvas 6.0 (Deneba Systems, Inc.). In effect, this method generates a flattened or "unrolled" surface from curved serial coronal sections as if viewed from above (the dorsal surface; see Figure 3.4D).

3.2.8 Identification of Cortical Regions. Multiple sources of information were integrated to position general areal boundaries in the developing cortex and locate injection sites. First, atlases of the adult hamster brain (Morin and Wood, 2000) and developing and adult rat brain (Paxinos and Watson, 1986; Bayer and Altman, 1991; Altman and Bayer, 1995) were used to establish the overall orientation and form of the map. It is well established that the topology of thalamocortical and corticothalamic projections is conserved from first innervation to adulthood, though maturational gradients in the cortex and the deformation of the cortex by overall growth alters the relative size of cortical regions (Lent, 1982; Crandall and Caviness, 1984; Miller et al., 1993; Molnar et al., 1998). The anterograde and/or retrograde transport of biocytin from injection sites to the thalamus, listed in Table 1, was used to fix the positions of the primary visual, auditory and somatosensory cortex and shift areal boundaries with respect to the adult

cortex as required, for each postnatal age. Published and unpublished hamster developmental studies from this laboratory were also used to help align regions of the developing cortex with respect to other adjoining telencephalic regions, such as the striatum and hippocampus, whose topological positions remain fixed from initial generation to adulthood (Miller et al., 1993; Windrem and Finlay, 1991; Kingsbury et al., 2000).

3.2.9 Axon Tracing. Thirty-six developing brains with well-labeled axons were completely analyzed microscopically and 24 representative brains were traced using a Neurolucida (25x) for more detailed morphological and statistical analysis, including ages (injected-recovered) P0-1 (n=7), P2-3 (n=4), P4-5 (n=3), P6-7 (n=4), P8-9 (n=3). Axons were identified by their coloring, thin uniform appearance, characteristic branching patterns, and, on many occasions, the presence of growth cones. Every visible intracortical axon in each traced section was drawn. Sections to be traced (typically over one half) were determined by the presence or absence of labeled axons, although as noted above, sections containing the furthest ventral and caudal levels of the white matter, thalamic complex, and caudate were always traced to obtain registration measurements for dorsal views.

3.2.10 Reconstruction of Axonal Projections. The tracings of coronal sections were then used to generate dorsal view reconstructions of the furthest distal points where labeled axons were found, as well as axon density plots of projections arising from injection sites. First, radial lines were drawn perpendicular to the middle layers of the gray matter and spanning the entire depth of the white and gray matter, spaced every 200μm beginning at the point of flexure and ending at

the rhinal fissure, with the last measurement the interval between the final 200 μm line and the rhinal fissure. Tangential substrates were then outlined using pseudo phase-contrast on unstained tissue and adjusted using counterstained sections (accounting for shrinkage, which was consistently less than 10%). The tangential substrate boundaries included the subjacent border of the cortex (layer VI), the subjacent border of the infracortical fasciculus (a cell-sparse area above the subplate neurons, also called "channel 2" in (Bayer and Altman, 1991), and the subjacent border of the subplate neurons, which corresponds to the superficial border of the white matter. Axons crossing each radial line were counted and tangential substrate subtotals obtained. Each of these counts was associated with a location (i, j) on the 60μm × 200μm grid, indicating that this is the count at the *i*th radial line in the *j*th section. The substrate subtotals were labeled $c_{i,j}^{Ctx}$, for those axons counted in cortical layers, and $c_{i,j}^{WM}$, for those in the white matter. We use $c_{i,j}^{Coll}$ to denote the collapsed count of all axons encountered at a radial line, i.e. for each count location $c_{i,j}^{Coll} = c_{i,j}^{Ctx} + c_{i,j}^{WM}$.

The tangential compartments are not uniformly identifiable in hamster cortex: in far anterior and posterior coronal sections, white matter fibers, subplate neurons and the infracortical fasciculus merge. Moving anterior to posterior in pup brains, white matter fibers are first noted at the level of orbital cortex where the rhinal fissure no longer clearly separates cortex and olfactory bulbs, followed approximately 0.5 mm posterior by a distinct layer of subplate neurons and approximately 0.5 mm further posterior by the band of fibers comprising the infracortical fasciculus. In far lateral regions of cortex, the subplate neurons seem to merge with neurons of the claustrum; in both far lateral and posterior cortex, the fasciculus is quite thick relative to

anterior sections (see also Reep (2000)). The position of isolated single axons or very sparse projections was always registered independent of the radial lines used for systematic sampling. Care was taken to ensure that counts did not include axons traveling to subcortical or callosal areas; however, although these axons travel different routes, some small uncertainty is unavoidable. Dorsal view reconstructions were produced for projections traveling from an injection site in each of the different substrates (cortical layers I-VI, infracortical fasciculus, subplate and white matter), as well as a "collapsed" view of the first three combined so as to represent the conventionally identified cortical gray matter.

3.2.11 Basic Quantification. The surface area covered by underlying axons within the borders of the cortex bounded by the point of flexure and rhinal fissure was determined for 20 traced pup brains using NIH Image. Total area of axon coverage (in mm^2) was analyzed for cortex, subplate, infracortical fasciculus, and for a category collapsed across these three, as well as for the white matter. These totals were expressed as a percentage of the total dorsal area or anterior/posterior (A/P) or medial/lateral (M/L) length in each individual brain. Schematized cortical areas were not used in statistical analysis; areas were determined for each individual brain at each age (see also Table 2). ANOVA was performed in Statview 5.0 to determine if axon extent in M/L or A/P planes varied based on injection site location or age, followed by Scheffe's Post-hoc test when appropriate.

3.3 Methods Part II: Characterization of Axon Outgrowth Distribution

3.3.1 Interpolating the Data. The data for each animal was recorded as a set of axon counts taken at points on a 2-D grid whose axes aligned with the medial/lateral (ML) and anterior/posterior (AP) axes of the flattened cortical hemisphere. Indexing each grid point (i, j) and calling the corresponding count $c_{i,j}$, these counts document the number of axons originating at the injection site which were detected at location (i, j) on the 200μm by 60μm grid of sample points. As described above, for each animal, three sets of count data were analyzed: axons found in the cortical layers only c^{Ctx}, axons in the white matter only c^{WM}, and a collapsed set c^{Coll}, where $c_{i,j}^{Coll} = c_{i,j}^{Ctx} + c_{i,j}^{WM}$.

In order to arrive at the desired description in terms of probability distribution functions of axon terminal sites, the following steps were carried out. Any missing counts from the interior of each dataset were interpolated. Each grid was re-centered such that the injection site (detected as the site having the maximum axon count $c_{\max}$) had index $(i, j) = (0,0)$. We assumed that the injection site is a point source of axons. To simplify further calculations, a 2-dimensional first order interpolating function was fitted to each grid (using Mathematica). With the interpolating function $c(x, y)$, it was possible to treat the count data as continuous over the 2-D domain with $c_{i,j} = c(i \times 200\mu\text{m}, j \times 60\mu\text{m})$.

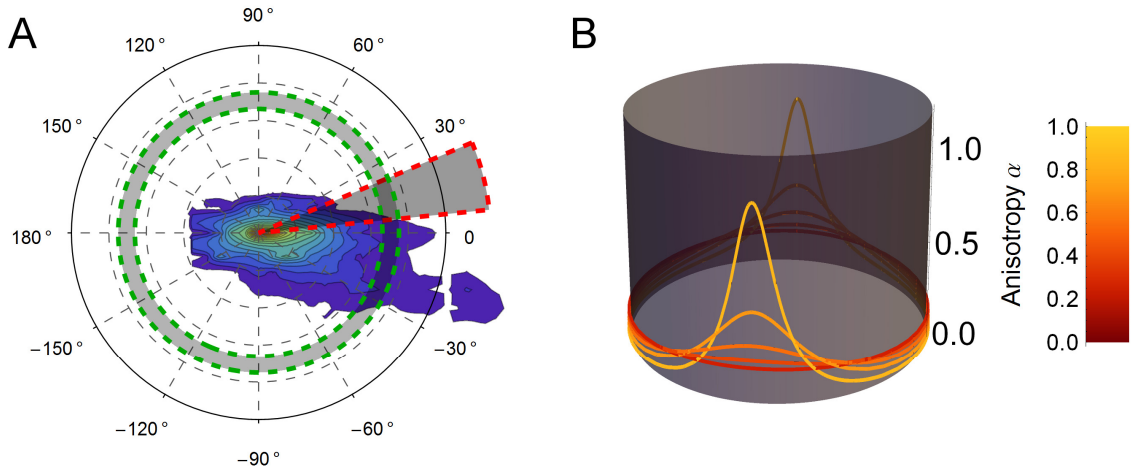

Figure 3.1. Characterizing axon outgrowth distributions. (A) The contour plot depicts a typical distribution of axon outgrowth from the site at the origin. The spatial distribution of axon outgrowth was described by an angular distribution function $\upsilon(\theta)$, quantifying the relative fraction of outgrowth volume in the infinitesimal sector of the plane centered at angle θ (shaded sector). A radial distribution function $S(r)$ quantifies the fraction of axon volume in the infinitesimal annulus at radius r. (B) The function $q(\theta;\alpha,\eta)$, with parameter α determining the height of its two diametrically opposed peaks, is graphed here on a circular domain for several different values of α. The tilt η is the same for each member of the family shown here, resulting in the peaks occurring at the same values of α and $\alpha+2\pi$ for each member. The distribution is almost uniform on the circle for values of α near zero. As α approaches 1, then $q(\theta;\alpha,\eta)$ becomes a delta function.

3.3.2 Angular Distribution of Outgrowing Axons. Two functions, calculated using $c(x,y)$, were used to characterize each dataset. The first, $\upsilon(\theta)=\int_0^\infty c(r\cos\theta, r\sin\theta)rdr$, accounts for the angular distribution of axons (see Figure 3.1A). The data exhibited a prevalence of growth along the direction of the ML axis in preference to the AP axis. To quantify this anisotropy, we fitted a double peaked function

$$q(\theta;\alpha,\eta)=\frac{1}{2}\left[\left(\frac{1}{2\pi}\right)u_{(\alpha)}(\theta-\eta)+\left(\frac{1}{2\pi}\right)u_{(\alpha)}(\theta-\eta-\pi)\right],$$

defined on $\theta\in[0,2\pi)$. Here $u_{(\alpha)}(\theta)=\frac{1-\alpha^2}{1-2\alpha\cos(\theta)+\alpha^2}$ with parameter $\alpha\in[0,1)$ is a probability distribution on the circle (see Figure 3.1B). The distribution is flat at $\alpha=0$ and approaches two delta spikes as $\alpha\to1$. For each animal, we calculated the values of α and η, or the *anisotropy* and *tilt* as we call them respectively, which minimized the least squares error between $q(\theta;\alpha,\eta)$ and $\upsilon(\theta)$ (see Supplementary Figure 3A.2 for fits to data). Thus $q(\theta;\alpha,\eta)$ is a probability distribution for the relative volume of outgrowth in each direction, parametrized in each case by anisotropy α and tilt η.

3.3.3 Radial Distribution of Outgrowing Axons. Arriving at the radial distribution function, characterizing the length distribution of the axons, requires taking into account the cumulative nature of the count data: $c(x,y)$ is the number of axons one would expect to find passing through any point (x,y), not the number of axons terminating there. Given that axons may trace more or less circuitous routes between their origin and terminal arbor, and may also branch en route, it will not be possible to exactly recover the density distribution of endpoints from the count data. To arrive at an approximation to the true distribution, we assume (i) that no branching occurs prior to arrival at the terminal site and (ii) that axons travel from the origin along straight trajectories. These assumptions are generally consistent with the data collected in this study and in earlier work (Miller et al., 1993). Given that our network model is constructed

using such straight-line axon trajectories, disregarding the (unknown) particulars of axons routes will not affect our simulated networks.

The quantity $S(r) = \frac{1}{2\pi c_{\max}} \int_0^{2\pi} c(r\cos\theta, r\sin\theta) d\theta$, under assumptions (i) and (ii) above, can be interpreted as the probability that an axon has length greater than or equal to r (see Figure 3.1A). The probability that it terminated at a length less than r is simply $P(r) = 1 - S(r)$ and so, in principle, $P(r)$ is an approximation to the cumulative distribution function (CDF) for the length of the axons. In practice however, portions of the empirical "CDFs" fail to meet the monotonicity property required of distribution functions. The difficulty arises near the origin, at small radii r, where the resolution of the experiment means that few count sites are contributing to the calculated value of $S(r)$. Furthermore, what counts are present may be noisy due to the high concentration of stained axons close to the injection site. For this reason, we chose to disregard the non-monotonic portions of the empirical functions $P(r)$ near the origin and fit analytical CDF's to the remaining monotonic data. However, it is that portion of the data, near the origin, which would otherwise provide the normalizing constant for our distributions (i.e. $c_{\max} = c(0,0)$). Hence, the fitting procedure must also provide an estimate for that normalizing constant. On inspection, the usable portion of the empirical distributions seemed to be well fit by gamma distributions, which have previously be used to model axon length distributions (Kaiser et al., 2009). So as to reduce the number of fitting parameters, we constrained the fitting procedure to use gamma distributions with a shape parameter equal to 2. Thus the radial

distribution of each outgrowth pattern was characterized by the mean ρ of its fitted gamma distribution, $p(r;\rho) = \frac{r}{\rho^2} e^{-r/\rho}$. See Supplementary Figure 3A.1 for fits to data.

3.4 Methods Part III: Network Modeling and Analysis of Networks

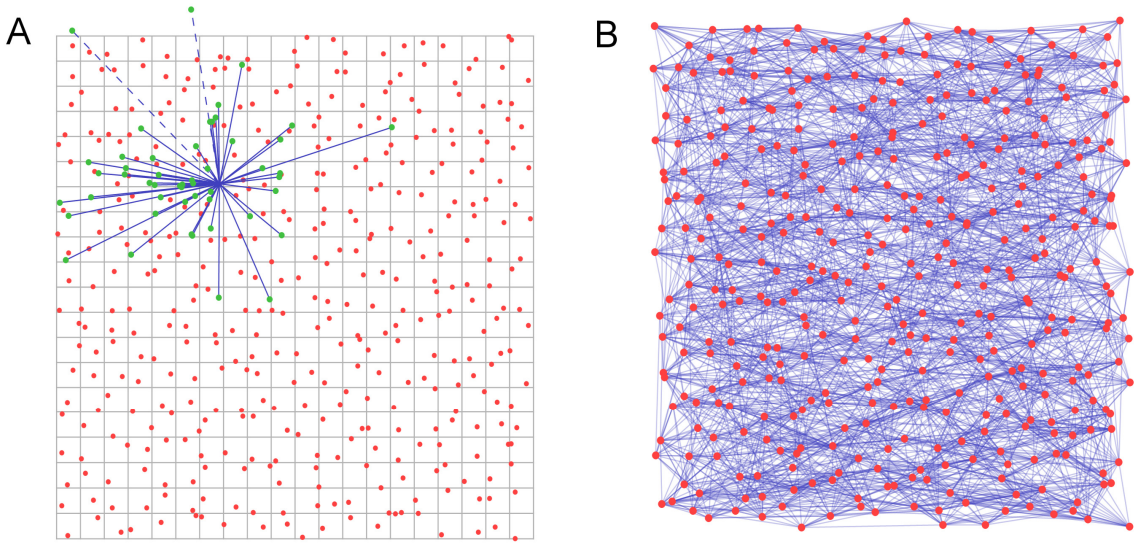

Figure 3.2. Generating spatial networks. (A) We begin with a grid of 100μm squares, each containing a node located uniformly at random within the square. For each node, a set of candidate end points for efferent links is drawn from under the probability distribution, those terminating outside the boundary of the region (such as the dashed lines here) will be discarded in favor of new candidates until the quota of n_{axons} has been reached. The ends of the candidate axons snap to the nearest node, and the links are recorded in the adjacency matrix. (B) Repeating the procedure in (A) for each node results in a network such as that depicted here. For clarity of display, the network in (B) is drawn on a grid of $N = 20 \times 20$ nodes having $n_{axons} = 10$. Networks used in our simulation have $N = 50 \times 50$ and $n_{axons} = 10$.

3.4.1 Generating Spatial Networks. We study a network model whose nodes are localized populations of neurons, linked by edges which model representative axons. The network is constructed as follows (see also Figure 3.2). We model the hamster's cortical hemisphere as comprising 2,500 idealized cortical units. Each unit represents the neural population under a 100μm×100μm square of cortex. Our model cortex is a grid of 50×50=2,500 of such units, thus mimicking a cortical sheet measuring 5mm×5mm. These units are the nodes in our network. With each node *i* we associate a location $p_i = (x_i, y_i)$, chosen uniformly at random within the corresponding unit's square footprint.

Emanating from each node are a fixed number, n_{axons}, of directed network edges, representing efferent axons. Edges are assigned to each node *i* by using the following procedure: *(i)* select a length r and a direction θ from under the empirically derived radial and angular probability distributions, $p(r)$ and $\upsilon(\theta)$, respectively; *(ii)* find the node *j* nearest to the point at distance r from node *i* in the direction θ; *(iii)* add a directed edge, pointing from node *i* to node *j*, to our network. There are two exceptions to the above procedure. First, if the randomly chosen length r and direction θ determine a point which lies outside the grid, we chose a new random r and θ, repeating until the chosen r and θ determine a point inside the grid. Second, self edges are disallowed – should one occur, we discard it and choose a new random endpoint such that the axon does not terminate at its node of origin. The procedure for generating edges is repeated until the node *i* has been assigned its full complement of n_{axons} edges. Edges are assigned to all nodes in the network in this manner. Once all edges have been assigned, in the *adjacency matrix* A, the entry A_{ij} records the number of directed edges from node *i* to node *j*.

We note that although the details of meandering axonal paths were ignored as we deduced $\upsilon(\theta)$ and $p(r)$, our method of generating networks does not require such details to reproduce the distribution of axon terminal sites. Our networks were created and visualized using Mathematica 7.0 (Wolfram Research, 2008).

3.4.2 Degree Distribution, Path Lengths and Clustering. We calculated several measures to analyze the networks generated by our spatial model. The *out-degree* $k_i^{out} = \sum_j A_{ij}$ of a node on a directed network counts the number of edges originating at that node. By construction, we have $k_i^{out} = n_{axons}$ for all nodes in our networks. The *in-degree* counts all edges terminating at a node: $k_i^{in} = \sum_j A_{ji}$. The number of edges comprising shortest network path between any pair of nodes, *i* and *j*, also known as the *distance* from *i* to *j*, is recoded as d_{ij}. The *average shortest path*, $l = \frac{1}{N(N-1)} \sum_{i \neq j} d_{ij}$, gives a characteristic length for the network paths. The *clustering* of a network gives the probability that if the edges $i \rightarrow j$ and $j \rightarrow k$ are both present then so too is the edge $k \rightarrow i$. The clustering, *C*, is given by $C = \frac{6 \times (\text{number of triangles in the network})}{(\text{number of paths of length 2})}$, where, for example, $i \rightarrow j \rightarrow k$ is a path of length 2 and a "triangle" refers to a case where the three edges ($i \rightarrow j$, $j \rightarrow k$ and $k \rightarrow i$) are present (Newman et al., 2006). A *small-world network* is characterized by having both the short path lengths typical of a random network and the high clustering typical of a more regularly wired (e.g. lattice) network. Using random networks as a baseline, the *small-world index*, *S*, makes the classification of networks as being small-world quantitative

(Humphries and Gurney, 2008). The small-world index of a network with N nodes, M edges, clustering C and average shortest path length l, is given by $S = \frac{C/C_r}{l/l_r}$, where C_r and l_r are, respectively, the clustering and average shortest path length of a random network also having N nodes and M edges. For a random network, $S = 1$, but S takes larger values for small-world networks.

3.4.3 Network Efficiency. *Global network efficiency* quantifies the efficiency of communication between all pairs of nodes on the network, under the assumption that information flows along the shortest paths available (Latora and Marchiori, 2001). Considering just one pair of nodes first, if an edge joins the two nodes, the path between them has length 1 and so communication is maximally efficient for that pair: we say that path has an efficiency of 1. If the shortest path between a pair of nodes (i and j) has length d_{ij}, then we say its efficiency is $1/d_{ij}$. The average value of that pairwise efficiency, taken over all pairs of nodes in the network, is the global efficiency: $E = \frac{1}{N(N-1)} \sum_{i \neq j} 1/d_{ij}$. Only a completely connected network (where all possible edges are present) has a global efficiency of 1. All other networks have an efficiency $E < 1$.

3.4.4 Node Centrality. The *betweenness centrality* of a node is a measure of how important that node is for efficient communication on the network (Newman et al., 2006). Considering the set of all shortest paths on the network, we see that some "central" nodes may feature in a greater number of shortest paths than do other less central nodes. The betweenness centrality of a node i

is the fraction of all shortest paths on the network which pass through *i*. Specifically, if σ_{st} is the number of shortest paths from *s* to *t*, and $\sigma_{st}(i)$ is the number of such paths containing the node *i*, the betweenness centrality of *i* is given by $b_i = \sum_{s \neq t \neq i} \sigma_{st}(i) / \sigma_{st}$.

3.4.5 Modularity. It can be useful to think of the nodes on a network as being members of different communities. To investigate the modular nature of our networks, we will assign nodes to non-overlapping communities whose membership is defined by location. If the communities are chosen well, one should observe a greater prevalence of intra-community edges over inter-community edges than would be found in a comparable random network (i.e. a randomly wired network with the same number of nodes and edges). The *modularity Q* quantifies the extent to which we have such a prevalence (Leicht and Newman, 2008). Assigning each node to a community, and denoting the node *i*'s community c_i, we can measure the modularity of the network with respect to that community assignment:

$$Q = \frac{1}{M} \sum_{i,j} \left[A_{ij} - \frac{k_i^{in} k_j^{out}}{M} \right] \delta_{c_i, c_j},$$

where *M* is the total number of edges in the network and δ_{c_i, c_j} is equal to 1 if $c_i = c_j$ and is zero otherwise. We measure the modularity of our networks with respect to two different, spatially defined, community assignments. First, we partition the nodes into 4 rectangular communities, roughly equal in size, aligned with the medial-lateral axis. Namely, the communities contain the nodes in rows 1 through 13, 14 through 25, 26 through 37 and 38 through 50 of our 50×50 grid, respectively). The communities are thus rectangles whose width spans the medial-lateral

dimension of our gird and whose height is about one fourth that of the grid. Second, we use a similar partitioning, but in this case assigning nodes by column number to one of four rectangular communities aligned with the anterior-posterior axis.

The NetworkX package (Hagberg et al., 2008) for Python was used to carry out the graph analysis of our networks.

3.4.6 Spatial Modeling of Links. Exploiting the spatially embedded nature of our network, we investigate how anisotropy may affect the volume requirement of axons via an altered number of axon encounters (see Figure 3.3). Modeling all the axons as straight lines in the plane, we count the number of axon encounters. Only encounters along the body of an axon are considered, those occurring at a node are disregarded. Axon encounters were enumerated using an algorithm implemented in c++.

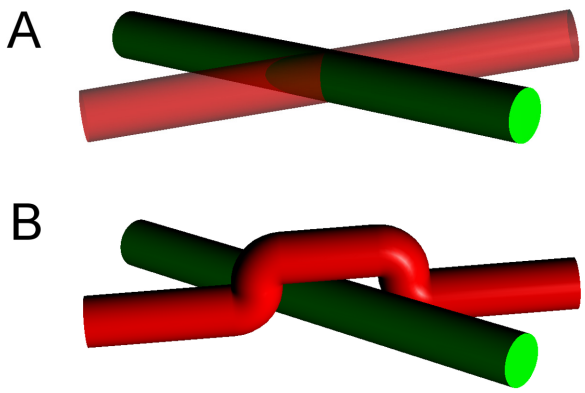

Figure 3.3. Extra volume cost due to axon encounters. Axons, whose paths were destined to intersect in (A) incur an extra volume cost as one or both alter their paths to avoid collision such

as in (B). The extra volume requirement of scenario (B) as compared with (A) is $(\pi - 1)4\pi r^3 \approx 26.9r^3$, where r is the axon radius.

3.5 Results

3.5.1 Characterization of Initial Axon Distribution in Empirical Data. Thirty-six developing brains were judged to have well-placed injections and well-labeled axons and form the empirical corpus on which the network modeling results are based. Injections were placed across the cortical field, although because of its small size, inaccessibility of the most lateral aspect, developing vascularization, and the relative immaturity of posterior regions at the earliest ages a uniform grid of sites is difficult to produce. Our method of representing initial transected axon counts is shown on a representative "unrolled" P0-1 cortex in Figure 3.4D.

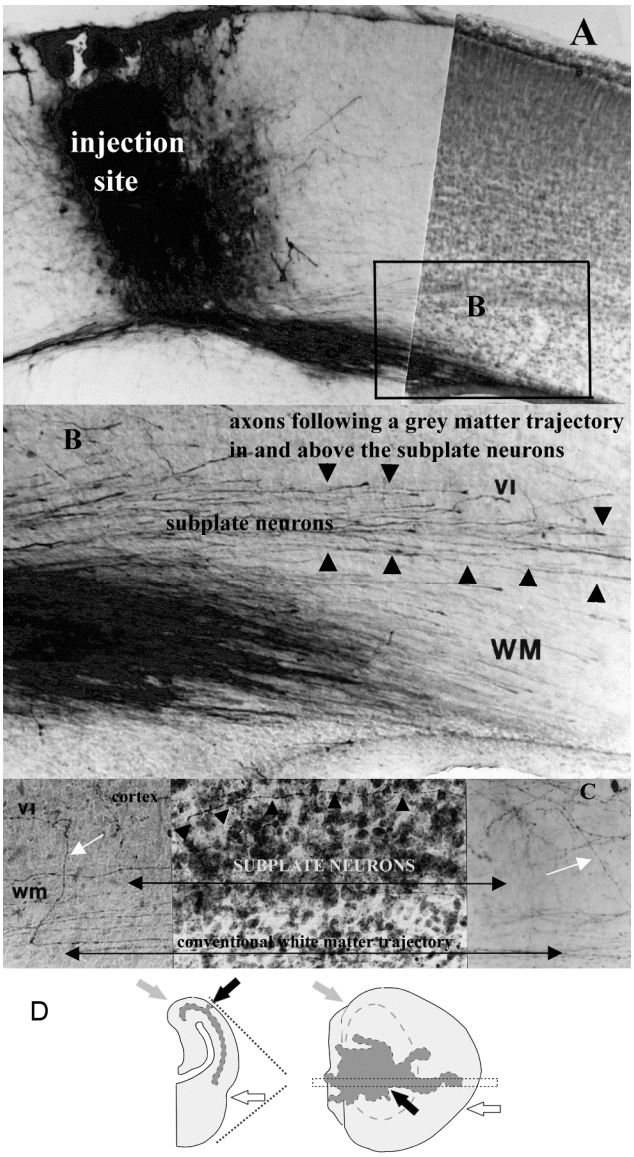

Figure 3.4. Representative injection site, axon travel in tangential substrates and initial reconstruction procedure. (A) Photomicrograph of a biocytin injection site spanning the cortical layers and avoiding the white matter at age P4-5 (injected-recovered). Note that this figure depicts a relatively large injection site, shown here to best illustrate axons traveling in the various tangential substrates. (B) High power photomicrograph of area outlined in (A) depicting axons coursing through the cortex, the infracortical fasciculus, and the subplate, as well as in the conventionally identified white matter. (C) Although some axons travel within the subplate neurons (visible in the Nissl-stained middle panel of the photomicrograph), others clearly avoid

this substrate (small black arrows). Arrowheads in B and C delineate the upper boundaries of the infracortical fasciculus (top), the subplate neurons (middle) and the conventionally identified white matter (bottom). Scale bars are approximately 100 μm. (D) Graphic depicting the method by which coronal tracings of axons are mapped onto unrolled dorsal views of the cortex, with the standard dorsal view superimposed in gray on the unrolled cortex. Unrolled cortex includes cortical areas ventromedial and ventrolateral to flexures and thus hidden in a standard ("rolled") dorsal view. Gray arrows indicate the medial point of flexure in both views; open arrows point to the rhinal fissure. Black arrows in both (A) and (B) indicate the site of the injection in a P0-1 animal (#675.1). Images in this figure were produced using digitally scanned negatives (1200 pixels per inch resolution on a flatbed scanner) processed using PhotoShop software (Adobe, Mountain View, California) to optimal contrast and sharpness, then cropped and lettered. No other adjustments were made.

For initial contrasts of differences in axon outgrowth patterns across the cortical surface, injection placement was assigned to one of three broad categories: "anterior" (presumptive motor), "middle" (presumptive somatosensory) and "posterior" (presumptive visual) cortex (Table 1). The assigned divisions take into account the location of anterograde and/or retrograde labeling found in thalamic regions as well as the position of the axons in the developing cortex. Tracer was typically deposited at each site throughout the layers of the cortex, avoiding the white matter; injections sites were very small compared to the dimensions of the primary cortical areas (Figure 3.4). The topography of axon extension in each tangential substrate, topography of extension within the cortex as a function of injection site and age, variations in trajectory patterns, and changes in the relative density of projections across ages were all quantified and contrasted.

3.5.2 Paths of Axon Extension. The greatest numbers of intracortically confined projections are local, extending in a radial fashion for short distances in the gray matter directly adjacent to the injection site. Longer-range projections traveling away from injection sites take multiple paths, coursing through the conventionally identified gray matter, the infracortical fasciculus, and among the subplate neurons, as well as in the white matter itself (see Figure 3.4B). In these small brains, axons reaching the most distant point from the injection site might equally be found traveling through the cortex or through subcortical white matter -- the route taken by an axon, within grey matter or white matter did not dictate the distance traversed. Although this study traces the distribution of a population of labeled axons, the trajectories of individual axons were noted when they could be followed. Some of the individual axons that could be traced from injection site to growth cone or terminal arbor traveled exclusively in one substrate, others switched pathways, for example, from the infracortical fasciculus to the white matter, avoiding the subplate (Figure 3.4C); or alternated travel between two substrates.

3.5.3 Overall axon extension by region, lamina and postnatal day. The mean of the available neural area in each substrate covered from the injections (expressed as a percentage of total dorsal cortical area) is as follows: cortex mean: 61.21%, SE: 3.24, white matter mean: 38.09%, SE: 3.16; subplate mean: 32.34%, SE: 2.59; infracortical fasciculus mean: 30.53%, SE: 2.97 (Figures 3.5 and 3.6). Thus, these small tracer injections resulted in extensive axon spread in the cortex, and insofar as it was possible to rank injection sites by size, the only difference associated with injection size was projection density, not extent.

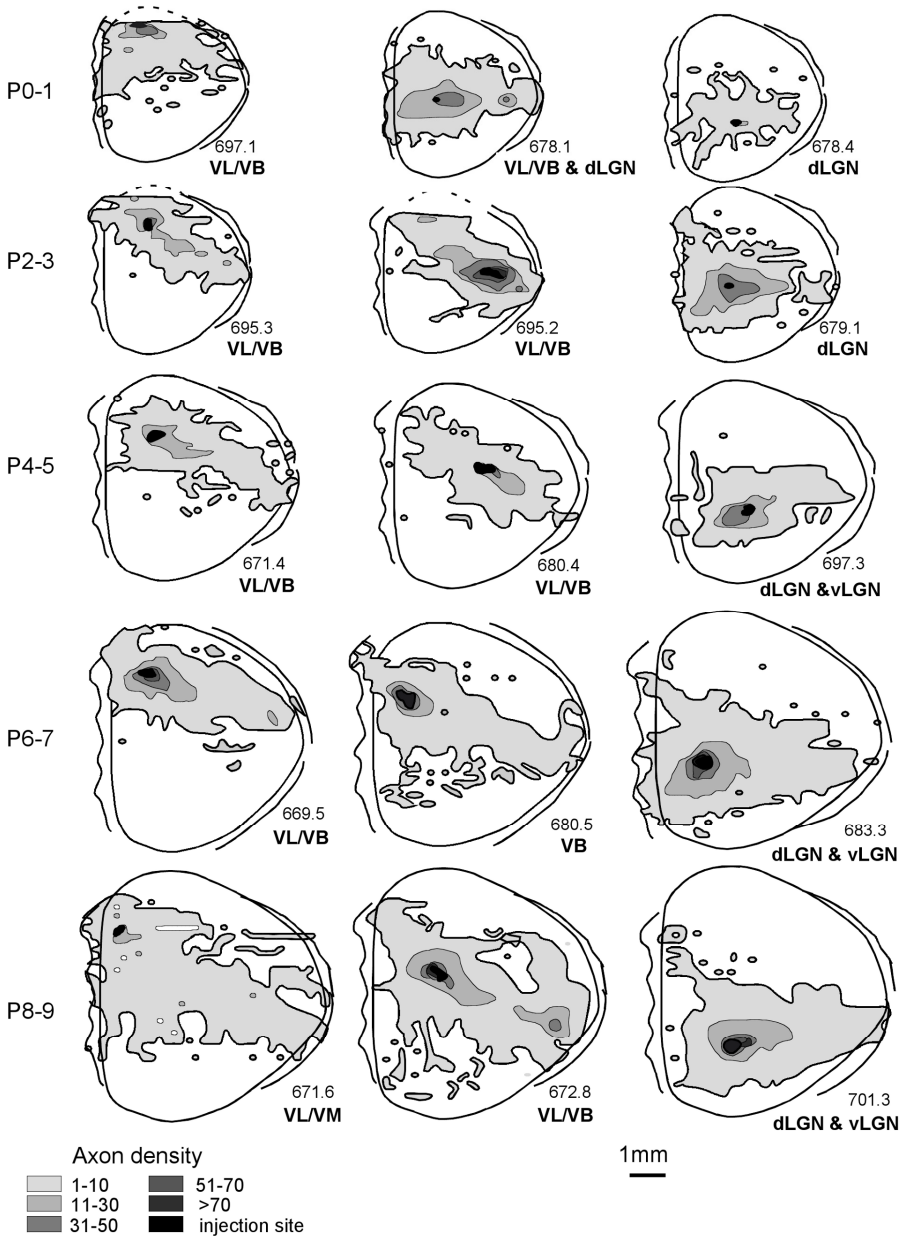

Figure 3.5. Axon extension in gray matter across early ages. Dorsal views depict representative axon extension in 15 cortices across the different developmental ages included in this study. For this figure, the three tangential substrates that make up the conventional rodent gray matter (subplate, infracortical fasciculus, cortex) are collapsed into one compartment. The abbreviations below each animal indicate the thalamic areas in which anterograde and/or retrograde labeling

was noted. Abbreviations: dorsal lateral geniculate nucleus, dLGN; ventrobasal nucleus, VB; ventrolateral nucleus, VL.

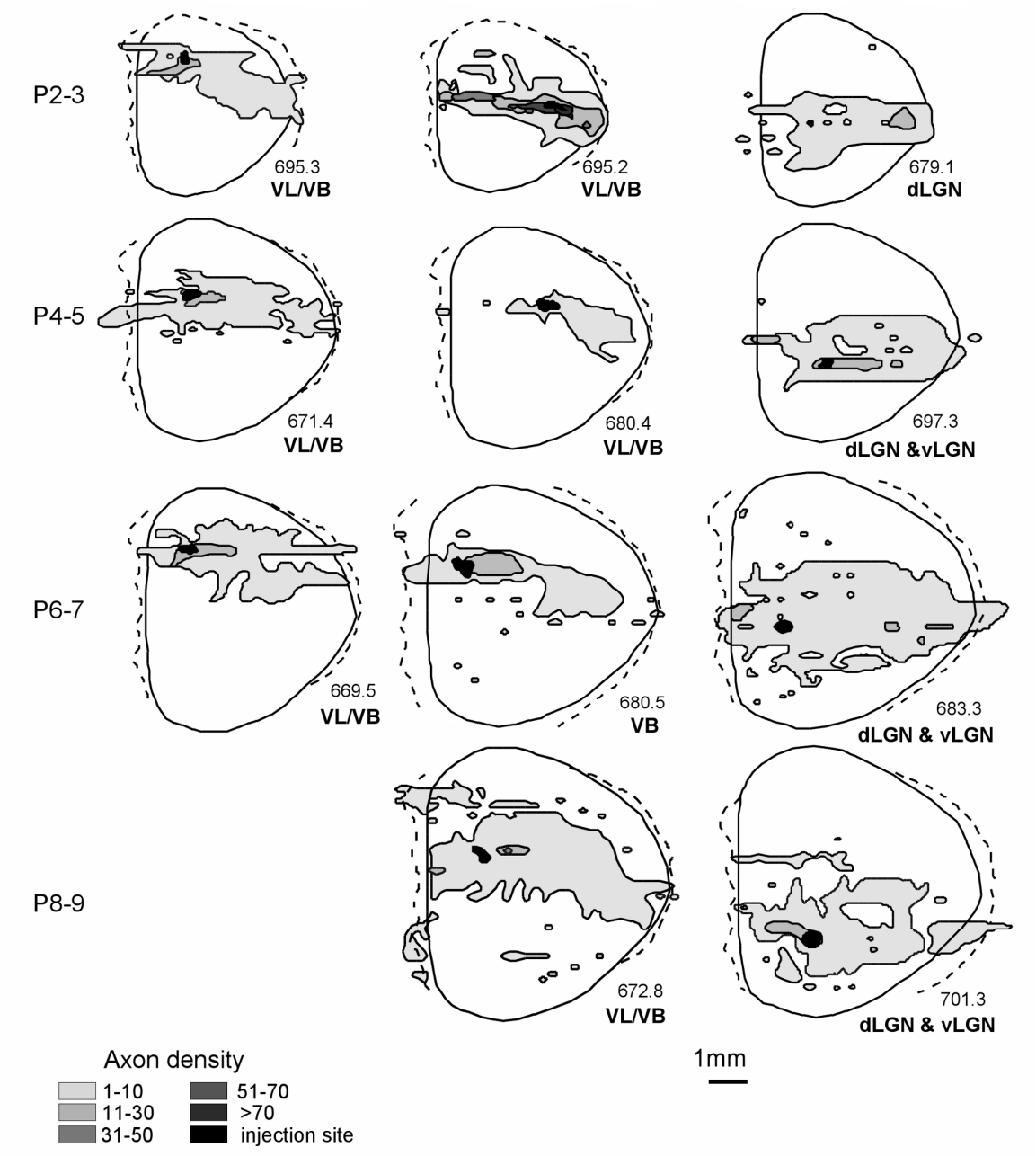

Figure 3.6. Axon extension in white matter. Dorsal views depicting representative axon extension in the white matter of the same animals depicted in Figure 3.5.

Even at the earlier age, connections from each site span almost the entire medial/lateral (M/L) distance of the cortex; this coverage persists as total cortical area more than doubles between ages P0-1 and P8-9 (Table 2). This widespread axon extension, evident across all locations, is illustrated in the dorsal reconstructions depicted in Figure 3.5. Because extension within the subplate and infracortical fasciculus was always less than extension within the cortex itself, in Figure 3.5 these three divisions are collapsed into one "gray matter" compartment. Qualitative inspection and statistical analyses indicate no significant differences in axon coverage from any site (anterior, middle or posterior) at any postnatal age, when total area of coverage was expressed as a percentage of total cortical area, regardless of the substrate of axon extension.

Tracer placements that happened to bridge more than one cortical area, as judged by retrograde labeling of both primary visual and somatosensory thalamic nuclei, might be expected to produce larger ranges of axon travel if each cortical area specifies a unique list of termination addresses, as contrasted with a model of initial axon outgrowth independent of cortical area identity. Though the number of cases we could use to address this question is small, examination of the area of cortex labeled by tracer injections in the several cases that resulted in retrograde label to both somatosensory and visual thalamic nuclei (45.0%, n=3, across ages) compared to injections that labeled either one or the other class (70.2%, n=7, across ages), however, showed the opposite, though non-significant trend.

Despite the general similarity of widespread coverage patterns from P1-P9, some local patterns were evident. As illustrated by the gradient outlines in Figure 3.5, long-range connections from anterior cortex extend asymmetrically posterior and laterally towards middle

cortex, not colonizing far posterior cortex. Axons labeled by injections in middle cortical areas appear reciprocally focused on anterior cortex with few posterior projections. The majority of developing intracortical projections from posterior cortex is confined to the posterior cortex itself, although from all sites a number of axons typically extend to presumed medial limbic regions.

3.5.4 Axon extension and trajectory changes in the white matter. Axon travel in the conventionally recognized pathway, the white matter, is summarized in Figure 3.6. Travel in the white matter is more confined than travel in the overlying substrates, and more anisotropic, as shown by a comparison of the axon coverage in Figure 3.6 to the outlines of axon coverage in the collapsed views illustrated in Figure 3.5.

Because intracortical axons travel in large numbers through the cortex as well as the conventionally identified white matter, these schematized dorsal representations of axon populations do not distinguish axons traveling intracortically from those which exit the cortex, travel in white matter, and re-enter cortex to terminate. The generally uniform picture of axon extension that the dorsal view reconstructions suggest is perhaps at odds with the presence of a large number of abrupt trajectory shifts in axon tracks which might suggest alteration axon extension by detection of an areal boundary (e.g., Figure 3.4C, left). Trajectory shifts in white-matter axons might indicate regions of cell-to-substrate recognition that specify unique termination zones. For the two distributions which most strongly suggested the development of a particular termination focus, one early and one late in development, we charted every axon that turned from a horizontal trajectory to travel vertically (Figure 3.7). The locations of abrupt

trajectory shifts populated the entire area of extension, however, producing a distribution that was simply a reduced form of the overall distribution. This pattern is more suggestive of random sampling of the substrate by the axon population prior to target selection (Bastmeyer et al., 1998; Bastmeyer and O'Leary, 1996). Overall these relatively uniform distributions resemble those seen in studies which reconstructed single-axon termination patterns within single areas in larger brains (White and Fitzpatrick, 2007).

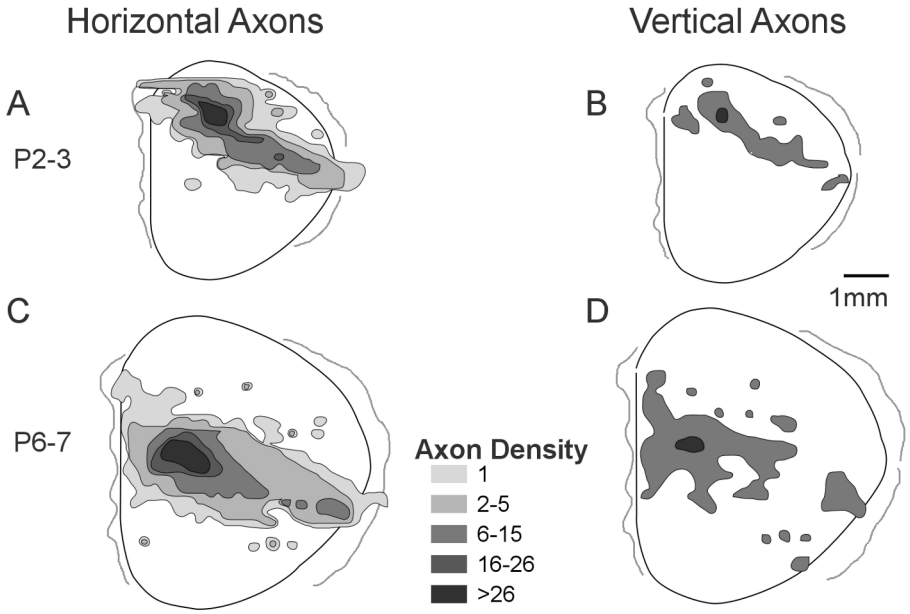

Figure 3.7. Vertically-turning axons. Comparative views of axon extension in cortex including gradients of only those axons extending horizontally and parallel to the white matter at ages P2-3 (A) and P6-7 (C) together with outlines of areas where vertically-oriented axons extending perpendicular to the white matter were found at each age (B and D). Outlines are representative of projections patterns found even at early ages in which labeled axons are found in areas both continuous and non-contiguous (possible target) with the injection site.

3.5.6 Synopsis of typical outgrowth pattern. Given the empirical observations above, we characterize the typical outgrowth pattern as having the following features: (i) having areal coverage larger than half of the cortical hemisphere; (ii) comprising axons travelling in both the white and gray matter which traverse comparable distances; (iii) having a footprint with greater extent along the ML axis than along the AP axis, with travel in the white matter being comparatively more constrained in this regard; (iv) being largely independent of the location of its source. With these features in mind, we developed the following framework to arrive at a quantitative description.

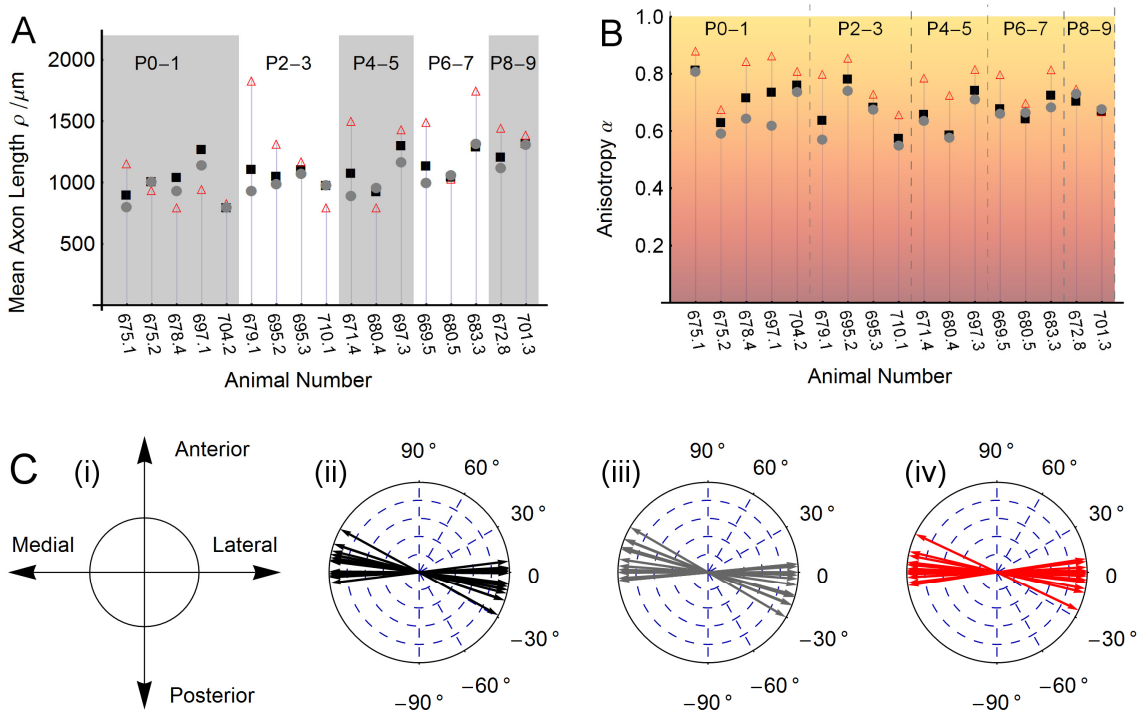

Figure 3.8. Fitting axon distributions. (A) The fitted mean length of an axon in the collapsed (black squares), cortex (gray dots) and WM (red triangles) outgrowth distributions for each animal (assuming a gamma distribution with shape parameter equal to 2). (B) Measured anisotropy in the collapsed (black squares), cortex (gray dots) and WM (red triangles) outgrowth

distributions for each animal. We note that white matter axons travel more anisotropically than those traversing gray matter. See Figure 3.1 and the Methods section for details of our approach to quantifying anisotropy in the measured distributions. (C) Preferred direction of travel. (i) Orientation of our coordinate system relative to the anterior/posterior and medial/lateral axes of the cortical hemisphere. The preferred axis of axon travel, shown here for each animal's (ii) collapsed, (iii) cortex and (iv) white matter distributions tends to align closely with the ML axis.

3.5.7 Modeling outgrowth distributions. Probability densities for the angular and radial components, denoted $q(\theta;\alpha,\eta)$ and $p(r;\rho)$, respectively, were fitted to the observed outgrowth distributions. The resulting values of the characteristic length ρ, anisotropy α and tilt η for each dataset are shown in Figure 3.8, and can be summarized as follows.

The radial distribution shows a marked departure from uniformity (see Figure 3.8B). The measured values of anisotropy α for collapsed distribution have mean 0.69 and standard deviation 0.07 on our 0 to 1 scale (see Supplementary Figure 3A.2 for fits to data). There is a clear tendency for white matter distributions to be more anisotropic ($\alpha^{WM} = 0.78 \pm 0.07$) than distributions measured only in the cortex ($\alpha^{Ctx} = 0.66 \pm 0.07$). The tilt η is such that the preferred direction of travel is almost collinear with the ML axis, as illustrated in Figure 3.8C ($\eta^{Coll} = 7° \pm 10°$).

The length distribution of axons in the white matter, gray matter and collapsed distributions were well fit by gamma distributions (see Supplementary Figure 3A.1 for fits to data), with mean lengths as shown in Figure 3.8A. There is a tendency for distributions measured in older animals to be longer and for white matter axons to travel greater distances. Taking the

ratio ρ^{WM} / ρ^{Ctx} for each animal, we find that ρ^{WM} is on average 119±33% as long as ρ^{Ctx} - indicating a trend of axons travelling in white matter reaching further than those traversing cortex only. This greater length is not incompatible with the lesser areal coverage of white matter axon distributions; travel in this compartment was also noted to be more anisotropic and therefore has a more slender footprint.

3.5.8 Spatial network modeling. We sought to create a model of the early cortical network which was faithful both to the qualitative characteristics and the measured distributions of axon outgrowth. We also wanted the nodes of this network to be biologically meaningful but representing neurons as individual nodes would have made our model computationally unwieldy. We instead take our nodes to be cortical populations or units, comprising all the neuronal cell bodies and local processes within a small volume of the cortical sheet, much like the "cortical output units" of Innocenti and Vercelli (2010). We define these units as 100μm×100μm squares on a 2-dimensioal cortical sheet, so that they have roughly the dimensions of a dendritic arbor. Hence our "local" length-scale is set at ~100μm. The number of nodes is thus conducive to constructing and analyzing our simulated networks on a desktop computer.

The simulated networks are found to have the small world property but are not scale free. The small world index is measured to be 4.57±0.17, indicating our networks possess short path lengths comparable with those of random networks while also having far higher clustering. This may have been anticipated given the form of the axonal distributions employed, which have a preponderance of local connections and relatively few long links. The networks are not in the class of so-called scale-free networks, with neither their in-degree nor out-degree having the

required power-law distributions. The out-degree is, by construction, the same for every node and is equal to the bespoke number of efferent axons per node, n_{axons}. The in-degrees are in close agreement with those for a random network, only differing slightly from the Poisson distribution one would encounter in that case. We can see why such an in-degree distribution arises: if we ignore boundary effects, then nodes attract afferent axons with a probability proportional to the area of their respective Voronoi cells, the polygons in the plane enclosing all points to which a given node is the closest node. Given our method of distributing nodes in the plane, the preponderance of Voronoi cells not adjacent to borders will have area comparable with that of our 100μm×100μm grid squares. Such nodes therefore attract afferent edges with approximately equal probability, thus giving rise to the observed narrow, near-Poisson distribution of in-degrees.

3.5.9 Anisotropy of axonal distributions: consequences for efficiency, robustness and modularity. Anisotropy in axonal distributions may lead to a more volume-efficient wiring scheme but would seem, prima facie, to entail negative repercussions for the resulting network structure. Given that increased anisotropy in laying down axons leads to a smaller ensemble of possible networks (to see this consider the limiting case where axons are restricted to travel along only one axis), we were curious as to what advantages it might bestow. While investigating the effect of varying anisotropy α on the topology of simulated networks, we also sought to determine whether increased α might lead to a more compact packing of axons in space. We begin with the observation that an axon's length, and thus its volume, is increased if it

must deviate to avoid another axon (see Figure 3.3). Therefore, encounters with other axons tend to increase the total volume requirement.

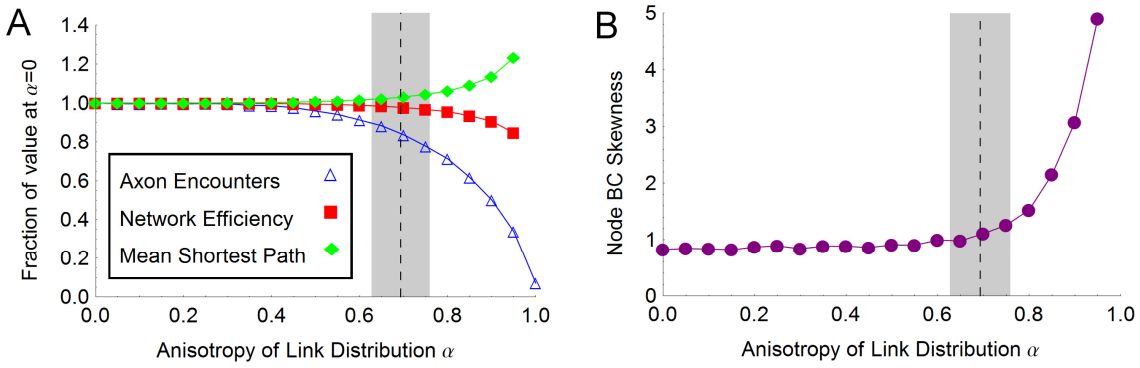

Figure 3.9. Effect of anisotropy. (A) Packing volume and network paths. In our simulations increased anisotropy α leads to a reduced number of axons encouters but also a decrease in network efficiency E and an increase in mean shortest path length l. The dashed line marks the mean empirical value of α for collapsed axon distributions and the extent of the shaded region indicates the standard deviation in that quantity. Each data point is the average result for 10 networks, each generated with $N = 2500$ nodes, having $n_{axons} = 10$, drawn from under a distribution having anisotropy as indicated and length distributed as a gamma-2 distribution with average length 1000µm. (B) Node betweenness centrality. Increased anisotropy α leads to an increased right-skewness in the distribution of node betweenness centrality in the generated networks. The dashed line and shaded region, respectively, denote the mean and standard deviation of the empirical values for α. These data were generated using the same network parameters as in (A). See also Supplementary Figure 3A.3 for a comparison of the histograms of the betweenness centrality distribution at $\alpha = 0.2$, $\alpha = 0.7$ and $\alpha = 0.9$.

Our spatial network model predicts that there exists a narrow range of values for the anisotropy parameter α which reduces the extra volume requirement of crossing axons without significantly impacting the ease of communication within the network, as measured by the efficiency E (see Figure 3.9A). Increasing the anisotropy beyond this range is predicted to reduce

network efficiency. We find that the empirically measured values of anisotropy fall within this range for both white matter and gray matter travel.

Increased anisotropy may lead to networks which are more vulnerable in the case of central nodes failing. The presence of such nodes is indicated by a more skewed distribution of node betweenness centrality (see Figure 3.9B; also Figure 3.S3 for histograms of betweenness centrality distributions). The betweenness centrality b_i of the node i quantifies the relative contribution of individual network elements to the collection of shortest paths on the network (see Figure 3.10). Conversely, it can be seen as a measure of how detrimental the removal of that element might be to the functioning of the network as a whole. We observe that increased anisotropy in the spatial distribution of links leads to an increased positive skew in the distribution of node betweenness centrality in simulated networks (Figure 3.9B). The right tail of the distribution becomes increasingly "heavy", signifying the emergence of a small number of nodes with betweenness centrality much higher than the average value. As studies in other complex networks have shown (Albert et al., 2000), the existence of such highly central nodes renders the network as a whole more vulnerable to functional disruption in the event of their failure. It is also the case, however, that communication on such a network is more robust to the failure of a typical node, i.e. one which is not among the few highly central nodes.

The possibility of nodes becoming overloaded may be another reason to disfavor highly anisotropic wiring schemes. Assuming that information is propagated along the shortest paths between nodes, betweenness centrality can be interpreted as a measure of how much traffic a node handles. Given the finite neural populations comprising our nodes, they will have a limited capacity to process or propagate information. Hence, with highly anisotropic wiring, nodes

which are very central may be at risk of becoming overloaded, thereby affecting the reliability of communication on the network.

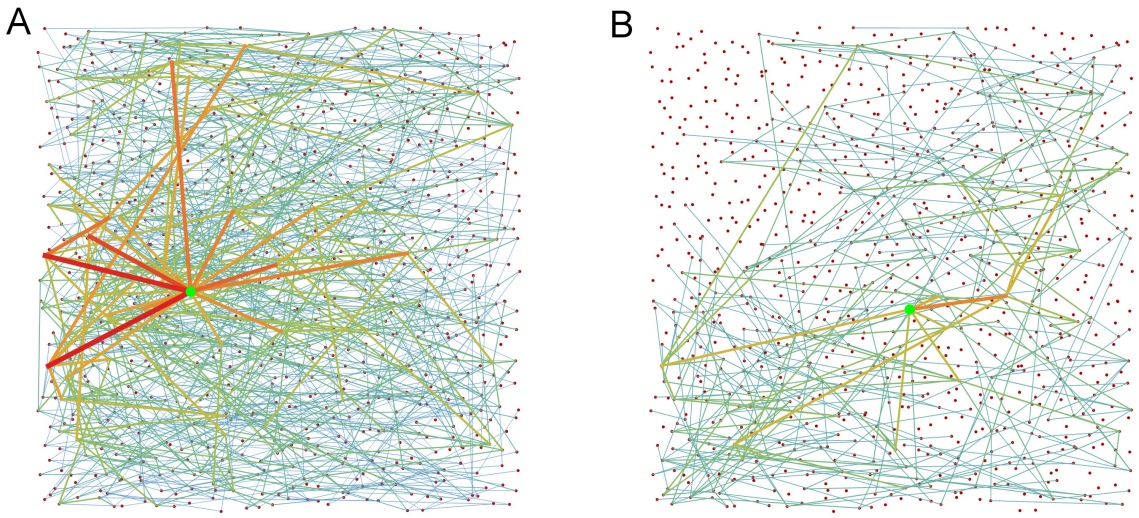

Figure 3.10. Contrasting nodes of high and low node betweenness centrality on the same network. (A) and (B) each show a different subset of the shortest paths on the same network. In (A), the node on the graph with the highest betweenness centrality is marked by the green dot. All the shortest paths which travel through that node are shown. Almost 1.5% of this directed graph's $N(N-1)$ paths pass through the node. The edges used by these paths have color and thickness reflecting the number of paths traversing that edge. By contrast, (B) shows a node of lower betweenness centrality which is on less than 0.1% of the network's shortest paths. The network has $N = 900$ nodes, $n_{axons} = 5$, average axon length 800 μm and $\alpha = 0.65$.

Looking at the modularity of our networks as anisotropy is increased, we observe that partitioning the network into communities aligned with the medial-lateral axis of our grid is increasingly favored over choosing communities aligned perpendicular to that axis (see Figure 3.11). This may favor a layout in which more strongly connected and functionally related cortical areas have that same axial alignment. We investigated modularity with respect to partitioning the

nodes into 4 spatially defined communities: first, communities which were (approximately) equally-sized rectangular blocks of nodes, aligned with the medial-lateral axis; second, a similar arrangement but with the rectangular blocks now parallel to the anterior-posterior axis. In both cases, the preponderance of short links, which leads to spatial clustering, ensured that our networks were more modular than the comparable network wired uniformly at random. However, the modularity was seen to increase significantly with anisotropy for the medial-lateral partitioning while decreasing for the anterior-posterior partitioning.

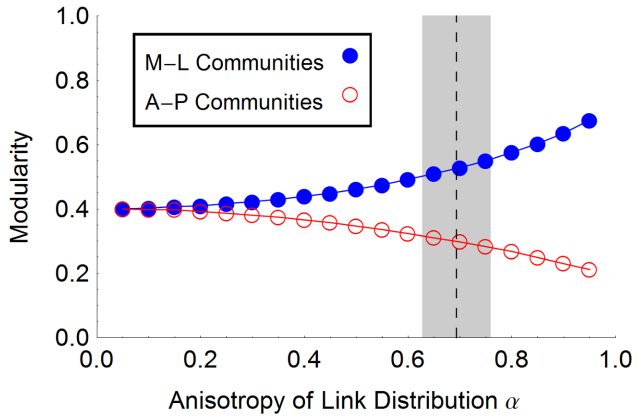

Figure 3.11. Modularity versus anisotropy of axon outgrowth. For the range of anisotropy values, we calculated the modularity of our networks with respect to two different community assignments. Assigning nodes to 4 approximately equal rectangular blocks, spanning the medial-lateral extent of our model cortex and having height equal to one fourth of the anterior-posterior extent, we see that modularity increases with anisotropy. However, using a partitioning which assigns nodes to communities extended along the anterior-posterior axis instead, we observe a decrease in modularity. In both cases, the networks are more modular than the comparable randomly wired network. This is because the prevalence of relatively short edges in our networks leads to clustering among nearby nodes in either set of communities.

3.6 Discussion

The neuroanatomical results we present in this paper show a surprising independence between the early patterns of axon outgrowth and the cortical region of their origin. In these small brains, axons extend to the limits of their growth through the cortex itself, and also in the white-matter tracts under the cortex. There is no obvious variation in axon "behavior" between axon populations arising from sites of origin near cortical boundaries, and axons traversing future borders of cortical areas. Axons originating from delimited regions cover a third to a half of the entire cortical area. The network model of cortical connectivity inferred from these outgrowth distributions suggests that at this scale the cortical network has a high small-world index and is not scale-free but rather has both in- and out-degrees which are narrowly distributed ("single-scale"). Our spatial model suggests that the unexpected anisotropy of initial axon outgrowth may represent a partial solution to the problem of minimizing the volume requirement of cortical connections while simultaneously maintaining network efficiency.

Reduced network efficiency has straightforward interpretations in the context of neural networks, where a primary goal is the cost-effective and timely exchange and integration of information. Increased average path lengths, too, can serve only to incur higher costs and error rates in propagating information on the cortical network. Further, the increasingly right-skewed distribution of node betweenness centrality with increased anisotropy in axon travel hints at yet another potential constraint: highly central nodes render the network liable to suffer a marked increase in path lengths in the event of their failure or overload. Clearly, some trade-off must

exist between these deleterious effects and any benefits arising from reduced wiring volume. We do not know what relative weights one should assign to such costs and benefits in order to achieve the optimal trade-off. However, our results suggest that the axonal patterns recorded in this study may achieve such a balance. Further, there is evidence that different mammalian orders may have evolved disparate solutions to the problem of supporting and connecting increased numbers of neurons in the neo-cortex (Herculano-Houzel et al., 2006; Herculano-Houzel et al., 2007). Anisotropy of axonal outgrowth patterns may be just one aspect of the various strategies available to taxa in solving this problem.

We suggest that two features of the outgrowth patterns described here may contribute to the layout of the cortex: highly central nodes in this developing cortex may seed future hub regions and modularity may favor certain spatial layouts for cortical areas. Regarding the former, one possible effect of a skewed node centrality distribution is to distinguish potential future hubs in our network of cortical units. Although network hubs typically have higher-than-average degree, the degree statistics of our nodes are narrowly distributed and uniform across 2-dimensional space. This is in contrast with reports of broader degree distributions in the adult cortical network (Sporns et al., 2007). However, in our model networks, nodes with high betweenness centrality begin to appear as anisotropy is increased. Such nodes are uniformly distributed in space, but may provide seed sites for the emergence, in interaction with activity from sub-cortical projections, of structural network hubs, and for a broader distribution of node degrees (Modha and Singh, 2010; Hagmann et al., 2008). As development proceeds, elevated centrality may lead activity at such sites to be correlated with that at distal regions of the cortex, leading to increased persistence of afferent projections. Secondly, we observed that the

modularity of our networks favors the formation of communities which extend parallel to the medial-lateral axis. The overall layout and separation of sensory and motor modalities in the cortex is established by the embryonic polarization of the cortical sheet (Fukuchi-Shimogori and Grove, 2001). That polarization may enable the emergent modularity of the cortical network we have modeled. Later in development, this modularity may itself guide the formation of features of cortical network structure.

In this study, we have only examined the connectivity structure "implied" by the pattern of axon outgrowth also making the assumption that an axon has exactly one arbor, occurring at the extent of its travel. We have neither demonstrated that synaptic connections have been made by these axons at the limits of their extents, nor that the connections are permanent. Axon tracing studies have demonstrated that a typical axon may branch once or more and may have arbors at sites other than its most distal arbor (Zhong and Rockland, 2003). As to the effects of such limitations in our approach, we expect the measured anisotropy of outgrowth to be largely unchanged (assuming that branches of the same axon proceed independently). The length distributions we have fitted, however, will have under-represented axon ramifications at shorter lengths. The effect of including more ramifications at shorter distances from the neuron's cell body would be to further increase the modularity and clustering (and hence, we expect, also the small-world index) of our networks.

Our network model presents a reduced representation of the cortical network by taking as its nodes "cortical units" rather than the greatly more numerous constituent neurons – an approach consistent with the notion, presented in several studies, that it is appropriate to consider computational units having the scale of, for example, ocular dominance columns (Innocenti and

Vercelli, 2010). Implicit in our model, however, is the further assumption that cortical connectivity at this intermediate scale can also be usefully depicted using a representative sample of "edges" far smaller in number than the axonal connections they hope to mimic. The cross-comparability of neural networks sampled at different scales and resolutions is a topic of current interest in the neuro-imaging community (Zalesky et al., 2010).

We note that travel in the white matter as measured in this study is only slightly longer than the cortex-only travel. For this reason, our network model contained only one class of links, modeling all axons as identical. From the empirical data it is clear that axons traversing the gray matter alone can span the cortex. However, while the axons travelling in the white matter are not very much longer than their gray matter counterparts, they do represent a significant portion of the total axon population. This fact suggests these axons, with their capacity for faster and more reliable spike propagation, bestow some functional advantage even in a small brain. Further, this length mismatch could suggest that the size of the hamster cortex lies near an upper limit for what can be spanned by gray matter axons alone.

Our model is easily extended to accommodate two (or more) classes of axon. One could, for example, employ a short class, to mimic unmyelinated axons having a reach less than the dimensions of the cortex, and a longer class, representing connections having a length-scale comparable with the extent of the cortex. In this manner our model may elucidate the empirically observed scaling of white matter volume with increased cortical size (Zhang and Sejnowski, 2000). This will necessitate deciding on some minimum threshold for network performance (in terms of efficiency, shortest path lengths, or similar), and then finding the possible distributions and number of white matter connections required to achieve that standard.

In conclusion, our goal was to succinctly capture the salient features of the empirically-measured initial outgrowth distributions in a simple model with a minimal number of parameters. Such a concise model, having a small parameter space, is well suited to exploring the developmental implications of changes in these parameters. Ultimately, we would like to test our model's predictions for connectivity in larger cortices, thereby gaining insight into how developmental programs have evolved to achieve efficient communication in larger mammalian brains.

Acknowledgements

We are grateful to Lawrence J. Cauller for advice during the initial stages of this study, and to Michael L. Anderson for his advice on a draft of this manuscript. Dipti Prasad, Michael Lipan, Mikhail Spektor, Mike Parsons, Anita Sung, Evan Bloom and Nicole Florance contributed to data collection and initial analysis, and Jeremy Yost provided technical support.

APPENDIX 3A

SUPPLEMENTARY INFORMATION FOR

CHAPTER 3: NETWORK STRUCTURE IMPLIED BY INITIAL AXON OUTGROWTH IN RODENT CORTEX: EMPIRICAL MEASUREMENT AND MODELS

Supplementary Tables

Table 3A.1. Details animals, tracer injections and labelled subcortical nuclei (continued overleaf).

	Age	Animal	Pup weight	A-P Length	Label	Placement
1	PO-1	704.4	2.9 g	3420µm	VL, VB, PoM	anterior
2	PO-1	697.1	2.4 g	3540µm	VL, VB	anterior
3	PO-1	675.2	2.8 g	3600µm	MD, VL, VB	anterior
4	PO-1	678.3	2.6 g	3660µm	VL, VB, R	middle
5	PO-1	704.2	2.7 g	3720µm	VL, VB, R	anterior
6	PO-1	678.1	2.6 g	3600µm	MD, VL, VB	anterior
7	PO-1	678.2	2.8 g	3720µm	VL, VB, dLGN	posterior
8	PO-1	675.1	2.7 g	3480µm	R, L	posterior
9	PO-1	678.4	2.6 g	3600µm	VB, L, dLGN	posterior
10	P2-3	674.3	2.6 g	3300µm	VB	anterior
11	P2-3	695.1	2.8 g	3900µm	VB	anterior
12	P2-3	695.3	2.8 g	3420µm	VL, VB, L	anterior
13	P2-3	710.1	4.4 g	3720µm	VL, VB, L	middle
14	P2-3	695.2	2.8 g	3540µm	VL, VB, R	middle
15	P2-3	679.1	3.6 g	4020µm	dLGN, vLGN	posterior
16	P2-3	710.4	4.0 g	4020µm	dLG	posterior
17	P4-5	671.4	4.4 g	4560µm	VL, VB, R	anterior
18	P4-5	680.4	4.2 g	4140µm	VL, VB, R	anterior
19	P4-5	681.2	4.0 g	4200µm	-	middle
20	P4-5	694.3	4.2 g	4140µm	R	middle
21	P4-5	697.3	6.8 g	4080µm	PoM, L, dLGN, vLGN	posterior
22	P4-5	694.2	4.2 g	4140µm	VL, R	posterior

23	P6-7	680.5	7.4 g	4500µm	VB	anterior
24	P6-7	669.5	6.2 g	4980µm	VL, VB, R	anterior
25	P6-7	694.4	7.8 g	4720µm	VL, VB, PoM, R	middle
26	P6-7	683.1	6.4 g	5040µm	VL, VB, L	middle
27	P6-7	707.1	5.1 g	4620µm	VL, VB, R, L	middle
28	P6-7	683.3	7.2 g	5040µm	L, dLGN, vLGN	posterior
29	P6-7	669.4	6.5 g	4800µm	L, dLGN, vLGN	posterior
30	P6-7	708.2	7.4 g	5340µm	R, L, dLGN, vLGN	posterior
31	P8-9	671.6	9.1 g	4920µm	VL, VM	anterior
32	P8-9	672.8	10.8 g	5100µm	VL, VM, PoM	anterior
33	P8-9	679.7	10.8 g	5100µm	VL	middle
34	P8-9	692.4	7.9 g	4380µm	VL, VB, R, L, dLGN, vLGN	middle
35	P8-9	701.3	10.0 g	4980µm	L, dLGN, vLGN	posterior
36	P8-9	701.1	9.2 g	5160µm	R, L, dLGN, vLGN	posterior

Table 3A.1. Injections of anterograde tracer were made into three cortical regions: anterior (presumptive motor), middle (presumptive somatosensory) and posterior (presumptive visual cortex). Because some variability is evident in the A/P length of brains at similar early ages, we also list pup weight in grams. The Label lists only those putative major thalamic nuclei in which we have a great degree of confidence in identification at these ages; other nuclei were also labeled (see also Jones (1998)).

Abbreviations: dorsal lateral geniculate nucleus, dLGN; lateral nucleus, L; mediodorsal nucleus, MD; posteromedial nucleus, PoM; reticular nucleus, R; ventrobasal nucleus, VB; ventrolateral nucleus, VL; ventral lateral geniculate nucleus, vLGN.

Table 3A.2 Statistics of measured axon disctributions.

	Age	Animal	Placement	Total Area	WM	Cortex	Subplate	Fasc.
1	P0-1	697.1	anterior	17.4mm^2	56.1%	60.1%	39.0%	35.7%
2	P0-1	675.2	anterior	15.0 mm^2	23.1%	50.8%	20.9%	20.0%
3	P0-1	704.2	anterior	16.0 mm^2	25.1%	36.1%	12.1%	16.9%
4	P0-1	678.1	anterior	15.6 mm^2	58.3%	62.6%	50.4%	53.9%
5	P0-1	678.2	posterior	18.1 mm^2	21.2%	38.1%	19.5%	33.2%
6	P0-1	675.1	posterior	16.4 mm^2	50.2%	73.6%	49.6%	56.7%
7	P0-1	678.4	posterior	17.5 mm^2	23.4%	55.7%	31.9%	35.0%
8	P2-3	695.3	anterior	18.3 mm^2	48.2%	66.1%	30.8%	37.1%
9	P2-3	710.1	middle	16.7 mm^2	67.0%	79.4%	32.8%	33.5%
10	P2-3	695.2	middle	19.2 mm^2	49.4%	88.2%	36.6%	46.4%
11	P2-3	679.1	posterior	25.0 mm^2	35.4%	59.0%	39.4%	22.8%
12	P4-5	671.4	anterior	30.8 mm^2	32.0%	59.1%	23.1%	17.9%
13	P4-5	680.4	middle	31.4 mm^2	20.5%	53.8%	16.1%	16.9%
14	P4-5	697.3	posterior	28.6 mm^2	35.7%	40.6%	31.0%	10.8%
15	P6-7	680.5	anterior	35.9 mm^2	32.1%	50.9%	29.2%	22.6%
16	P6-7	669.5	anterior	40.2 mm^2	25.6%	71.3%	22.7%	24.9%
17	P6-7	683.3	posterior	44.6 mm^2	48.7%	52.2%	43.3%	29.1%
18	P8-9	672.8	anterior	39.6 mm^2	46.3%	81.2%	47.1%	48.0%
19	P8-9	671.6	anterior	37.2 mm^2	22.8%	73.4%	23.7%	14.8%
20	P8-9	701.3	posterior	35.7 mm^2	40.9%	71.8%	47.5%	33.6%

Table 3A.2. Statistical analysis was performed using these measurements from 20 pup brains and 2 adult brains. Total isocortical area is expressed in mm^2 and axonal coverage in each substrate is expresses as a fraction of total isocortical area. Abbreviation: white matter, WM; infracortical fasciculus, fasc.

Supplementary Figures

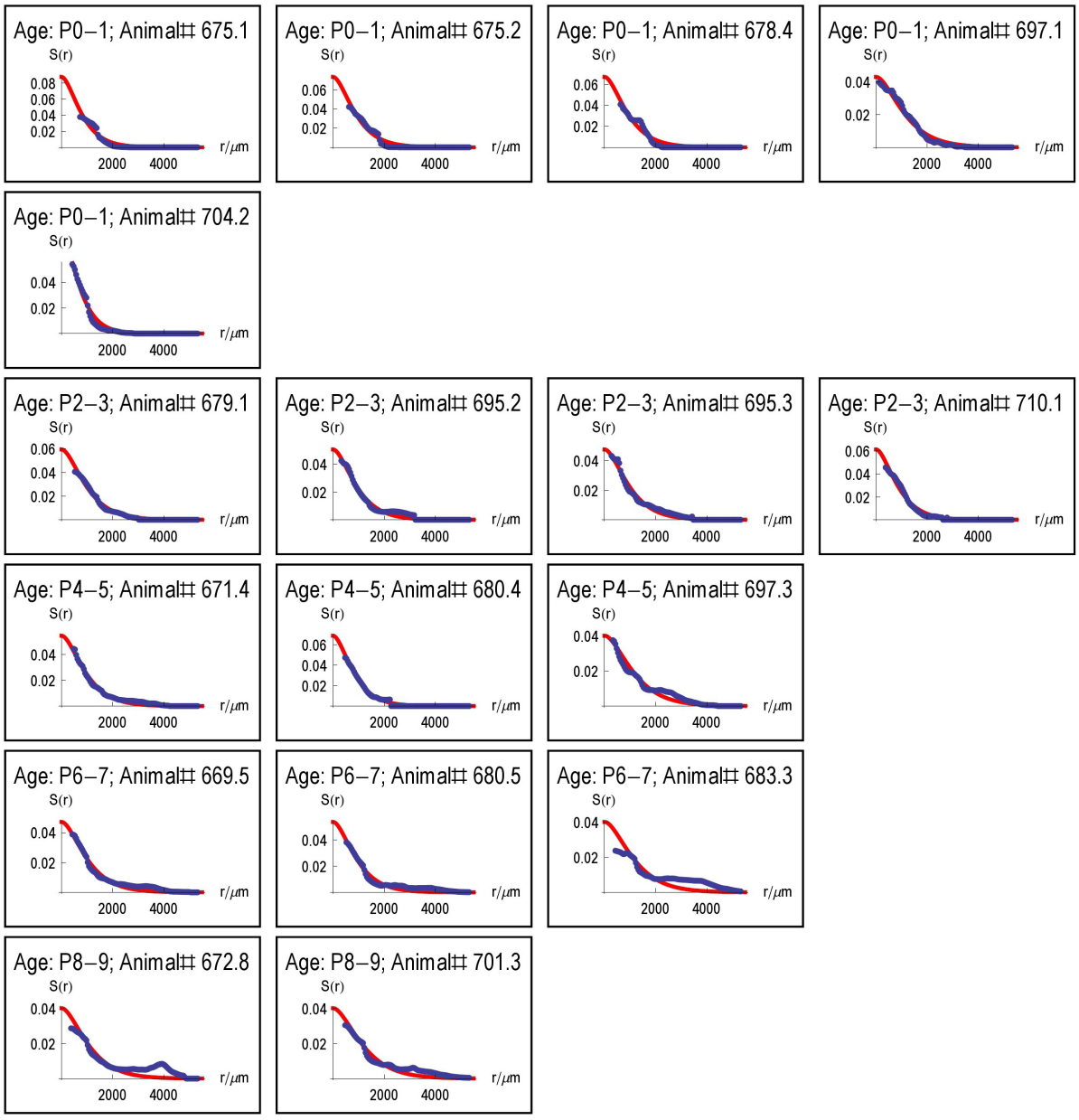

Figure 3A.1. Fits to data for the length distribution function. Shown here in blue is the empirically measured function $S(r)$ and, in red, our model, $n(1-C(r;\rho))$, where n is a normalizing constant and $C(r;\rho)$ is the cumulative distribution function of the gamma(2) distribution, $p(r;\rho)=\frac{r}{\rho^2}e^{-r/\rho}$.

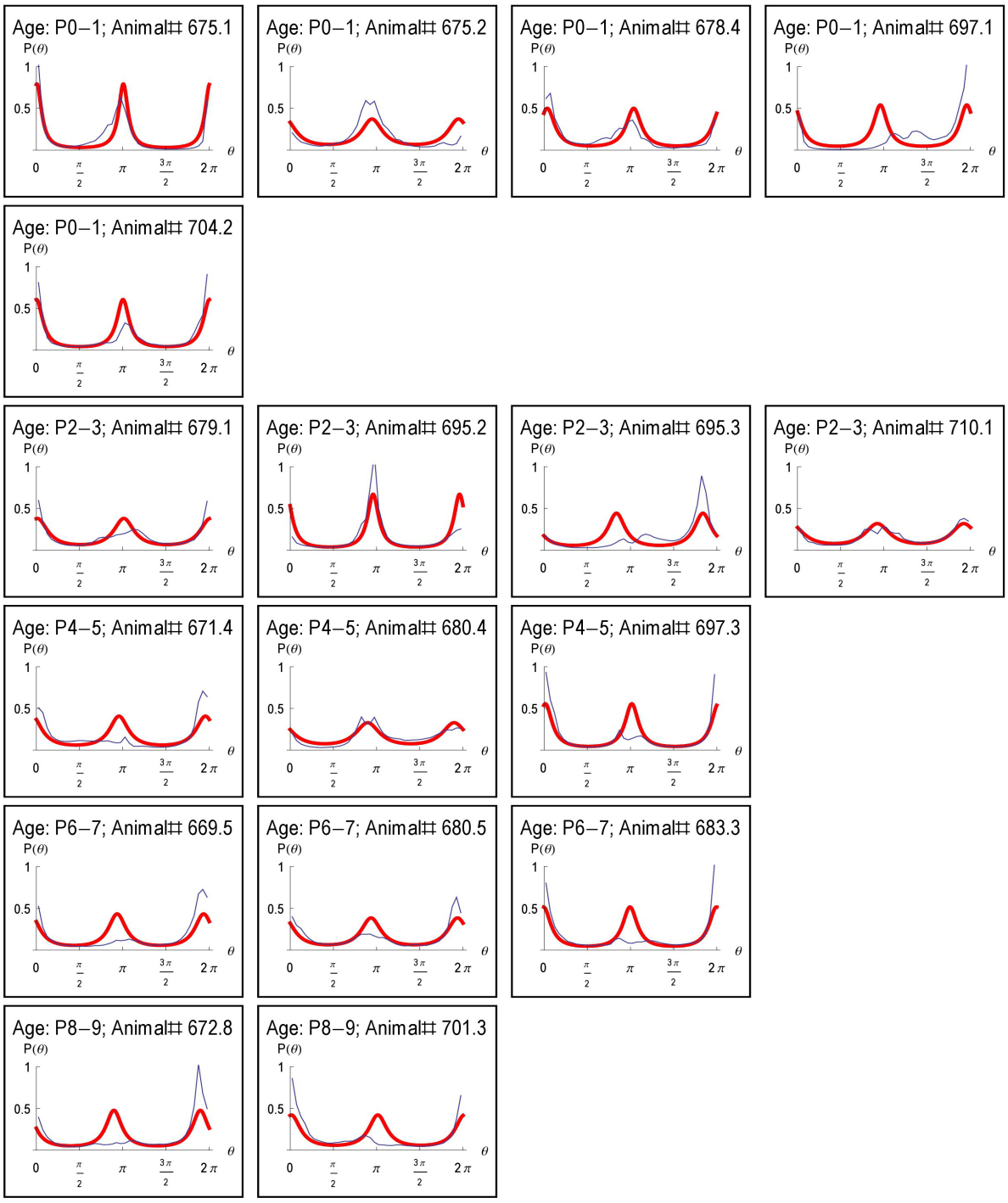

Figure 3A.2. Fits to data for the angular distribution function . Shown here in blue is the empirical function $\upsilon(\theta)$ and, in red, the fitted angular probability distribution $q(\theta;\alpha,\eta)$ for the

collapsed axon distributions. The parameter α ("anisotropy") determines the height of both peaks and η ("tilt") determines the location on the circle of the diametrically opposed peaks.

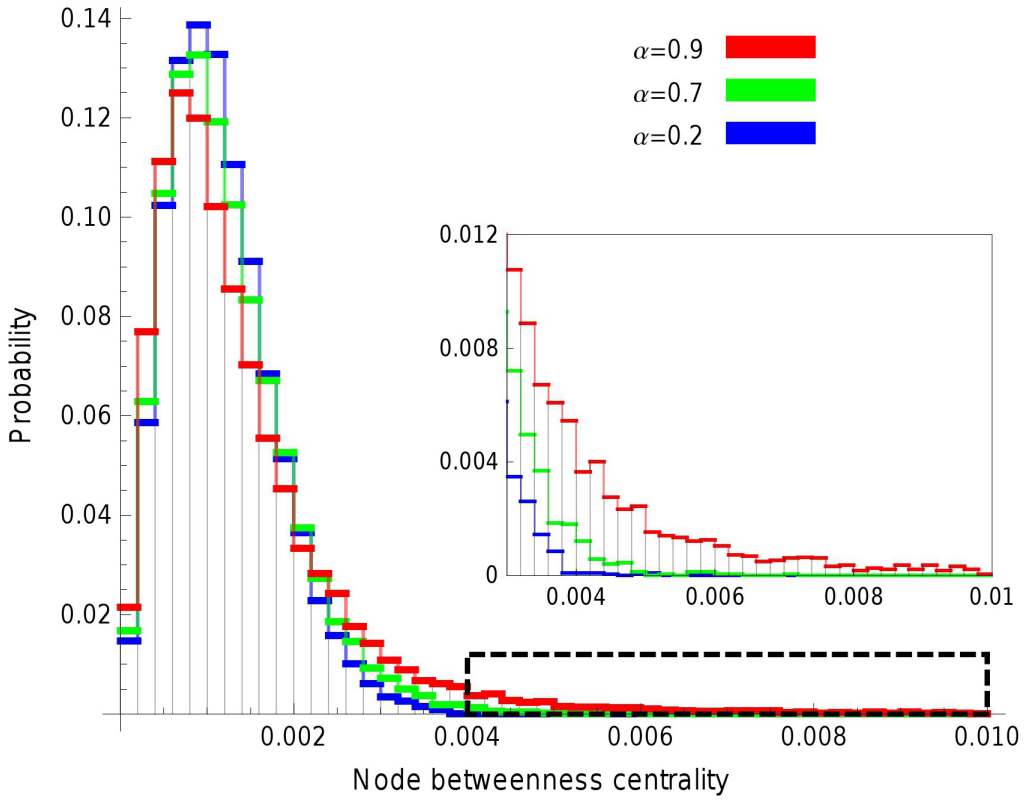

Figure 3A.2. Histograms of node betweenness centrality for several values of values of anisotropy α. The right tail of the distributions of betweenness centrality values is seen to become heavier with increased anisotropy α of the axon distribution. The inset provides an enlarged view of the area demarked by the dashed rectangle.

BIBLIOGRAPHY

Albert, R., Jeong, H., and Barabasi, A.-L. (2000). Error and attack tolerance of complex networks. *Nature* 406, 378–382.

Altman, J., and Bayer, S. A. (1995). *Atlas of Prenatal Rat Brain Development*. Boca Raton, Florida: CRC Press.

Anderson, M. L. (2010). Neural reuse: A fundamental organizational principle of the brain. *Behav Brain Sci* 33, 245–266.

Badre, D. (2008). Cognitive control, hierarchy, and the rostro-caudal organization of the frontal lobes. *Trends in Cognitive Sciences* 12, 193–200.

Bar, M. (2007). The proactive brain: using analogies and associations to generate predictions. *Trends in Cognitive Sciences* 11, 280–289.

Barone, P., Batardiere, A., Knoblauch, K., and Kennedy, H. (2000). Laminar Distribution of Neurons in Extrastriate Areas Projecting to Visual Areas V1 and V4 Correlates with the Hierarchical Rank and Indicates the Operation of a Distance Rule. *The Journal of Neuroscience* 20, 3263 –3281.

Bassett, D. S., Greenfield, D. L., Meyer-Lindenberg, A., Weinberger, D. R., Moore, S. W., and Bullmore, E. T. (2010). Efficient Physical Embedding of Topologically Complex Information Processing Networks in Brains and Computer Circuits. *PLoS Comput Biol* 6, e1000748.

Bastmeyer, M., Daston, M. M., Possel, H., and O'Leary, D. D. M. (1998). Collateral branch formation related to cellular structures in the axon tract during corticopontine target recognition. *Journal of Comparative Neurology* 392, 1–18.

Bastmeyer, M., and O'Leary, D. D. M. (1996). Dynamics of target recognition by interstitial axon branching along developing cortical axons. *Journal of Neuroscience* 16, 1450–1459.

Bayer, S. (1991). *Neocortical development*. New York: Raven Press.

Bayer, S. A., and Altman, J. (1991). *Neocortical development*. New York: Raven Press.

Beaulieu, C., and Colonnier, M. (1989). Number of neurons in individual laminae of areas 3B, 4 gamma, and 6a alpha of the cat cerebral cortex: a comparison with major visual areas. *J. Comp. Neurol.* 279, 228–234.

Bressler, S. L., and Menon, V. (2010). Large-scale brain networks in cognition: emerging methods and principles. *Trends in Cognitive Sciences* 14, 277–290.

Brodmann, K. (1913). Neue Forschungsergebnisse der Grosshirnrindenanatomie mit besonderer Berücksichtigung anthropologischer Fragen. *Verhandlungen der Gesellschaft deutscher Naturforscher und Ärzte* 85, 200–240.

Buffalo, E. A., Fries, P., Landman, R., Liang, H., and Desimone, R. (2010). A backward progression of attentional effects in the ventral stream. *Proc. Natl. Acad. Sci. U.S.A* 107, 361–365.

Bullmore, E., and Sporns, O. (2009). Complex brain networks: graph theoretical analysis of structural and functional systems. *Nature Reviews Neuroscience* 10, 186–198.

Burek, M. J., and Oppenheim, R. W. (1996). Programmed Cell Death in the Developing Nervous System. *Brain Pathology* 6, 427–446.

Burton, H. (2003). Visual cortex activity in early and late blind people. *J. Neurosci.* 23, 4005–4011.

Cahalane, D. J., Charvet, C. J., and Finlay, B. L. (2012). Systematic, balancing gradients in neuron density and number across the primate isocortex. *Front. Neuroanat* 6, 28.

Cahalane, D. J., Clancy, B., Kingsbury, M. A., Graf, E., Sporns, O., and Finlay, B. L. (2011). Network Structure Implied by Initial Axon Outgrowth in Rodent Cortex: Empirical Measurement and Models. *PLoS ONE* 6, e16113.

Caviness, V. S., Goto, T., Tarui, T., Takahashi, T., Bhide, P. G., and Nowakowski, R. S. (2003). Cell output, cell cycle duration and neuronal specification: a model of integrated mechanisms of the neocortical proliferative process. *Cereb Cortex* 13, 592–598.

Chalfin, B. P., Cheung, D. T., Muniz, J. A. P. C., de Lima Silveira, L. C., and Finlay, B. L. (2007). Scaling of neuron number and volume of the pulvinar complex in new world primates: Comparisons with humans, other primates, and mammals. *J. Comp. Neurol.* 504, 265–274.

Charvet, C. J., Darlington, R. B., and Finlay, B. L. (2013). Variation in human brains may facilitate evolutionary change toward a limited range of phenotypes. *Brain Behavior and Evolution* 81, 74–85.

Chen, C.-H., Gutierrez, E. D., Thompson, W., Panizzon, M. S., Jernigan, T. L., Eyler, L. T., Fennema-Notestine, C., Jak, A. J., Neale, M. C., Franz, C. E., et al. (2012). Hierarchical Genetic Organization of Human Cortical Surface Area. *Science* 335, 1634–1636.

Chklovskii, D. B., and Koulakov, A. A. (2004). Maps in the brain: what can we learn from them? *Annu Rev Neurosci* 27, 369–92.

Christensen, J. R., Larsen, K. B., Lisanby, S. H., Scalia, J., Arango, V., Dwork, A. J., and Pakkenberg, B. (2007). Neocortical and hippocampal neuron and glial cell numbers in the rhesus monkey. *The Anatomical Record: Advances in Integrative Anatomy and Evolutionary Biology* 290, 330–340.

Clancy, B., Darlington, R. B., and Finlay, B. L. (2001). Translating developmental time across mammalian species. *Neuroscience* 105, 7–17.

Collins, C. E. (2011). Variability in Neuron Densities across the Cortical Sheet in Primates. *Brain Behav Evol* 78, 37–50.

Collins, C. E., Airey, D. C., Young, N. A., Leitch, D. B., and Kaas, J. H. (2010a). Neuron densities vary across and within cortical areas in primates. *Proceedings of the National Academy of Sciences* 107, 15927 –15932.

Collins, C. E., Young, N. A., Flaherty, D. K., Airey, D. C., and Kaas, J. H. (2010b). A Rapid and Reliable Method of Counting Neurons and Other Cells in Brain Tissue: A Comparison of Flow Cytometry and Manual Counting Methods. *Front Neuroanat* 4.

Crandall, J. E., and Caviness, V. S. (1984). Thalamocortical connections in newborn mice. *Journal of Comparative Neurology* 228, 542–556.

Dehay, C., and Kennedy, H. (2007). Cell-cycle control and cortical development. *Nat Rev Neurosci* 8, 438–450.

Ding, S. L., and Elberger, A. J. (1995). A modification of biotinylated dextran amine histochemistry for labeling the developing mammalian brain. *J Neurosci Methods* 57, 67–75.

Duncan, J., and Owen, A. M. (2000). Common regions of the human frontal lobe recruited by diverse cognitive demands. *Trends in Neurosciences* 23, 475–481.

Economo, C., and Koskinas, G. (2008). *Atlas of cytoarchitectonics of the adult human cerebral cortex*. 1st English ed. Basil, New York: Karger.

Elman, J. L., Bates, E. A., Johnson, M. H., Karmiloff-Smith, A., and Plunkett, K. (1998). *Rethinking innateness : a connectionist perspective on development*. Cambridge: MIT Press.

Elston, G. N., Oga, T., and Fujita, I. (2009). Spinogenesis and Pruning Scales across Functional Hierarchies. *The Journal of Neuroscience* 29, 3271 –3275.

Van Essen, D., Anderson, C., and Felleman, D. (1992). Information processing in the primate visual system: an integrated systems perspective. *Science* 255, 419–423.

Fedorenko, E., Behr, M. K., and Kanwisher, N. (2011). Functional specificity for high-level linguistic processing in the human brain. *Proceedings of the National Academy of Sciences* 108, 16428 –16433.

Felleman, D. J., and Van Essen, D. C. (1991). Distributed hierarchical processing in the primate cerebral cortex. *Cerebral Cortex* 1, 1–47.

Finlay, B. L., and Darlington, R. B. (1995). Linked regularities in the development and evolution of mammalian brains. *Science* 268, 1578–1584.

Finlay, B. L., Hinz, F., and Darlington, R. B. (2011). Mapping behavioural evolution onto brain evolution: the strategic roles of conserved organization in individuals and species. *Phil. Trans. R. Soc. B* 366, 2111–2123.

Finlay, B. L., and Pallas, S. L. (1989). Control of cell number in the developing mammalian visual system. *Progress in Neurobiology* 32, 207–234.

Finlay, B. L., and Slattery, M. (1983). Local Differences in the Amount of Early Cell Death in Neocortex Predict Adult Local Specializations. *Science* 219, 1349–1351.

Fischl, B. (2000). Measuring the thickness of the human cerebral cortex from magnetic resonance images. *Proceedings of the National Academy of Sciences* 97, 11050–11055.

Fitzpatrick, D. (1996). The Functional Organization of Local Circuits in Visual Cortex: Insights from the Study of Tree Shrew Striate Cortex. *Cereb.Cortex* 6, 329–341.

Fox, M. D., and Raichle, M. E. (2007). Spontaneous fluctuations in brain activity observed with functional magnetic resonance imaging. *Nat.Rev.Neurosci.* 8, 700–711.

Fukuchi-Shimogori, T., and Grove, E. A. (2001a). Neocortex patterning by the secreted signaling molecule FGF8. *Science* 294, 1071–1074.

Fukuchi-Shimogori, T., and Grove, E. A. (2001b). Neocortex Patterning by the Secreted Signaling Molecule FGF8. *Science* 294, 1071–1074.

Gohlke, J. M., Griffith, W. C., and Faustman, E. M. (2007). Computational Models of Neocortical Neuronogenesis and Programmed Cell Death in the Developing Mouse, Monkey, and Human. *Cereb. Cortex* 17, 2433–2442.

Goldman-Rakic, P. S. (1987). Development of Cortical Circuitry and Cognitive Function. *Child Development* 58, 601–622.

Hagberg, A. A., Schult, D. A., and Swart, P. J. (2008). Exploring network structure, dynamics, and function using NetworkX. in *Proceedings of the 7th Python in Science Conference (SciPy2008)* (Pasadena, CA USA), 11–15.

Hagmann, P., Cammoun, L., Gigandet, X., Meuli, R., Honey, C. J., Wedeen, V. J., and Sporns, O. (2008). Mapping the Structural Core of Human Cerebral Cortex. *PLoS Biol* 6, e159.

Hawrylycz, M. J., Lein, E. S., Guillozet-Bongaarts, A. L., Shen, E. H., Ng, L., Miller, J. A., Lagemaat, L. N. van de, Smith, K. A., Ebbert, A., Riley, Z. L., et al. (2012). An anatomically comprehensive atlas of the adult human brain transcriptome. *Nature* 489, 391–399.

Haydar, T. F., Nowakowski, R. S., Yarowsky, P. J., and Krueger, B. K. (2000). Role of founder cell deficit and delayed neuronogenesis in microencephaly of the trisomy 16 mouse. *J. Neurosci.* 20, 4156–4164.

Herculano-Houzel, S., Collins, C. E., and Wong, P. and K. (2007). Cellular scaling rules for primate brains. *Proc Nat Acad Sci Usa* 104, 3562–3567.

Herculano-Houzel, S., and Lent, R. (2005). Isotropic Fractionator: A Simple, Rapid Method for the Quantification of Total Cell and Neuron Numbers in the Brain. *The Journal of Neuroscience* 25, 2518 –2521.

Herculano-Houzel, S., Mota, B., and Lent, R. (2006). Cellular scaling rules for rodent brains. *Proc Nat Acad Sci Usa* 103, 12138–12143.

Hilgetag, C. C., and Grant, S. (2000). Uniformity, specificity and variability of corticocortical connectivity. *Philosophical Transactions of the Royal Society of London B* 355, 7–20.

Hubel, D. H., and Wiesel, T. N. (1965). Binocular interaction in striate cortex of kittens reared with artificial squint. *Journal of Neurophysiology* 28, 1041–1059.

Humphries, M. D., and Gurney, K. (2008). Network "Small-World-Ness": A Quantitative Method for Determining Canonical Network Equivalence. *PLoS ONE* 3, e0002051.

Hutsler, J. J., Lee, D.-G., and Porter, K. K. (2005). Comparative analysis of cortical layering and supragranular layer enlargement in rodent carnivore and primate species. *Brain Res* 1052, 71–81.

Huttenlocher, P. R., and Dabholkar, A. S. (1997). Regional differences in synaptogenesis in human cerebral cortex. *The Journal of Comparative Neurology* 387, 167–178.

Innocenti, G. M., and Vercelli, A. (2010). Dendritic bundles, minicolumns, columns, and cortical output units. *Frontiers in Neuroanatomy* 4.

Jackson, C. A., Peduzzi, J. D., and Hickey, T. L. (1989). Visual cortex development in the ferret. I. Genesis and migration of visual cortical neurons. *J. Neurosci.* 9, 1242–1253.

Jerison, H. J. (1973). *Evolution of the brain and intelligence,*. New York: Academic Press.

Johnson, M. H., and Vecera, S. P. (1996). Cortical differentiation and neurocognitive development: The parcellation conjecture. *Behavioural Processes* 36, 195–212.

Jones, E. G. (1998). Viewpoint: The core and matrix of thalamic organization. *Neuroscience* 85, 331–345.

Kaas, J. H. (1987). The organization of neocortex in mammals: Implications for theories of brain function. *Annual Review of Psychology* 38, 129–151.

Kaas, J. H., and Hackett, T. A. (2004). "Auditory Cortex in Primates: Functional Subdivisions and Processing Streams," in *The cognitive neurosciences* (Cambridge Mass.: MIT Press), 215.

Kaas, J. H., Schüz, A., and Miller, R. (2002). "Cortical areas and patterns of cortico-cortical connections," in *Cortical areas: unity and diversity* (London: Taylor and Francis), 179–191.

Kaiser, M., Hilgetag, C. C., and van Ooyen, A. (2009). A Simple Rule for Axon Outgrowth and Synaptic Competition Generates Realistic Connection Lengths and Filling Fractions. *Cereb.Cortex* 19, 3001–3010.

Kang, H. J., Kawasawa, Y. I., Cheng, F., Zhu, Y., Xu, X., Li, M., Sousa, A. M. M., Pletikos, M., Meyer, K. A., Sedmak, G., et al. (2011). Spatio-temporal transcriptome of the human brain. *Nature* 478, 483–489.

Kanwisher, N., McDermott, J., and Chun, M. M. (1997). The Fusiform Face Area: A Module in Human Extrastriate Cortex Specialized for Face Perception. *The Journal of Neuroscience* 17, 4302 –4311.

Kaskan, P. M., Franco, E. C. S., Yamada, E. S., de Lima Silveira, L. C., Darlington, R. B., and Finlay, B. L. (2005). Peripheral variability and central constancy in mammalian visual system evolution. *Proceedings of the Royal Society B: Biological Sciences* 272, 91–100.

Kingsbury, M. A., and Finlay, B. L. (2001). The cortex in multidimensional space: where do cortical areas come from? *Developmental Science* 4, 125–142.

Kingsbury, M. A., Graf, E. R., and Finlay, B. L. (2000). Altered development of visual subcortical projections following neonatal thalamic ablation in the hamster. *J Comp Neurol* 424, 165–78.

Korbo, L., Pakkenberg, B., Ladefoged, O., Gundersen, H. J., Arlien-Søborg, P., and Pakkenberg, H. (1990). An efficient method for estimating the total number of neurons in rat brain cortex. *J. Neurosci. Methods* 31, 93–100.

Kornack, D. R., and Rakic, P. (1998). Changes in cell-cycle kinetics during the development and evolution of primate neocortex. *Proceedings of the National Academy of Sciences* 95, 1242 –1246.

Kornack, D. R., and Rakic, P. (1995). Radial and horizontal deployment of clonally related cells in the primate neocortex: relationship to distinct mitotic lineages. *Neuron* 15, 311–21.

Lashley, K. S. (1931). Mass action in cerebral function. *Science* 73, 245–254.

Latora, V., and Marchiori, M. (2001). Efficient Behavior of Small-World Networks. *Phys. Rev. Lett.* 87, 198701.

Leicht, E. A., and Newman, M. E. J. (2008). Community Structure in Directed Networks. *Phys. Rev. Lett.* 100, 118703.

Lent, R. (1982). The organization of subcortical projections of the hamster's visual cortex. *Journal of Comparative Neurology* 206, 227–242.

Lewis, J. (2008). From Signals to Patterns: Space, Time, and Mathematics in Developmental Biology. *Science* 322, 399–403.

Lukaszewicz, A., Savatier, P., Cortay, V., Giroud, P., Huissoud, C., Berland, M., Kennedy, H., and Dehay, C. (2005). G1 Phase Regulation, Area-Specific Cell Cycle Control, and Cytoarchitectonics in the Primate Cortex. *Neuron* 47, 353–364.

Luskin, M. B., and Shatz, C. J. (1985). Neurogenesis of the cat's primary visual cortex. *The Journal of Comparative Neurology* 242, 611–631.

Merker, B. (2004). Cortex, Countercurrent Context, and Dimensional Integration of Lifetime Memory. *Cortex* 40, 559–576.

Miller, B., Chou, L., and Finlay, B. L. (1993). The early development of thalamocortical and corticothalamic projections. *Journal of Comparative Neurology* 335, 16–41.

Miller, M. W., and Kuhn, P. E. (1995). Cell Cycle Kinetics in Fetal Rat Cerebral Cortex: Effects of Prenatal Treatment with Ethanol Assessed by a Cumulative Labeling Technique with Flow Cytometry. *Alcoholism: Clinical and Experimental Research* 19, 233–237.

Miyama, S., Takahashi, T., Nowakowski, R. S., and Caviness, V. S., Jr (1997). A gradient in the duration of the G1 phase in the murine neocortical proliferative epithelium. *Cereb. Cortex* 7, 678–689.

Modha, D. S., and Singh, R. (2010). Network architecture of the long-distance pathways in the macaque brain. *Proceedings of the National Academy of Sciences* 107, 13485–13490.

Molnar, Z., Knott, G. W., Blakemore, C., and Saunders, N. R. (1998). Development of thalamocortical projections in the south American gray short-tailed opossum (Monodelphis domestica). *J Comp Neurol* 398, 491–514.

Morin, L. P., and Wood, R. I. (2000). *A stereotaxic atlas of the Golden Hamster Brain*. San Diego: Academic Press.

Murre, J. M. J., and Sturdy, D. P. F. (1995). The connectivity of the brain: multi-level quantitative analysis. *Biol Cybern* 73, 529–545.

Newman, M. E. J., Barabasi, A. L., and Watts, D. J. (2006). *The Structure and Dynamics of Networks*. Princeton, New Jersey: Princeton University Press.

O'Leary, D. D. (1989). Do cortical areas emerge from a protocortex? *Trends Neurosci.* 12, 400–406.

O'Leary, D. D., Schlaggar, B. L., and Tuttle, R. (1994). Specification of neocortical areas and thalamocortical connections. *Annual Review of Neuroscience* 17, 419–439.

O'Toole, A. J., Jiang, F., Abdi, H., and Haxby, J. V. (2005a). Partially distributed representations of objects and faces in ventral temporal cortex. *Journal of Cognitive Neuroscience* 17, 580–599.

O'Toole, A. J., Jiang, F., Abdi, H., and Haxby, J. V. (2005b). Partially Distributed Representations of Objects and Faces in Ventral Temporal Cortex. *Journal of Cognitive Neuroscience* 17, 580–590.

Pakkenberg, B., and Gundersen, H. J. G. (1997). Neocortical neuron number in humans: Effect of sex and age. *The Journal of Comparative Neurology* 384, 312–320.

Pallas, S. L. (2001). Intrinsic and extrinsic factors that shape neocortical specification. *Trends Neurosci.* 24, 417–423.

Paxinos, G., and Watson, C. (1986). *The Rat Brain in Stereotaxic Coordinates*. Orlando, Florida: Academic Press.

Rakic, P. (1982). Early developmental events: cell lineages, acquisition of neuronal positions, and areal and laminar development. *Neurosci Res Program Bull* 20, 439–451.

Rakic, P. (2002a). Neurogenesis in adult primate neocortex: an evaluation of the evidence. *Nat Rev Neurosci* 3, 65–71.

Rakic, P. (1974a). Neurons in Rhesus Monkey Visual Cortex: Systematic Relation between Time of Origin and Eventual Disposition. *Science* 183, 425–427.

Rakic, P. (1974b). Neurons in rhesus monkey visual cortex: systematic relation between time of origin and eventual disposition. *Science* 183, 425–427.

Rakic, P. (2002b). Pre- and post-developmental neurogenesis in primates. *Clinical Neuroscience Research* 2, 29–39.

Rakic, P. (1988). Specification of Cerebral Cortical Areas. *Science* 241, 170–176.

Rakic, P., Bourgeois, J.-P., Eckenhoff, M. F., Zecevic, N., and Goldman-Rakic, P. S. (1986). Concurrent Overproduction of Synapses in Diverse Regions of the Primate Cerebral Cortex. *Science* 232, 232–235.

Reep, R. L. (2000). Cortical layer VII and persistent subplate cells in mammalian brains. *Brain Behav. Evol.* 56, 212–234.

Reillo, I., and Borrell, V. (2012). Germinal Zones in the Developing Cerebral Cortex of Ferret: Ontogeny, Cell Cycle Kinetics, and Diversity of Progenitors. *Cereb. Cortex* 22, 2039–2054.

Rockel, A. J., Hiorns, R. W., and Powell, T. P. S. (1980). The Basic Uniformity in Structure of the Neocortex. *Brain* 103, 221–244.

Rosa, M. G. P., and Tweedale, R. (2005). Brain Maps, Great and Small: Lessons from Comparative Studies of Primate Visual Cortical Organization. *Phil. Trans. R. Soc. B* 360, 665–691.

Roth, G., and Dicke, U. (2005). Evolution of the brain and intelligence. *Trends in Cognitive Sciences* 9, 250–257.

Sansom, S. N., and Livesey, F. J. (2009). Gradients in the Brain: The Control of the Development of Form and Function in the Cerebral Cortex. *Cold Spring Harbor Perspectives in Biology* 1, a002519–a002519.

Saxe, R., and Kanwisher, N. (2003). People thinking about thinking people. The role of the temporo-parietal junction in "theory of mind." *NeuroImage* 19, 1835–1842.

Scannell, J. W., Blakemore, C., and Young, M. P. (1995). Analysis of connectivity in the cat cerebral cortex. *J Neurosci* 15, 1463–1483.

Scannell, J. W., Burns, G. A. P. C., Hilgetag, C. C., O'Neil, M. A., and Young, M. P. (1999). The Connectional Organization of the Cortico-thalamic System of the Cat. *Cereb.Cortex* 9, 277–299.

Smart, I. H. (1983). Three dimensional growth of the mouse isocortex. *J Anat* 137, 683–694.

Smart, I. H. M., Dehay, C., Giroud, P., Berland, M., and Kennedy, H. (2002). Unique Morphological Features of the Proliferative Zones and Postmitotic Compartments of the Neural Epithelium Giving Rise to Striate and Extrastriate Cortex in the Monkey. *Cereb. Cortex* 12, 37–53.

Smith, M. L., Fries, P., Gosselin, F., Goebel, R., and Schyns, P. G. (2009). Inverse Mapping the Neuronal Substrates of Face Categorizations. *Cerebral Cortex* 19, 2428–2438.

Sporns, O., Chialvo, D. R., Kaiser, M., and Hilgetag, C. C. (2004). Organization, development and function of complex brain networks. *Trends Cogn.Sci.(Regul.Ed.)* 8, 418–425.

Sporns, O., Honey, C. J., and Kötter, R. (2007). Identification and Classification of Hubs in Brain Networks. *PLoS ONE* 2, e1049.

Sporns, O., Tononi, G., and Edelman, G. M. (2000). Theoretical neuroanatomy: Relating anatomical and functional connectivity in graphs and cortical connection matrices. *Cereb Cortex* 10, 127–141.

Stephan, H., Frahm, H., and Baron, G. (1981). New and revised data on volumes of brain structures in insectivores and primates. *Folia Primatol* 35, 1–29.

Takahashi, T., Nowakowski, R., and Caviness, V. (1995). The cell cycle of the pseudostratified ventricular epithelium of the embryonic murine cerebral wall. *The Journal of Neuroscience* 15, 6046 –6057.

Takahashi, T., Nowakowski, R. S., and Caviness, V. S., Jr (1996). The leaving or Q fraction of the murine cerebral proliferative epithelium: a general model of neocortical neuronogenesis. *J. Neurosci.* 16, 6183–6196.

Thomaidou, D., Mione, M. C., Cavanagh, J. F., and Parnavelas, J. G. (1997). Apoptosis and its relation to the cell cycle in the developing cerebral cortex. *J. Neurosci.* 17, 1075–1085.

Underwood, E. (2013). Why Do So Many Neurons Commit Suicide During Brain Development? *Science* 340, 1157–1158.

White, L. E., and Fitzpatrick, D. (2007). Vision and Cortical Map Development. *Neuron* 56, 327–338.

Williams, R. W., von Bartheld, C. S., and Rosen, G. D. (2003). "Counting Cells in Sectioned Material: A Suite of Techniques, Tools, and Tips," in *Current Protocols in Neuroscience* (John Wiley & Sons, Inc.). Available at: http://dx.doi.org/10.1002/0471142301.ns0111s24.

Windrem, M. S., and Finlay, B. L. (1991). Thalamic ablations and neocortical development: alterations of cortical cytoarchitecture and cell number. *Cerebral Cortex* 1.

Wolfram Research, I. (2008). Mathematica.

Workman, A. D., Charvet, C. J., Clancy, B., Darlington, R. B., and Finlay, B. L. (2013). Modeling Transformations of Neurodevelopmental Sequences across Mammalian Species. *J. Neurosci.* 33, 7368–7383.

Yamamori, T. (2011). Selective gene expression in regions of primate neocortex: Implications for cortical specialization. *Progress in Neurobiology* 94, 201–222.

Yopak, K. E., Lisney, T. J., Darlington, R. B., Collin, S. P., Montgomery, J. C., and Finlay, B. L. (2010). A conserved pattern of brain scaling from sharks to primates. *PNAS*. Available at: http://www.pnas.org/content/early/2010/06/24/1002195107 [Accessed December 3, 2012].

Zalesky, A., Fornito, A., Harding, I. H., Cocchi, L., YÃ¼cel, M., Pantelis, C., and Bullmore, E. T. (2010). Whole-brain anatomical networks: Does the choice of nodes matter? *Neuroimage* 50, 970–983.

Zhang, K., and Sejnowski, T. J. (2000). A universal scaling law between gray matter and white matter of cerebral cortex. *Proceedings of the National Academy of Sciences of the United States of America* 97, 5621–5626.

Zhong, Y.-M., and Rockland, K. S. (2003). Inferior Parietal Lobule Projections to Anterior Inferotemporal Cortex (Area TE) in Macaque Monkey. *Cerebral Cortex* 13, 527–540.